University of Alberta

Development of new fluorescent protein biosensors

by

Ahmed Saied F. Belal

A thesis submitted to the Faculty of Graduate Studies and Research
in partial fulfillment of the requirements for the degree of

Doctor of Philosophy

Department of Chemistry

Fall 2013
Edmonton, Alberta

Abstract

The discovery of green fluorescent protein (GFP) from the *Aequorea victoria* Jellyfish followed by the extensive efforts of protein engineers to produce other fluorescent proteins (FPs) spanning the visible color spectrum made fluorescent proteins indispensable biochemical tools in the scientific community. Experimental biologists have utilized FPs as genetically encoded markers for the imaging of subcellular structures and protein dynamics in live cells. Another important application of FPs is their design for use in biosensors for either enzymes or small biological molecules of interest. The work described in this thesis is an attempt to portray different experimental designs of FP based biosensors with the final objective of either modifying previously reported or introducing novel biosensors.

We addressed the FP biosensors based on the principle of intramolecular Förster resonance energy transfer (FRET) in two projects. In the first project we demonstrated a modification of a methodology of development and optimization of FRET-based biosensor for a post translational modification. The end result of this project has led to improving a previously reported protein kinase B (PkB) biosensor and the discovery of a new cyclin B1- cyclin dependent kinase 1 (Cyclin B1-CDK1) biosensor of a higher dynamic range than previously published one.

In the second project our efforts were directed to develop a matrix metallo proteinase 2 (MMP2) FRET based biosensor, with the ultimate goal of using this biosensor in live cell imaging of cardiomyocytes to explore postulated MMP2 intracellular role in ischemia-reperfusion injury**.** We designed protein constructs based on both previously reported MMP2 substrate sequences and potential cardiac protein target sequences. After testing and characterizing the designed constructs, the expression of the best candidate in neonatal

cardiomyocytes cell lines is undertaken by our collaborator Professor Richard Schulz, Department of Pharmacology, University of Alberta.

In the third and final project we utilized single FP-based biosensor concept in trying to develop Hydrogen peroxide biosensors of different hues. Our efforts were fruitful in discovering two green biosensors, one is with direct and the other is with inverse response to hydrogen peroxide.

TABLE OF CONTENTS

LIST OF TABLES

LIST OF FIGURES

LIST OF ABBREVIATIONS

ADP	Adenosine diphosphate
ATP	Adenosine triphosphate
avGEP	*Aequorea victoria* green fluorescent protein
BCA	Bicinchoninic acid
BiFC	Bimolecular fluorescence complementation
bp	Base pair
BKAR	B kinase activity reporter
BSA	Bovine serum albumin
CaM	Calmodulin
cGMP	Cyclic guanosine monophosphate
CCD	Charged couple device
CDK1	Cyclin dependent kinase 1
cpFP	Circularly permuted fluorescent protein
CyPet	Cyan fluorescent protein for energy transfer
Cys	Cysteine
DNA	Deoxyribonucleic acid
dNTP	Deoxyribonucleotide triphosphate
dsDNA	Double stranded deoxyribonucleic acid
DsRed	*Discosoma* species red fluorescent protein
E	FRET efficiency
E. coli	*Escherichia coli*
ECFP	Enhanced cyan fluorescent protein

EGFP	Enhanced green fluorescent protein
EYFP	Enhanced yellow fluorescent protein
FACS	Fluorescence activated cell sorting
FBS	Fetal bovine serum
FHA2	Forkhead associated domain 2
FRET	Fluorescence resonance energy transfer
ε	Extinction coefficient
FP	Fluorescent protein
FACS	Fluorescence activated cell sorting
GECO	Genetically encoded Ca^{+2} indicator for optical imaging
GFP	Green fluorescent protein
Gln	Glutamine
Glu	Glutamate
Gly	Glycine
HeLa	Cervical cancer cell line originating from Henrietta Lacks
His	Histidine
kb	Kilobases
KDa	Kilodalton
IDT	Integrated DNA technology
IPTG	Isopropyl β-D-1-thiogalactopyranoside
KIE	kinetic isotope effect

LB	Lauria-Bertani medium
MBSU	Molecular biology service unit at University of Alberta
MMP2	Matrix Metalloproteinase-2
MRE	Molecular recognition element
mTFP1	Monomeric teal fluorescent protein 1
Ni-NTA	Ni+2 nitrilotriacetate
PBS	Phosphate buffered saline
PCR	Polymerase chain reaction
PDB	Protein data bank
PH	Pleckstrin homology
Phe	Phenylalanine
PIP3	Phosphatidylinositol (3,4,5)-triphosphate
PKB	Protein kinase B
PVDF	Polyvinylidene fluoride
φ	Quantum yield
RFP	Red fluorescent protein
R_o	Förster radius
roGFP	Redox-sensitive GFP
SDS-PAGE	Sodium dodecyl sulfate polyacrylamide gel electrophoresis
Ser	Serine
TAE	Tri-acetate EDTA

TnI	Troponin-I
Tyr	Tyrosine
WT	Wild type
YFP	Yellow fluorescent protein
YPet	Yellow fluorescent protein for energy transfer

CHAPTER 1
GENERAL INTRODUCTION

1.1 FLUORESCENCE

Photoluminescence is the process of light emission from a species that has been electronically excited as a result of absorption of photons. Depending on the nature of the electronic excited state it has two forms: fluorescence and phosphorescence (1).

Once a molecule becomes electronically excited to the S_1 state via irradiation with a source of electromagnetic radiation of appropriate energy, it has several ways to relax back to the ground state (S_o). If the molecule has been excited to a higher vibration sublevel of the S_1 state, it can rapidly (10^{-12} s or less) relax to the lowest vibration level of S_1 in a process known as internal conversion. The molecule can then further relax directly to S_o through either non-radiative relaxation (e.g., solvent quenching or dipole-dipole interaction with neighboring fluorophore) or emitting a photon of light in the process of fluorescence. The energy of the emitted fluorescence is lower than that of excitation light owing to fact that internal conversion precedes the emission process via fluorescence. This loss of energy results in a wavelength shift between excitation and emission peak wavelengths that known as the Stokes shift (1). Another possibility is intersystem crossing which involves a change in spin multiplicity to form the triplet state. Relaxation from the triplet state to S_o via another change in spin multiplicity gives rise to the long-lived emission phenomenon known as phosphorescence (1). The best conceptual illustration of the photoluminescence mechanisms is the Jablonski diagram (Figure 1.1) that is named after Professor Aleksander Jabłoński who developed the modern theory of the fluorescence mechanism.

The intrinsic ability of a molecule to exhibit fluorescence depends on two main factors: extinction coefficient (ε) and quantum yield (φ). Extinction coefficient (also known as molar absorptivity) is a measure of how strongly a species can absorb light at a certain wavelength.

Quantum yield is the ratio of the number of photons emitted to the number of photons absorbed. The intrinsic brightness is also another parameter used to describe species exhibiting fluorescence and is simply the product of extinction coefficient and quantum yield (1).

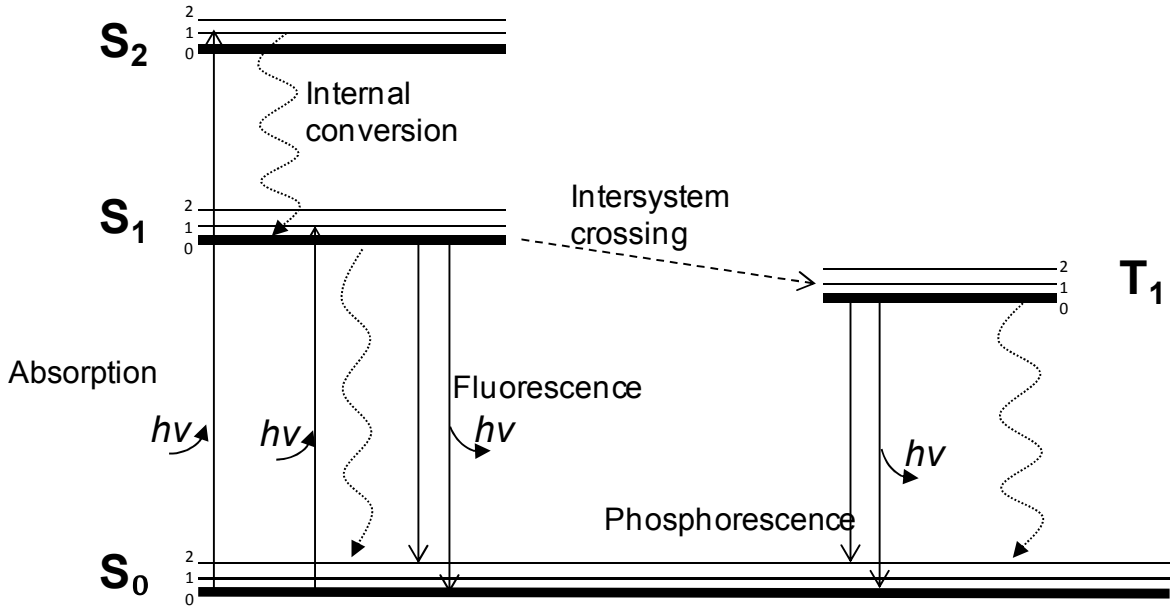

Figure 1.1 Simplified Jablonski diagram. Solid arrows show absorption or emission of photons while dashed arrows show non-radiative relaxation processes.

In 1942 Coons *et al*. reported the staining of pneumococcal antigen by a fluorescently labeled antibody (2), thus demonstrating the first example of immunofluorescence detection. The widespread popularity of this technique introduced the field of experimental biology to the sensitivity of fluorescence as a detection technique, and served as a corner stone in establishing molecular cell biology. Since that initial demonstration, immunofluorescence has enabled the detection and visualization of a wide spectrum of intra- and extracellular components including proteins, hormones, metabolites secondary messengers and even posttranslational modifications (3-6). The related technique of fluorescent analogue cytochemistry (7, 8) and the use of fluorescent chemical indicators (9) allowed, with some limitations, temporal and spatial

observation of specific intracellular processes. Overall, these scientific breakthroughs paved the way for the eventual introduction of genetically encoded fluorescent proteins (FPs), which revolutionized the ability of researchers to observe intracellular processes using fluorescence imaging.

1.2 *AEQUOREA VICTORIA* GREEN FP

Although it has been noted earlier that *Aequorea victoria* jellyfish carries fluorescent component, Osamu Shimumora of the Princeton University was the first one to realize that the fluorescent component is actually a protein, which later came to be known as *Aequorea victoria* green FP (avGFP) (10). Soon after its initial discovery, the avGFP fluorescence emission spectrum was reported and it was proposed that it was acting as the acceptor for Förster-like energy transfer from the luminescent donor protein aequorin. This proposal provided a consistent explanation for the fact that Aequorea exhibited greenish *in vivo* luminescence of Aequorea yet purified aequorin emitted blue luminescence (11). Again, it was Shimomura who determined the chemical structure of avGFP chromophore. Using purified protein, he subjected it to cycles of thermal denaturation, enzymatic digestion and chromatographic separation of the fragments. His results from these experiments, along with his chemical intuition, allowed him to reach the conclusion that the avGFP chromophore is a 4-(p-hydroxybenzylidene)-5-imidazolidinone moiety covalently linked within the polypeptide chain (12). Although the chromophore structure proposed by Shimumora was essentially correct, the substitution pattern and the amino acid sequence in which the chromophore exists was later corrected by Cody *et al*. (13).

It took almost 30 years after the initial discovery of avGFP for the primary amino acid sequence to be determined by Prasher *et al*. (14). The key revolutionary breakthrough in the development of FP technology, and hence in its broad use in experimental biology, was the

heterologous expression of avGFP in organisms other than jellyfish. Specifically, in the first demonstrations, the gene encoding avGFP was expressed in the sensory neurons of the worm *Caenorhabditis elegans* (15) and also in *Escherichia coli* (16). The heterologous expression convincingly demonstrated that the lone polypeptide gene product was self-sufficient to undergo the post-translational modifications necessary for chromophore formation.

The formation of the avGFP chromophore proceeds through an autocatalytic process that involves three key steps: cyclization, dehydration and oxidation. The exact sequence of steps has been controversial due to conflicting results from multiple studies. Tsien and co-workers (17, 18) suggested that chromophore formation starts first with distortion of the polypeptide backbone which in turn brings the Ser65 carbonyl carbon into close proximity to the Gly67 amide nitrogen. The latter attacks the adjacent serine carbonyl via its lone pair of electrons to form hydroxylated imidazolidinone, which subsequently undergoes dehydration to form an imidazolone ring. Finally Cα-Cβ of Tyr66 undergoes oxidation by molecular oxygen leading to the formation of the mature chromophore as shown in Figure 1.2 (17, 18).

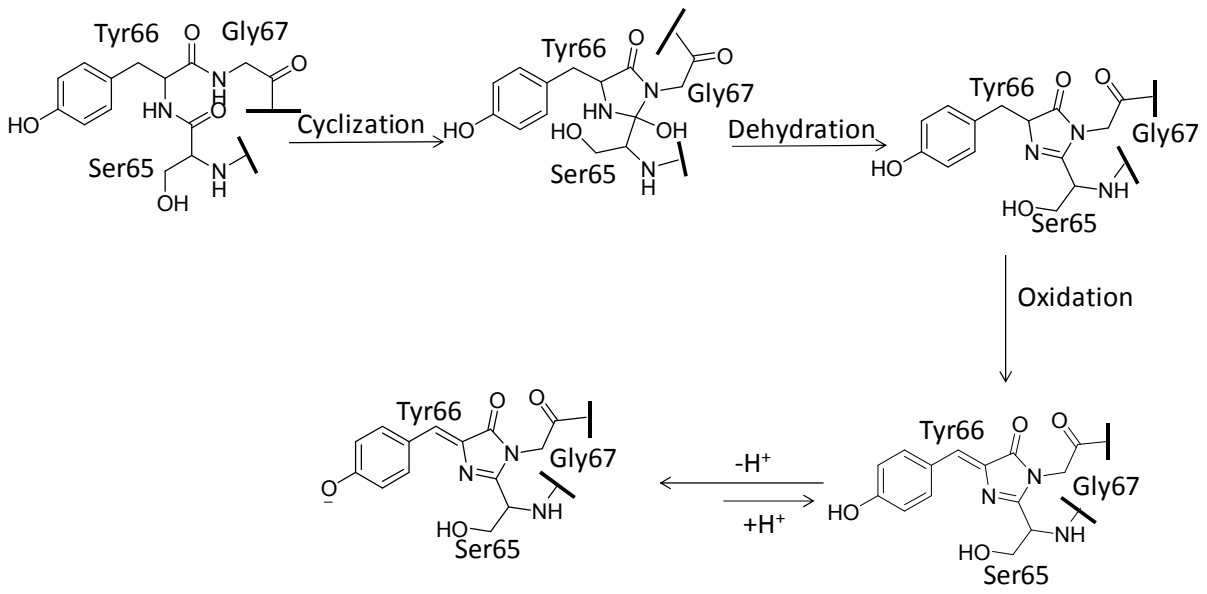

Figure 1.2 Tsien and co-workers suggested mechanism of chromophore formation of avGFP.

However, the mechanism postulated by Tsien and co-workers was in conflict with a crystallographic study of a non-fluorescent GFP Y66L mutant (19). In the GFP Y66L structure, it was observed that the chromophore-forming tripeptide had undergone the cyclization step but still existed as a hemiaminal, indicating that the dehydration step had not yet taken place. Furthermore, Cα of Leu66 had a triagonal planar geometry that strongly suggested the presence of a double bond formed by the oxidation step (19). Consequently, the authors of the crystallography study proposed a modification of Tsien's mechanism in which oxidation step comes after the initial cyclization. In this sequence, formation of the hydroxylated cyclic imine is followed by the dehydration step that involves benzylic Tyr66 Cβ leading to formation of the mature chromophore (19). Zhang *et al*. had reported the production of hydrogen peroxide preceding chromophore maturation (20). Interestingly, Pouwels and coworkers revealed that there was not any kinetic isotope effect associated with hydrogen peroxide production during chromophore formation of a GFP contained dideuterated Tyr66 Cβ (21). Consequently, chromophore formation is most likely to proceed via cyclization, then oxidation, then dehydration, as illustrated in Figure 1.3.

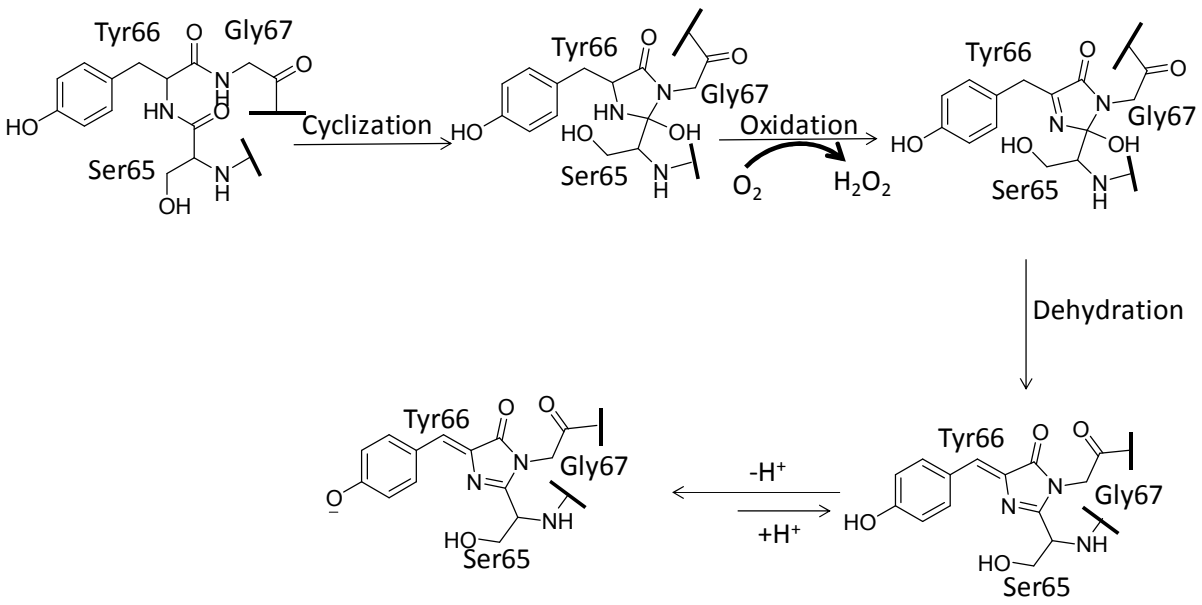

Figure 1.3 The revised mechanism of avGFP chromophore formation.

Along similar lines, the chromophore formation in the red FP isolated from *Discosoma* coral (DsRFP) has been studied extensively by various research groups. DsRFP is a homotetramer that contains both green and red chromophores (22, 23). It was first thought that an avGFP-like green chromophore is the precursor of the red chromophore and that it undergoes an additional oxidation step involving the Cα-N of Gln66 residue extending the π conjugation system and shifting the fluorescence emission to give the red hue (24). Nevertheless, Strack *et al*. (25) have demonstrated new experimental findings that supported a branched mechanism where the branch point is a hydroxylated cyclic imine similar to that formed with avGFP (Figure 1.4). One branch of the mechanism follows the green chromophore maturation pathway similar to that of avGFP. The second branch of the mechanism involves an oxidation to a short lived blue intermediate that is subsequently converted to the red chromophore (Figure 1.4). The blue species suggested by Strack *et al*. is a cationic chromophore with a 10-electron π-system (Figure 1.4; intermediate II) (25). In contrast, on the basis of ab initio and QM/MM calculations Bravaya

et al. proposed that the blue species is an anionic chromophore with a 12-electron π-system (Figure 1.4; intermediate I). The involvement of intermediate I might explain the key role of Lys70 for the DsRFP-like chromophore maturation, which was verified experimentally by directed mutagenesis (26). Specifically, the side chain of Lys70 may have a key role in stabilizing the enolate moiety of intermediate I.

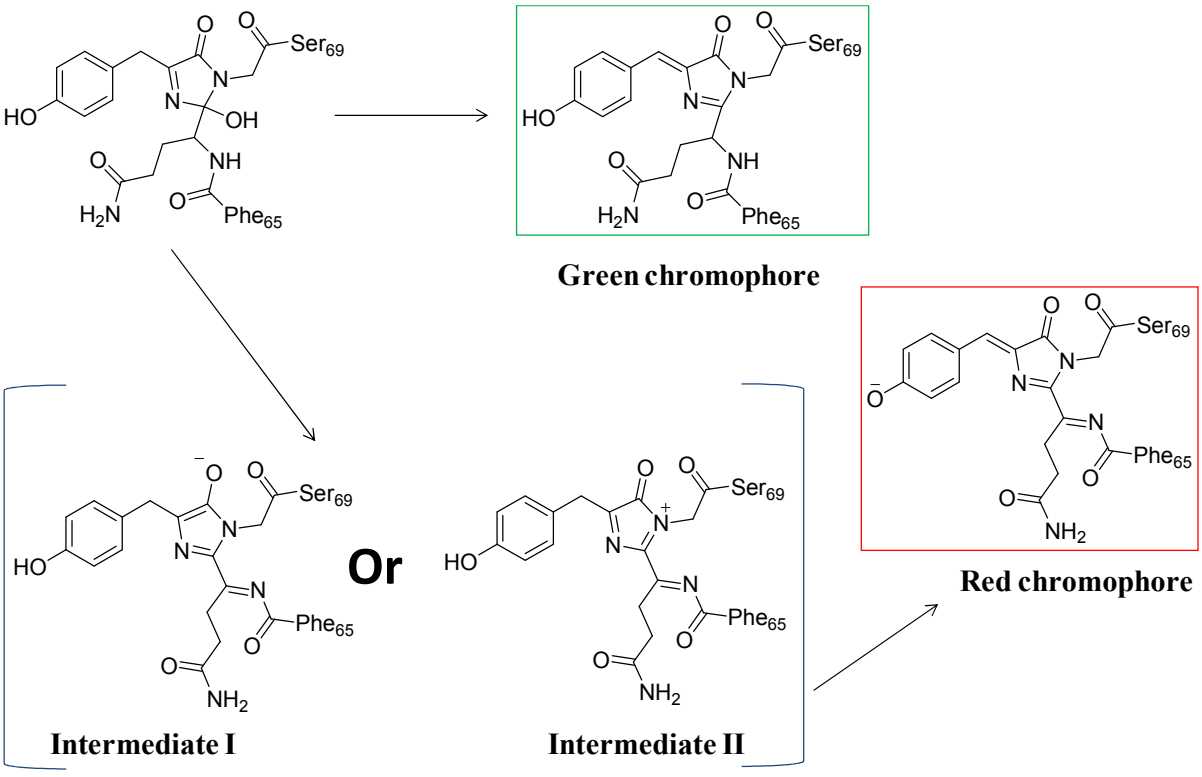

Figure 1.4 Branched mechanism of DsRFP chromophore formation.

1.3 THREE-DIMENSIONAL STRUCTURE OF avGFP

The optical properties of the different FPs are the result of both the chromophore structure and the microenvironment created by the amino acids surrounding the chromophore. In

1996, the crystal structure of avGFP was reported by two independent research groups (27, 28). AvGFP adopts a 'β-can' fold comprised of an 11-stranded β-sheet polypeptide wrapped into a pseudosymmetric cylinder with a length of ~42 Å and cross section of ~24 Å (27). At the center of the β-can lies an α-helix that connects the third and the fourth β-strands and bears the chromogenic tripeptide Ser65-Tyr66-Gly67. This tripeptide is buried in the core of β-can and is isolated from the surrounding solvent (27, 28).

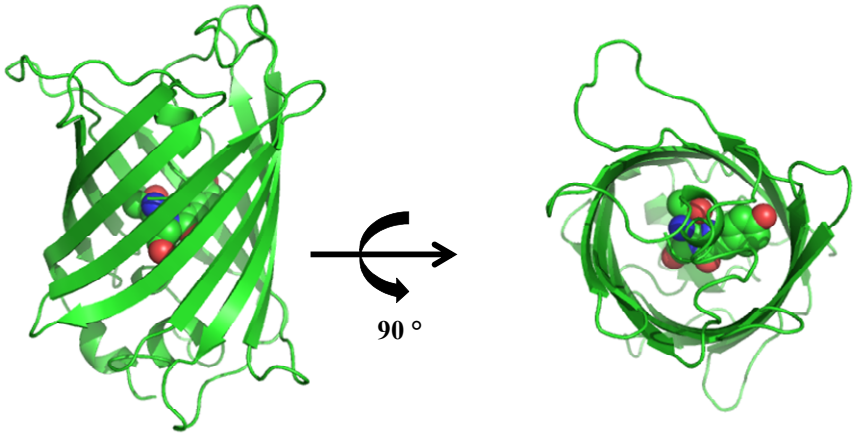

Figure 1.5 A cartoon representation of the three-dimensional structure of avGFP (PDB ID 1EMA). Graphical representation was prepared with PyMol (www.pymol.org).

1.4 FPs OF DIFFERENT COLORS

Soon after avGFP was cloned in 1994 (15, 16), it was well on its way to becoming a practically indispensable tool to many biochemists. Nevertheless, the wild-type avGFP suffered from some limitations including the fact that only one color of the protein was available, and it was sub-optimal in terms of folding if cloned into a biological context other than the one that naturally exists in (e.g., expression at 37 °C versus colder temperatures of ocean waters). These limitations prompted protein engineers to develop new variants with different colors and

enhanced properties. The color hues that are provided by FPs can be categorized into six classes based on their emission maxima: blue (440-470 nm) (29); cyan (470-500 nm) (17); green (500-520 nm), yellow (520-550 nm) (29); orange (550-575 nm) (30); and red (575-610 nm). Figure 1.6 illustrates respresentative chromophore structures associated with common FPs from each of the aforementioned classes.

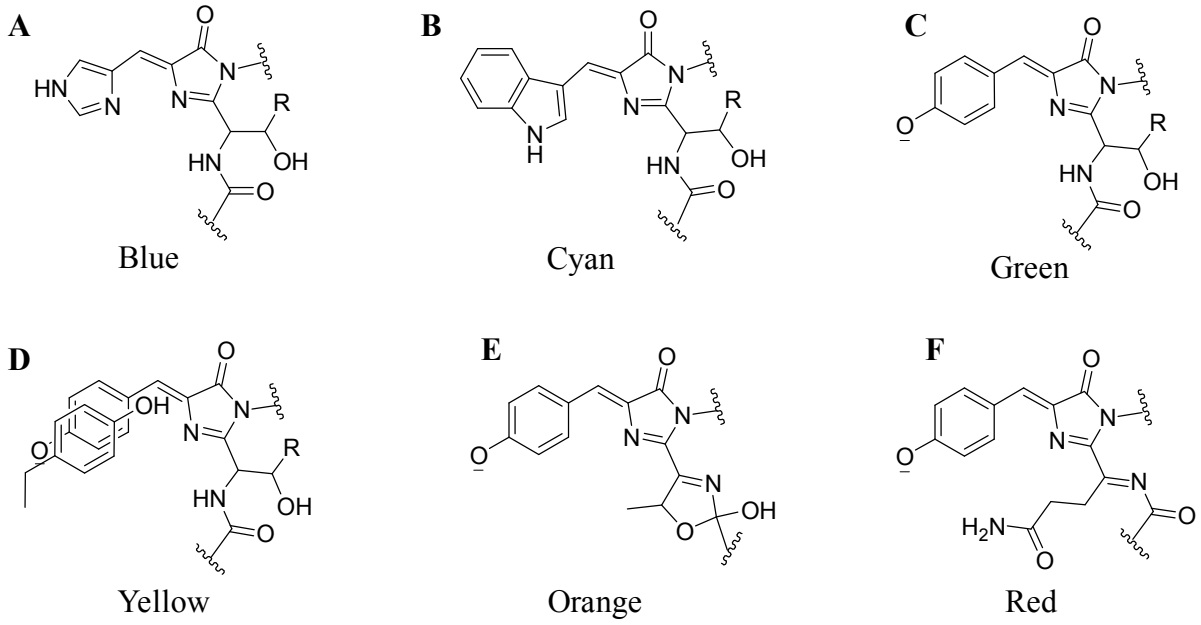

Figure 1.6 Chromophore structures of various FP color classes.

A variety of mutagenesis strategies have been applied to avGFP to create variants with either modified chromophore structures (as shown in Figure 1.6 A, B, E and F) or modified chromophore environments. An example of the former approach is the avGFP-derived cyan FP (CFP) variants (Figure 1.6B) in which the Tyr66Trp mutation has changed the chromophore structure and blue shifted the excitation and emission (31). An example of the latter approach is the avGFP-derived yellow FP (YFP) variant (Figure 1.6 D) in which the Thr203Tyr mutation has lead to an aromatic side chain π-stacking with the chromophore as confirmed by X-ray crystal

structure. This π-stacking interaction decreases the energy of the excited state resulting in red-shifted excitation and emission (29, 32).

Besides jellyfish, corals provide another source of avGFP homologues with fluorescence hues ranging from cyan to red (22). The first red FP (DsRFP) was cloned from coral *Discosoma* coral (22). Later studies revealed that the chromophore was similar to the avGFP chromophore, but the conjugated system was extended by an additional acylimine moiety (Figure 1.6 F) (24, 33, 34). DsRFP became a target for rational protein engineering and, following an extensive process of directed evolution, eventually gave rise to the mFruit series of variants which has hues that span the yellow to far-red region of the spectrum (30, 35, 36).

1.5 APPLICATIONS OF FPs

Among the earliest applications enabled by the advent of FP technology was their use as whole cell markers or reporter of gene promoter activities (18, 37). This was soon followed by applications in which FPs were used as tags that could be genetically fused to a protein of interest and hence allow the imaging of the localization and dynamics and the resulting protein chimera (37). The existence of a broad palette of FPs, coupled with the parallel developments in fluorescence microscopy, has enabled the imaging of the localization and dynamics of multiple FP tagged proteins simultaneously (37, 38).

In addition to their use as organelle and protein localization markers, FPs have several desirable features that enable them to be used in intracellular biosensing. A broad definition of a biosensor is that it is a molecule or device that couples a molecular recognition element (MRE) to a signal transducer (39). By design, the interaction of the MRE with the biological analyte of interest will modulate the signal output of the transducer (39). Needless to say, the sensitivity of fluorescence plus the ability of FPs to be genetically encoded paved the way to their inclusion in

the design of molecular biosensors for detection of intracellular analytes and biochemical events. FP-based biosensors generally fall into three categories: Förster resonance energy transfer (FRET)-based biosensors, complementation-based biosensors, and single FP-based biosensors.

1.5.1 FRET-based biosensors

FRET is the phenomenon of non-radiative energy transfer between an excited blue-shifted donor fluorophore and a red-shifted acceptor fluorophore (Figure 1.7). An absolute requirement is the spectral overlap of the donor emission and acceptor excitation spectra (40, 41). The FRET phenomenon is best quantified by the FRET efficiency. FRET efficiency exhibits a sixth power dependence on the distance separating two fluorophores and is related to the distance by the following equation (42):

$$E = \frac{1}{1 + \left(\frac{r}{R_0}\right)^6}$$

where r is the distance between the two fluorophores and R_o is the Förster radius. The Förster radius is defined as the distance at which 50% of FRET efficiency is obtained assuming a random relative orientation of the two fluorophores (42).

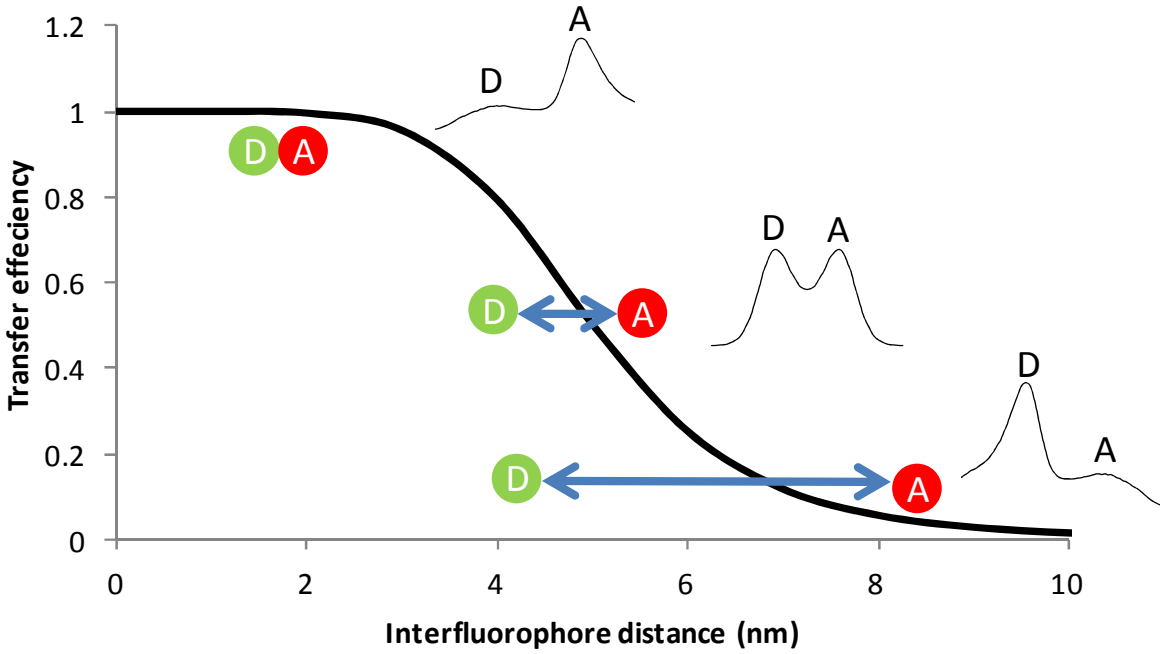

Figure 1.7 The dependence of FRET efficiency (E) on inter-fluorophore distance.

The Förster radius for a particular donor/acceptor fluorophore pair can be calculated using the equation:

$$R_0{}^6 = 8.75 * 10^{-28}\, \kappa^2\, \eta^{-4}\, \Phi_D\, J$$

where κ^2 is the dipole orientation factor of two fluorophores, η is the refractive index of the medium, and Φ_D is the quantum yield of the donor. The κ^2 orientation factor can have a value ranging between 0-4 for perpendicular to co-linear relative orientation of the donor and acceptor transition dipoles. When the donor and acceptor are freely rotating relative to each other, the dipole orientations are assumed to be random and κ^2 has a value of 2/3 (42). The J term is the overlap integral of the two chromophores which is calculated using the formula (42):

$$J = \int_0^\infty I_D\,(\lambda)\, \varepsilon_A\,(\lambda)\lambda^4\, d\lambda$$

where $I_D(\lambda)$ and $\varepsilon_A(\lambda)$ are the donor fluorescent intensity and acceptor extinction coefficient, respectively, at a given wavelength (λ). From these equations it should be apparent that the FRET efficiency change occurring during a certain experiment is a function of the change in distance (r) and/or orientation (κ^2) between fluorophores and can be described mathematically using the equation (42):

$$\Delta E = \frac{1}{1 + \left[\frac{r_{final}^6}{C\kappa_{final}^2}\right]} - \frac{1}{1 + \left[\frac{r_{initial}^6}{C\kappa_{initial}^2}\right]}$$

where C is a constant. Based on the sixth power distance dependence of FRET efficiency, FRET is considered a useful spectroscopic ruler for measuring distance changes between two fluorophores (42).

A variety of FP-based FRET biosensor design strategies have been described in the literature (43). All these strategies share the common feature of including molecular recognition element(s) between a pair of FPs that show an appropriate spectral overlap. The most common choice for a FP-based FRET pair is CFP and YFP. Nevertheless there are other pairs that have proven to be successful (44-46). A summary of the most popular design strategies is illustrated in Figure 1.8.

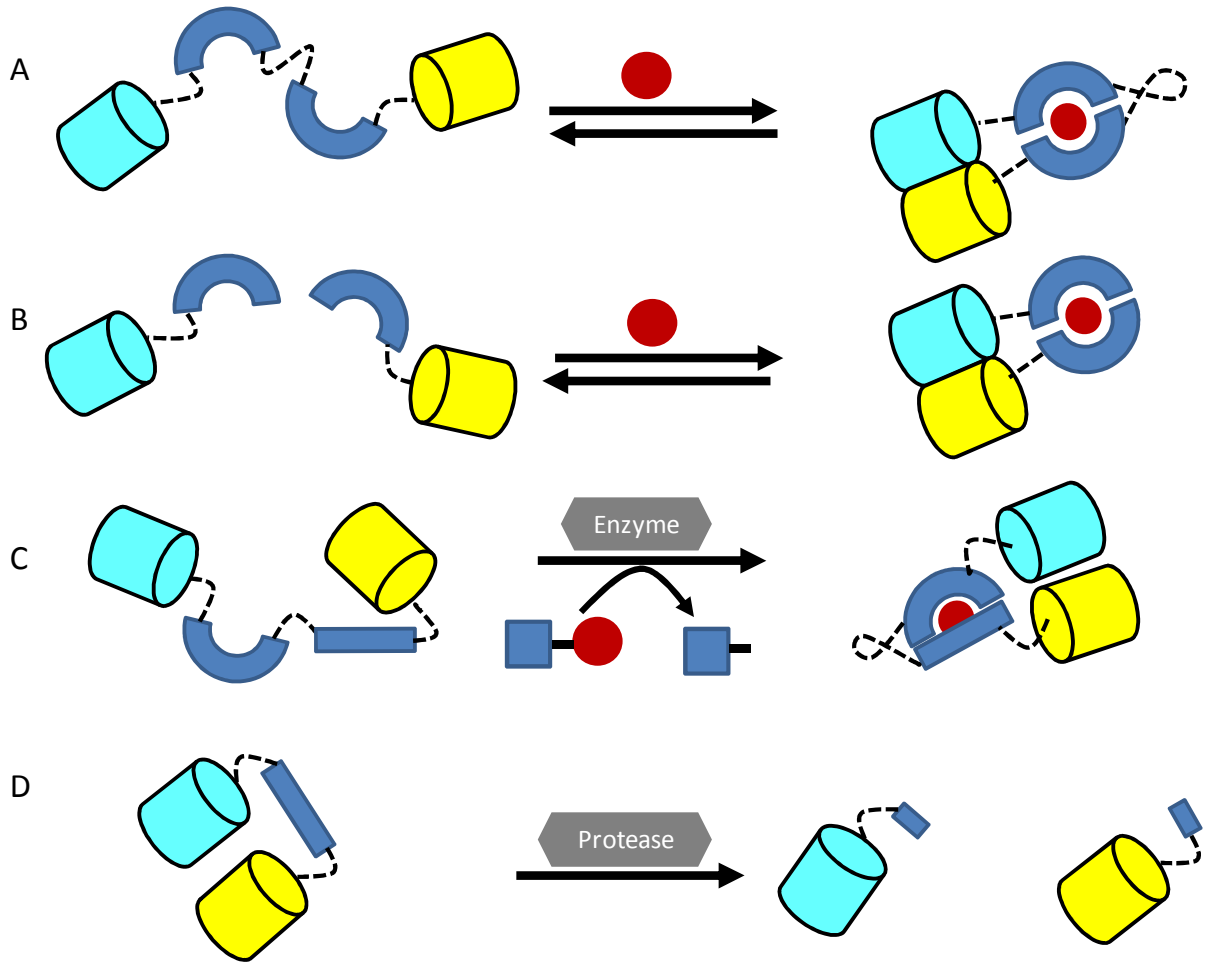

Figure 1.8 Design strategies for FP-based FRET biosensors. (A) Intramolecular biosensors in which MRE undergoes a conformational change in response to a small molecule. (B) Intermolecular biosensors of small molecules. (C) Biosensors of post-translational modification where modifying a peptide substrate (represented by a circle) makes it bind to a binding domain and cause a change in FRET. (D) Protease biosensors in which FRET pair are linked by a protease-specific substrate.

FP-based FRET biosensors to detect small molecules can be designed in either intermolecular or intramolecular form (Figure 1.8AB). In both cases the MRE used is a protein domain or domains that undergo a conformational change upon binding to the small molecule. The prototypical example for these designs is the class of cameleon Ca^{2+} FRET biosensors (47, 48). In a cameleon-type biosensor, the donor FP is fused to a Ca^{2+} binding module called

calmodulin (CaM) and an acceptor is fused to the M13 peptide that forms a complex with Ca^{2+}-bound CaM (47). Both parts can be joined in a single chimera showing robust change in FRET in response to Ca^{2+} concentration changes in live cells (47-49). Other interesting examples of this class of FRET biosensors are those employing periplasmic binding proteins, the motion of which can be described as a clam shell-like movement (50, 51). This module had been successfully used in engineering a wide variety of biosensors that responded to numerous analytes such as sugars (e.g., ribose (52), glucose (53) and sucrose (54)), amino acids (e.g., glutamate (55) and tryptophan (56)), and ions (e.g., phosphate (57)).

FP-based FRET biosensors can also be designed to report post-translational modifications (Figure 1.8C). These biosensors usually contain the sequence of a specific substrate for the enzyme that catalyzes the post-translational modification of interest. They also contain a binding domain that binds preferentially to the post-translationally modified peptide. In the most common design, the substrate and binding domain are sandwiched between donor and acceptor FPs. The conformational change induced by the post-translational modification produces a change in FRET efficiency via modulation of distance and/or dipole orientation between the FPs of the FRET pair. This strategy has been successfully used to probe activities of various post-translational modification enzymes. Some important examples include kinases (58), histone lysine methyltransferase (59), and O-GlcNac transeferase (60).

Another popular FRET biosensor design strategy is to effectively create genetically encoded FRET-based substrates for protease activities of interest. In this case the biosensor is composed of a protease cleavable substrate motif tethered to a FRET FP pair (Figure 1.8D). Protease enzymatic activity is detected by a decrease in FRET efficiency. This design has been

used in reporting a large number of proteases such as caspase-3 (44, 61) and proteases of viruses like human enterovirus (62), hepatitis C (63), and poliovirus 2A (64).

1.5.2 Bimolecular complementation biosensors

Complementation can be defined as the ability of two inactive fragments of a reporter protein, when brought to close proximity, to interact spontaneously and restore activity (65) (Figure 1.9). This technique has been frequently utilized for detection of protein-protein interactions by fusing the reporter fragments to the potential interacting proteins (65). Some of the most commonly used reporter proteins are ubiquitin (66), FPs (67-69), dihydrofolate reductase (70), β-galactosidase (71, 72), TEV protease (73), and luciferase (74). Reporter systems based on this principle typically are producing changes in a reporter protein function that can be measured using fluorescence or absorbance-based assays. When the reporter protein is an enzyme, a fluorogenic, colorimetric, or luminescent substrate must be added to aid detection.

AvGFP was successfully introduced into the complementation technology in 2000, by splitting the gene into two fragment and fusing each to leucine zipper domains capable of dimerization (75). It has become standard practice to refer to FP complementation as bimolecular fluorescence complementation (BiFC).

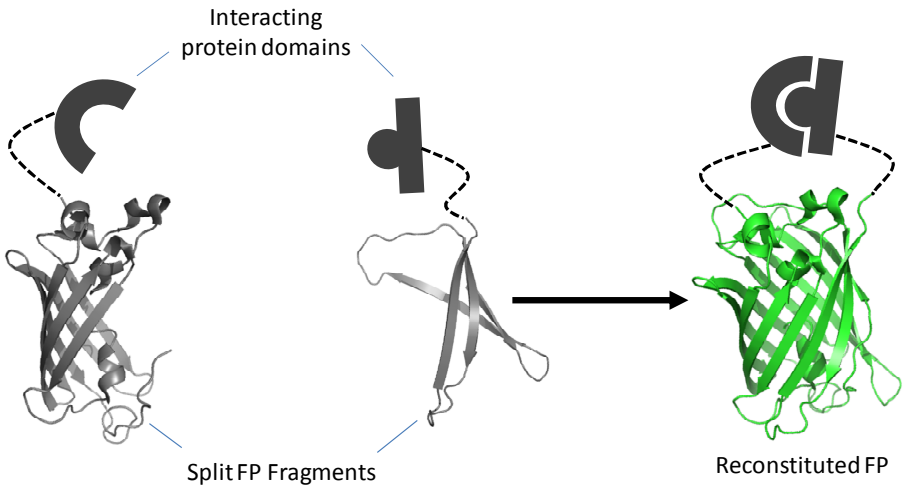

Figure 1.9 Schematic model of bimolecular fluorescence complementation biosensor design. Non-fluorescent split FP fragments are irreversibly reconstituted when brought in close proximity via protein-protein interaction and hence fluorescence is generated.

BiFC-based biosensors have been utilized to visualize a variety of protein-protein interactions in live cells (76, 77). BiFC has also been employed in high-throughput screening to detect and map previously unknown protein–protein interactions (76-79). Nevertheless, some disadvantages to this technology are the irreversible nature of complementation and slow kinetics of fluorescence complementation (76, 77).

Interestingly the color palette of BiFC has been expanded to include a variety of hue-shifted variants including: CFP (80), YFP (80, 81), RFP (68, 82), and far red FPs (83). These developments have allowed for simultaneous imaging of more than one protein-protein interaction event in live cells (84, 85).

1.5.3 Single FP-based biosensors

This class of genetically encoded FP-based biosensors utilizes a single FP that produces an optical response to change in the concentration of an analyte of interest or some other change that affects the fluorophore microenvironment (86). The optical response is typically an intensiometric change in FP emission, though some examples of ratiometric changes in FP excitation or emission profile have been reported (86, 87).

Single FP-based biosensors can be categorized into two classes. The first class are those with endogenous biosensing ability (86) (Figure 1.10A). That is, for the first class the FPs themselves are the molecular recognition element and thus an exogenously fused molecular recognition element is not required. For example some FPs have been developed to show spectral changes in response to pH changes (88-94), halides (95, 96), and even intracellular redox potential (97-99).

The second class of single FP-based biosensors are those in which the FP is fused to an exogenous molecular recognition element capable of sensing the analyte of interest (86) (Figure 1.10B). The molecular recognition event should induce, through conformational change, a modulation in the FP structure or chromophore microenvironment that eventually will be translated to a change in spectral output (86). The FP variants used in this subclass of biosensors should be capable of tolerating protein insertion and circular permutation at certain locations (86). Circular permutation is the process of genetically joining the original N- and C-termini of a protein accompanied with the creation of new N- and C-termini elsewhere in the protein structure. In the case of FPs, circular permutation is typically used to create variants with new termini in the vicinity of the chromophore (86). The molecular recognition domain(s) can then be

attached to these new termini. This design has been applied for the biosensing of Ca^{+2} (87, 100-103), Zn^{+2} (104), cGMP (105), and ATP:ADP ratio (106).

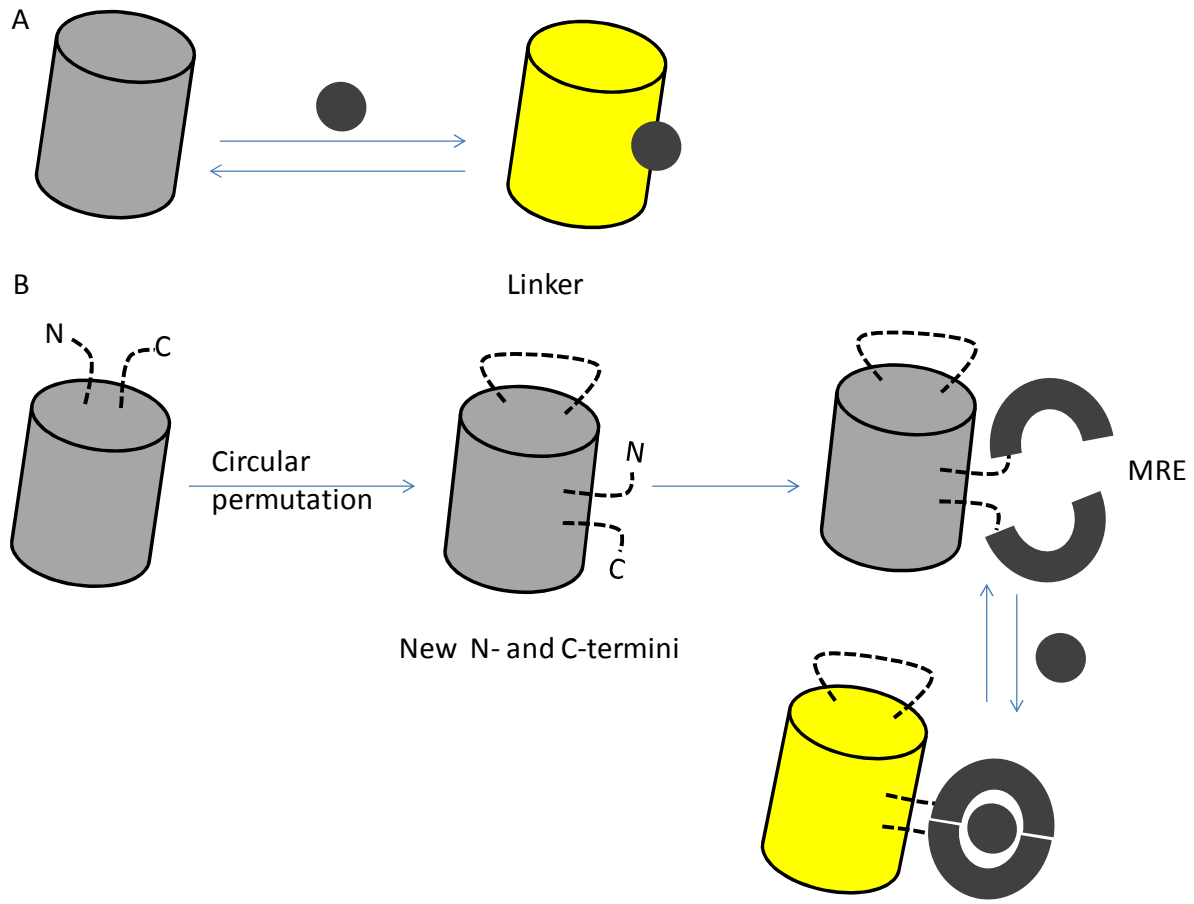

Figure 1.10. Schematic representation of single FP-based biosensor designs. (A) Single FP-based biosensor with endogenous biosensing capabalities. The fluorescence emission of the FP changes in response to analyte such as Cl^- and H^+. (B) Single FP-based biosensor with exogenous molecular recognition element, FP is first subjected to circular permutation in which the original N- and C-termini are joined by a linker and new termini are created in the vicinity of the chromophore. The new termini are used for MRE fusion, following the rationale that conformational changes in response to the analyte will perturb the microenvironment around the chromophore and hence a change in spectral properties will be observed.

1.6 RESEARCH OBJECTIVES

In this dissertation I present several different applications of using the different strategies of FP-based biosensors. The second and third chapters describe applications of two different FRET-based methodologies. The fourth chapter describes an application of single FP-based biosensor fused with an exogenous molecular recognition element.

In the second chapter I describe the modification of a screening methodology for optimizing FRET-based biosensors for post-translational modification that our lab had reported earlier (107). This modified screening methodology was applied to the optimization for a previously reported FRET-based biosensor for protein kinase B and to the development of a new FRET-based biosensor for cyclin-dependent kinase 1/cyclin B activity.

The third chapter deals with the development of a matrix metalloproteinase-2 FRET-based biosensor for the final goal of its utilization in revealing potential MMP2 intracellular roles in cardiac muscle cells. The design of biosensor, *in vitro* validation experiments, and kinetic characterization studies will be discussed.

In the fourth chapter, development of homologues of different hue for the earlier reported single FP-based hydrogen peroxide biosensor (known as HyPer) will be demonstrated.

Concluding remarks and suggestions of future directions will be described in the fifth and final chapter.

Chapter 2

DEVELOPMENT AND OPTIMIZATION OF FRET BASED BIOSENSORS FOR PROTEIN KINASE B AND CYCLIN B1-CYCLIN DEPENDENT KINASE 1

2.1 INTRODUCTION

Förster (or fluorescence) resonance energy transfer (or simply FRET) is the process of non-radiative energy transfer from a blue shifted donor fluorophore to a neighboring red shifted acceptor chromophore. If the acceptor chromophore is also a fluorophore, it will exhibit fluorescence at its characteristic emission wavelength without being directly excited at its characteristic excitation wavelength (108). Three main factors control the efficiency of FRET namely; spectral overlap between donor emission and acceptor absorption, the distance between the donor and acceptor molecules, and finally the relative dipole orientation between them (42, 109).

Aequorea green fluorescent protein (GFP) and homologous fluorescent proteins (FPs) from other marine organisms have been engineered to absorb and fluoresce at a wide variety of wavelengths ranging from the blue to far red regions of the visible spectrum. The availability of these various colours of FP has enabled researchers to apply the FRET phenomenon to intracellular biosensing applications. This has been made possible by the fact that FPs are genetically encoded so that, contrary to other fluorescent probes like synthetic dyes and quantum dots, they can be introduced to the cells in non-invasive manner by simple molecular biology procedures (42, 43). The design of FP FRET-based biosensors relies on the inclusion of molecular recognition element(s) between FRET pairs of FPs, where the former's response to a biological molecule or a triggered cellular event leads to a conformational change modifying the distance and/or dipole orientation between the latter. This distance or orientation change causes a modulation of FRET efficiency which is experimentally observed as a change in emission ratio (42, 43). A design of particular interest to the work described here is the inclusion of an enzyme substrate domain fused to a post-translationally modified peptide-binding domain between the

FRET pair. Such a design can be employed to detect the activity of enzymes, such as kinases and lysine methyltransferases, which catalyze post-translational modifications of specific amino acids in the context of a peptide substrate. When the enzyme activity of interest modifies the substrate domain, the modified peptide will bind to the binding domain, causing a large conformational change and hence a change in FRET (42, 43).

Since the first report of an intracellular FP FRET-based biosensor 16 years ago (47), numerous research groups have developed a large number of FP FRET-based biosensors for various biological molecules and events. Nonetheless, developing these biosensors remains a difficult and laborious undertaking, owing to the fact that even with good structural information, outcomes in terms of performance are hard to predict. Accordingly, essentially all of the work to improve the performance of these biosensors depends on trial and error. An illustrative example of this problem is a study in which 176 FRET-based glutamate biosensors, with variation only in the interdomain linkers, had to be constructed and tested individually to come up with just one variant with a useful FRET change (55). Despite the fact that FP FRET-based biosensor optimization tends to be highly tedious, the effort has been justified by the high impact of useful sensors that can provide unprecedented insight into spatial and temporal dynamics of biochemical processes as they happen in live cells. Technological developments that accelerate the development of useful FRET-based biosensors have the potential to both shorten the investment of effort required to optimize new sensors, and also to attract a wider range of researchers to attempt the development of new biosensors customized for their particular applications.

To date, there have been a few reports of improved strategies for accelerating the process of FP FRET-based biosensor optimizaiton. For example, one study attempted to develop an

optimized backbone for FRET biosensors by first optimizing donor and acceptor FPs separately. They focussed on cyan and yellow variants by trying different combinations or previously reported variants, and eventually came to the conclusion that enhanced CFP and Turquoise served as the best donors with the use of YPet as the best acceptor. They also used a mathematical model to design a very long linker (116 amino acids) that would eliminate dimerization of FRET pair rendering the FRET efficiency mostly dependant on the distance between the FRET pair (110). Although the optimized backbone succeeded in improving the FRET response of previously published biosensors of ERK, PKA, Ras and RacI, it did not show a reasonable improvement in biosensors of Akt and PKCβ (110). The authors attributed the mixed results to lower phosphorylation efficiency (i.e., lower efficiency of modification of the substrate part of the biosensor). However, one problem with this explanation is that the authors adopted substrate peptides from previously reported consensus sequences that had been already used in the construction of successful biosensors. A more likely explanation of the mixed results is that no one proposed model can be universally applied for all biosensor designs, and optimization must be done on a case-by-case basis.

In another interesting effort to accelerate the rate of FRET biosensor development, the authors proposed a semi-automated FRET-based biosensor optimization of two calmodulin-binding proteins in mammalian cells by the combined use of plasmid DNA arrays and fluorescence microscopic imaging (111). The plasmid DNA arrays were used to achieve the reverse transfection of mammalian cells on the array, such that they expressed the biosensor variant of interest (111). This approach offered the advantage of screening the biosensor variants in the same biological system that it will finally be applied to. One disadvantage of this approach

is that the throughput was limited by individual plasmid preparation of different clones and the transfection efficiency of the mammalian cells (111).

Our lab had previously reported our own screening strategy for rapid optimization of FP FRET-based biosensors. In this strategy the biosensor library is expressed in colonies of *E. coli* along with an inducible version of the enzyme that catalyzes the post-translational modification. By imaging of the colonies before and after induction of the expression of the modifying enzyme, biosensors with greater response can be identified. Both the biosensor and enzyme are expressed from a single expression vector. This approach enabled us to improve the dynamic range of previously reported biosensor of histone H3 lysine 27 methyltransferase activity (107). We note that the co-transfection of a biosensor library with a second plasmid encoding the enzyme activity of interest would be an alternative approach to achieving the same goal. Indeed, such an approach was adopted by Schifferer *et al*. in developing an RNA aptamer FRET-based biosensor (112). Nevertheless, we believe that our approach has distinct advantages such as the lack of need for multiple transformations and having more than one resistance marker. This simplifies the experimental procedure and enhances the overall throughput due to higher transformation efficiency. In this work we report a modified version of this strategy and apply it to the optimization of a previously reported protein kinase B (PKB) (also known as Akt) biosensor and to the development of a new cyclin B1-cyclin dependent kinase 1 (CDK1) biosensor.

2.2 MATERIALS AND METHODS

2.2.1 General Materials and Methods

Unless otherwise indicated all chemicals and reagents were purchased from Fisher Scientific (Ottawa, ON, Canada) or Sigma-Aldrich Canada (Oakville, ON, Canada). All primers

were purchased from Integrated DNA Technologies (Coralville, IA, USA). Polymerase chain reactions (PCRs) were performed using either Taq DNA polymerase (Invitrogen, Burlington, ON, Canada) or Pfu DNA polymerase (Fermentas, Burlington, ON, Canada) according to the provided manufacturer's protocols. Deoxyribonucleotide triphosphate (dNTP) solutions used in PCRs were purchased from Invitogen. Fast Digest Endonucleases (Fermentas, Burlington, ON, Canada) were used for restriction digests of all PCR products and plasmids. PCR products and products of restriction digestion were purified by gel electrophoresis and extracted using GeneJet gel extraction kit (Fermentas, Burlington, ON, Canada). DNA ligation was performed using T4 DNA ligase (Invitrogen, Burlington, ON, Canada). *E. coli* ElectroMax DH10B ^{TM} (Invitrogen, Burlington, ON, Canada) was used for transformation and subsequent plasmid propagation. Dye terminator cycle sequencing using BigDye (Applied Biosystems, Burlington, ON, Canada) was used to confirm the complete DNA sequencing of all fusion constructs. Sequencing reactions were analyzed at University of Alberta Molecular Service Unit (MBSU).

2.2.2 Construction of the PKB biosensor library

The pUADE (University of Alberta Dual Expression plasmid) dual expression plasmid was previously constructed in our lab (107). This plasmid can be used to express one gene under control of the tac promoter (P_{tac}) and another gene under control of the araBAD promoter (P_{BAD}). The pUADE plasmid was modified downstream of the P_{tac} promoter to include restriction sites compatible with insertion of the genes for constitutively active PKB and its reporter BKAR. Consequently, a DNA fragment encoding *AvrII*-linker-*SalI*-Linker-*SbfI*-Linker-*EagI* has been amplified by PCR using primers YLS-FRET-FD and YLS-FRET-BK, digested with *AvrII* and *EagI* restriction enzymes and ligated into similarly digested pUADE. An *Xho1* site and a *HindIII* site were already present in the plasmid at the 5' and 3' ends of the insertions site, respectively.

Successful ligation of the desired DNA was checked by analytical double digestion. The gene encoding mTFP1 was PCR amplified, double digested with *XhoI* and *AvrII* restriction enzymes and ligated into this modified pUADE after it had been similarly digested. Site-directed mutagenesis by overlap-extension PCR was used to remove an undesirable *XhoI* restriction site in the phosphoserine/threonine binding domain FHA2. Two PCR reactions were carried out using the pRSET B-BKAR as a template (Addgene, Plasmid 14877). The first reaction used a forward primer carrying *AvrII* and a reverse primer that mismatch annealed to the Xho1 site and carried a silent mutation to destroy the restriction site. The second reaction used a reverse primer carrying a *SalI* restriction site and a forward primer that was the reverse complement of the reverse primer in the first reaction. The two resulting PCR products were gel purified, mixed in equal proportions, and used as the template for a third PCR reaction with the *AvrII* and *SalI* containing primers. The resulting PCR product was double digested by *AvrII* and *SalI* and ligated into similarly digested modified pUADE containing mTFP1 as described above. Similar plasmid digestion and ligation steps with appropriately digested PCR product were used to insert the PKB substrate sequence and YFP between *SalI*/*SbfI* and *SbfI*/*HindIII* sites respectively. Finally the gene encoding constitutively active PKB (PKB-T308D, S473D) was PCR amplified from a template of Addgene plasmid 14751 (pcDNA3 backbone). The PCR product was doubly digested with *EcoRI* and *BglII* and ligated downstream of P_{BAD} in the modified pUADE from the last step.

The next step in the library preparation required that we insert a variety of cyan FPs and yellow FPs into the appropriate sites of the biosensor scaffold. Primers for cyan FPs (CFP, TFP, CyPet, cpTFP193, and cpTFP207) were designed to introduce *XhoI* and *AvrII* at the 5' and 3' ends, respectively. Similarly, primers for yellow FPs (YFP, Ypet, mCitrine, cpVenus173) were

designed to introduce an *SbfI* at the 5' end and a stop codon followed by *HindIII* at the 3' end. PCR amplifications were performed individually, and resulting PCR products for members of each group were mixed in equimolar amounts and subjected to double digestion with appropriate enzymes. Following ligation of the cyan FP group into similarly digested modified pUADE, 2 µl were used to transform 50 µl of electrocompetent *E. coli* and the whole reaction mixture was added to 4 ml LB medium containing 0.04% ampicillin and incubated at 37 °C with shaking at 220 rpm for 16 hours followed by plasmid DNA extraction. The extracted plasmid was then appropriately digested and ligated with the similarly digested pool of yellow FPs. The resulting plasmid library with various combinations of CFPs and YFPs, was used to transform competent *E. coli*. Plasmid extraction was performed as described above for insertion of the cyan FP pool. The cDNA encoding the substrate part of BKAR was prepared by overlap PCR amplification using a forward primer appending *SalI* followed by the '218' linker and a reverse primer appending an *SbFI* restriction site. This cDNA was used as the PCR amplification using the same 3' primer and a variety of 5' primers. These different 5' primers encoded for different lengths of linker at the 5' end. The PCR products were mixed in equimolar amounts, double digested, and ligated into the above mentioned biosensor library containing both the cyan pool and yellow pool. The resulting plasmid-based library was designated pUADE-PKB.

2.2.3 Construction of CDK1 biosensor library

Further modification of pUADE was performed to ensure compatibility of the restriction sites with the constitutively active enzyme gene (CDK1, encoded by the CDC28 gene) and its corresponding activity biosensor gene. An *XmaI* site was inserted between the *EcoRI* and *BglII* sites of the P_{tac} multiple cloning site. Polycistronic CDC28-CAK1-CKS1-CLB5 was PCR amplified from GEX6P-1/CDC28-CAK1-CKS1-CLB5 (a kind gift from Professor David Stuart)

using primers that appended *XmaI* and *BglII* sites at 5' and 3' ends, respectively. The resulting PCR product was double digested and ligated into similarly digested pUADE (previously modified to contain the *XmaI* site). Introduction of the cyan FP gene pool was performed as described above. The cDNA for the CDK1 substrate region was constructed by an overlap PCR that left a *KpnI* restriction site at the 3' end. The yellow FP pool was PCR amplified with appropriate primers with *KpnI* and *SbfI* sites at 5' and 3' respectively. Single digestion of both the CDK1 substrate cDNA and the yellow FPs gene pool with *KpnI* was performed. These were then mixed in equimolar proportion and ligated for 1 hour. The ligated product was then used as a template for further PCR amplifications. Specifically, the 3' primer was the *SbfI*-containing primer mentioned above, and the 5' primer was a mixture of primers encoding various lengths of linker and ending in a *SalI* restriction at the 5' end. The resulting PCR products were purified, double digested with *SalI* and *SbfI*, and ligated with similarly digested modified pUADE that already carried the cyan FP library pool. The resulting plasmid-based library was designated pUADE-CDK1.

2.2.4 Primary library screen in colonies

As described above, we had prepared two distinct plasmid-based libraries, pUADE-PKB and pUADE-CDK1, of biosensor variants in dual expression plasmids together with the corresponding enzymes that would catalyze their post-translational modification. *E. coli* was transformed with either pUADE-PKB or pUADE-CDK1, and transformants were plated on LB-agar with 0.04% ampicillin, 1 mM IPTG and 20 mM D-glucose in polystyrene Petri dishes and incubated at 37 °C overnight. The imaging system used for colony screening in our lab has been previously described (113). Briefly, it is composed of a 175 W xenon-arc lamp (Sutter instrument company, Novato, CA) as a source of excitation light; band-pass filters housed in a

filter wheel for the wavelength selection of the excitation light; a bifurcated fibre optic bundle (Newport corporation, Stratford, CT) to guide the filtered excitation light to a compartment with a circular recession to fit a 10 cm diameter Petri dish; a second set of band-pass filters housed in a filter wheel for selection of emission wavelength positioned vertically above the illuminated Petri dish; and a Retiga 1300i 12-bit CCD camera (QImaging, Burnaby,BC) just behind the emission filter wheel to snap pictures of the fluorescent colonies grown in the Petri dish. For FRET imaging using this system, fluorescence images of the untreated plates were acquired in both donor (excitation 420-440 nm; emission 460-500 nm) and acceptor (excitation 420-440 nm; emission 520-550 nm) fluorescence channels. Plates were then sprayed with 1 M L-arabinose solution, left at room temperature for 2 hours and images were acquired again for both the donor and acceptor fluorescence channels. Custom macros running in Image Pro Plus (Media Cybernetics Inc., Silver Spring, MD) were used to process the acquired images and create a spreadsheet showing donor and acceptor intensities for each colony both pre- and post-spray. The spreadsheets were exported to Microsoft Excel where the ratio of emission intensity of acceptor to emission intensity of donor ($I_{Acceptor}/I_{Donor}$) was calculated for each colony pre- and post-spray. The emission ratio change was calculated as $\Delta R/R_{min}$ % and colonies showing the highest ratio changes (typically $\Delta R/R_{min} > 15\%$) were isolated, propagated, and their plasmid DNA extracted and sequenced.

2.2.5 Secondary library screen with purified protein

As a secondary screen of clones identified during the primary colony based screen, each clone was subjected to 2 separate protein expression conditions. In the first condition, the biosensor was co-expressed with constitutively active enzyme and in the second condition the biosensor was expressed alone. The first condition was obtained by inoculating 500 ml Lysogeny

Broth (LB) medium supplemented with 0.04% ampicillin, 1 mM IPTG and 10 mM L-arabinose with a single colony of *E. coli* that had been transformed with pUADE carrying the gene for a specific biosensor variant. The second condition was obtained by inoculating 500 ml LB medium supplemented with 0.04% ampicillin, 1 mM IPTG and 30 mM D-glucose with an identical colony. All cultures were incubated at 37 °C for 24 hours with shaking at 250 rpm (Innova 4330 shaker, New Brunswick Scientific). Cells were harvested by centrifugation at 8000 rpm (Beckmann Rotor centrifuge) and re-suspended in lysis buffer (50 mM sodium phosphate, 300 mM sodium chloride, 10 mM imidazole, pH 7.5) and lysed by a cell disruptor (Constant Systems, Daventry, Northants, UK). Insoluble cell debris was separated by centrifugation at 14000 rpm, and biosensor proteins (carrying an N-terminal His_6 tag) were then purified by Ni-NTA affinity chromatography (Amersham, Amersham, Buckinghamshire, UK) and exchanged into PBS buffer (37 mM NaCl, 10 mM phosphate, 2.7 mM KCl, pH of 7.4) using Amicon Ultra-4 Centrifugal filter units (Millipore) with a molecular weight cut-off of 50 kDa. All protein expressions are done in at least 4 replicates to confirm reproducibility and statistical significance.

2.2.6 Gel electrophoresis and Western blotting

Gel electrophoresis and Western blotting was used to assess protein expression and degree of biosensor phosphorylation of expressed proteins. The concentration of proteins expressed as described above was determined using bicinchoninic acid (BCA) protein assay following the manufacturer's protocol (Pierce). Each of the expressed proteins (1 µg) was subjected to tricine-SDS-polyacrylamide gel electrophoresis as described earlier (114) in two parallel experiments. The first gel was stained with Coomassie Brilliant Blue R-250 and the second gel was subjected to Western blotting. Western Blotting was perfomed via electroblotting the bands on the SDS-polyacrylamide gel into PVDF membrane (Millipore) followed by

blocking the membrane by immersion in 5% bovine serum albumin (BSA) in TTBS Buffer (Tris-buffered saline pH 7.4 containing 0.1% tween-20) overnight at 4 °C. The membrane was then washed and incubated with rabbit anti-phosphoserine/phosphothreonine (pS/pT) polyclonal primary antibody (Life technologies) overnight at 4 °C. The membrane was then washed again and incubated with a horseradish peroxidase (HRP) conjugate of goat anti-rabbit IgG secondary antibody (Life technologies) for 2 hours at 4 °C. Bands were visualized using ECL-chemiluminescence substrate (Pierce) and ImageQuant RT ECL imager (GE Healthcare life sciences).

2.3 RESULTS AND DISCUSSION

2.3.1 Rationale for colony-based screening strategy

Our lab has previously reported a strategy for screening biosensor constructs for improved ratio change in colonies of *E. coli* (107). One of the keys to this strategy is a dual expression system designated as pUADE which can express two different proteins simultaneously under two different promoters (P_{tac} and P_{BAD}) (107). In the initial report of this screening strategy, we reported its application to the optimization of a biosensor for histone lysine methylation. We reasoned that this system could also be used for screening biosensors of kinase activity by cloning genes for a constitutively active kinase and its corresponding biosensor into the two different expression sites in the pUADE dual expression vector (107). We choose to clone the gene for the kinase downstream of the P_{BAD} promoter ensure tight control of its expression as L-arabinose will selectively turn it on and D-glucose will shut it off. The kinase FRET-based biosensor was cloned downstream of the P_{tac} promoter. These biosensors are composed of a FRET pair of fluorescent proteins joined by a kinase-specific substrate sequence bound by a linker to an appropriate phosphoaminoacid-binding domain. Turning on kinase expression with L-arabinose will artificially induce post-translational modification of the reporter and hence the biosensor will exhibit a different emission ratio (attributable to a change in FRET efficiency) relative to the biosensor expressed while the enzymatic expression is shut off by D-glucose as shown in Figure 2.1.

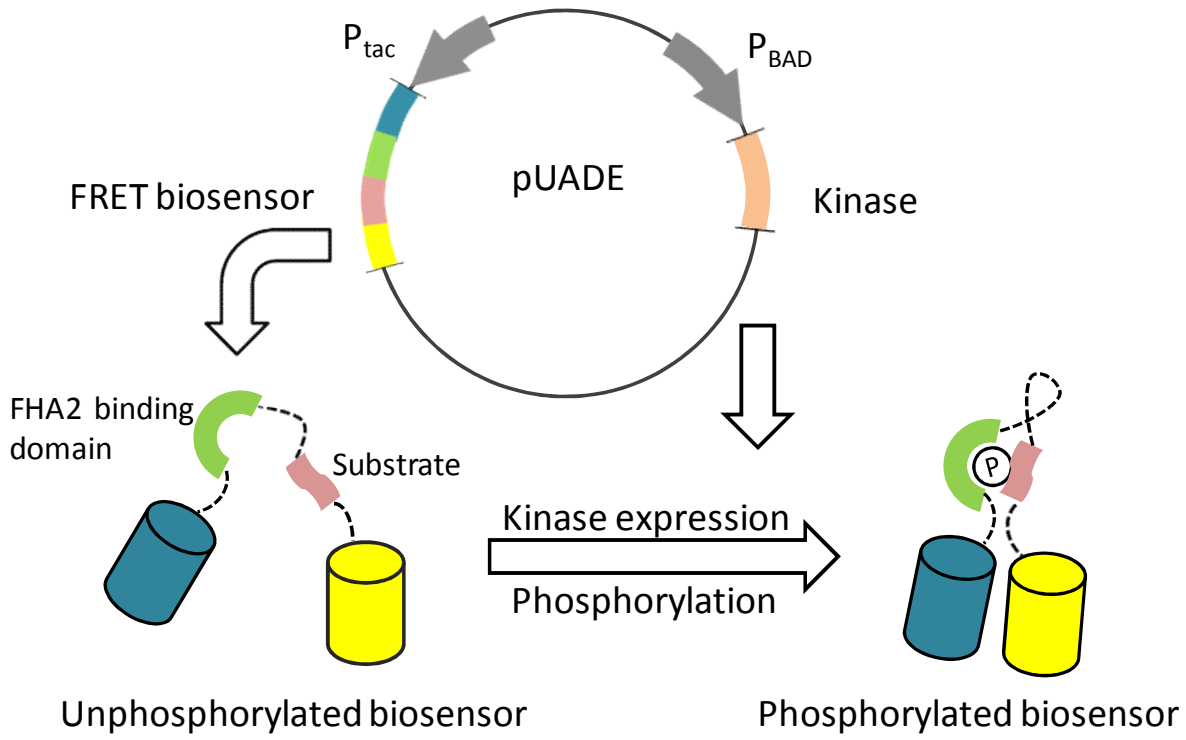

Figure 2.1 A schematic presentation of protein expression system pUADE that contains constitutively kinase gene downstream of L-arabinose-inducible (and D-glucose-repressible) promoter P_{BAD} and kinase biosensor downstream of IPTG-inducible promoter P_{tac}. Activation of P_{BAD} promoter via L-arabinose leads to the expression of the kinase, which in turn phosphorylates the biosensor and hence causes FRET change.

This dual expression strategy has previously enabled in-colony screening for a histone lysine methyltransferase activity biosensor using a replica spotting technique in which single colonies were spotted onto both D-glucose and L-arabinose agar plates in ordered arrays. Both plates were imaged and a comparison of the ratio of donor to acceptor emission channel intensities was performed for all colonies (107). One shortcoming of this previous approach was that the replica spotting was labour intensive and this limited the throughput of the screening system. In the present work we explored a different approach. Specifically, we expressed libraries of biosensors of serine/threonine kinases PKB and Cdk1-Cylin B1 with variations in FRET pair FPs and internal linkers (as shown in Figure 2.2) on D-glucose plates. These plates were imaged, sprayed with L-arabinose, and then imaged a second time. Digital processing of

images acquired pre- and post-spray enabled us to identify the colonies that biosensor clones that exhibited the larges ratio changes (Figure 2.3).

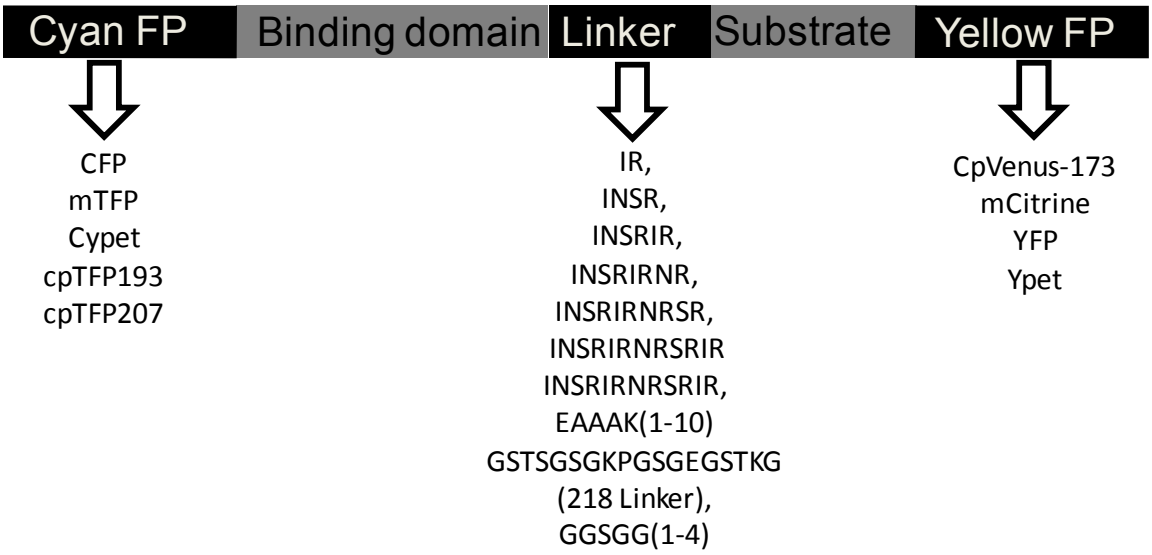

Figure 2.2 An overview of FRET construct library consisting of a pool of cyan FPs (donor), an FHA2 phosphoprotein binding domain, a linker of various lengths and compositions, a kinase substrate peptide, and a pool of yellow FPs (acceptor).

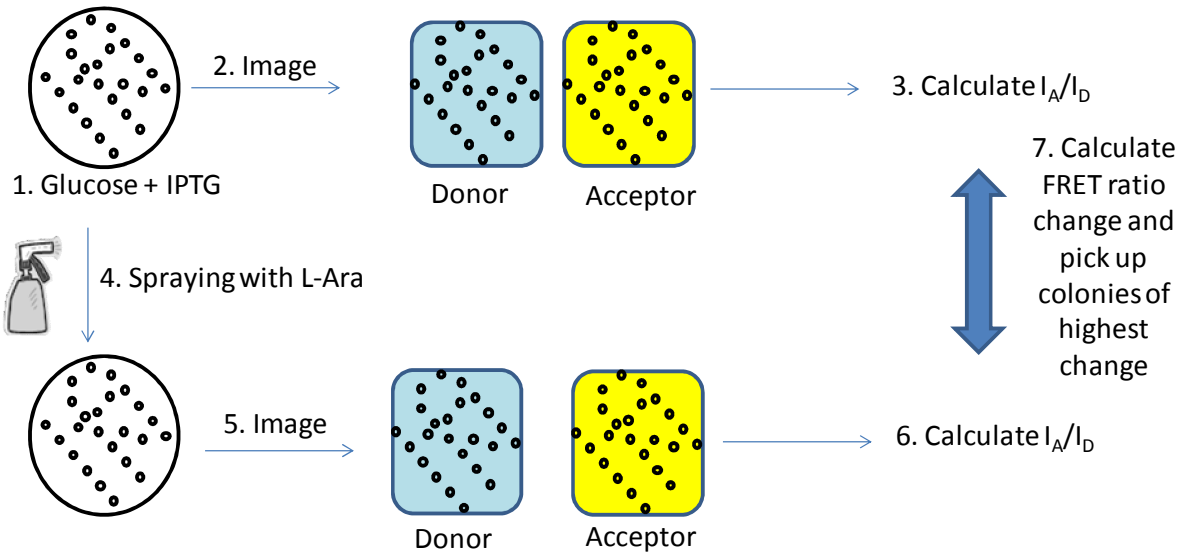

Figure 2.3 Screening methodology used in this work. Colonies of *E. coli* previously transformed with plasmid library are grown on D-glucose/IPTG plates, images are taken on both donor and acceptor channels and hence emission ratios are calculated for each individual colony. Afterwards, plates are sprayed with L-arabinose solution followed by taking images as

previously described. FRET ratio changes are calculated for each colony and colonies with highest changes are picked up and a secondary screen with purified proteins is performed.

2.3.2 Optimization of PKB (Akt) FRET biosensor

The serine-threonine kinase known as Akt or protein kinase B (PKB) is a pivotal member in phosphatidylinositol-3-kinase (PI3K)/Akt signaling pathway. It plays a central role in various cellular processes including cellular proliferation and growth, metabolism, and apoptosis (115). Not coincidentally, PKB itself has been identified as an oncogene that is often highly active in cancer cells (116, 117). Moreover, defects in PKB or upstream and downstream members in its particular signalling pathway, have been identified in various diseases including numerous types of cancers (118) and type 2 diabetes (119). PKB itself is composed of three distinct domains: the N-terminal plecksterin homology (PH) domain; the kinase domain (active site); and the C-terminal regulatory domains (120). Activation of growth factor receptors will lead to the activation of phosphatidylinositol 3-kinase which produces phosphatidylinositol 3,4,5-triphosphate at the plasma membrane which in turn will recruit PKB to the membrane due to binding to the PH domain (121-123).

Kunkel *et al*. have reported the development of a PKB activity FRET-based biosensor designated B-kinase activity reporter (BKAR). BKAR was constructed by incorporating the PKB phosphorylation consensus substrate sequence RKKRDRLGTLGI fused to phosphoaminoacid binding domain forkhead-associated domain-2 (FHA2) between mCFP and mYFP. This biosensor gave a 30% ratio change upon phosphorylation (124) and showed phosphorylation specificity for PKB over both PKA and PKC. Later efforts by Gao *et al*. to improve the signal amplitude of BKAR were not fruitful, and they ended up switching their focus to the development of a new biosensor called Akt activity reporter (AktAR). AktAR is based on the

PKB substrate sequence (PRPRSCTWPDPRPEF) fused to phosphoaminoacid binding domain forkhead-associated domain-1 (FHA1) sandwiched between Cerulean and cpVenus-172. AktAR exhibits a 40% increase in emission ratio in serum-starved NIH 3T3 cells upon PDGF stimulation (125). Intrigued by the apparent challenge of improving the response of BKAR, we chose to focus our efforts on trying to improve its dynamic range as a test case for our screening strategy.

One of the primary challenges of our colony based biosensor optimization strategy is to identify a constitutively active kinase that has the required specificity and can fold correctly when expressed in *E. coli*. Following translocation of PKB to the plasma membrane, the enzyme is activated via two sequential phosphorylation steps on Thr308 and Ser473 (126-129). Mutation of both PKB phosphorylation sites to aspartic acid has been shown to render PKB constitutively active (130, 131). Presumably, aspartic acid is acting as a mimic of the phosphorthreonine/serine. We used the gene of double aspartic acid mutant of bovine PKB1 (*B. taurus*) as a source of constitutively active PKB and we cloned it downstream of P_{BAD} promoter.

We constructed a library of BKAR variants composed of 5 different cyan FPs, 22 different internal linkers, and 4 different yellow FPs. Overall, there were 5*22*4 = 440 different variants in this library. The internal linkers chosen are a combination of flexible and rigid linkers. Flexible linkers adopted are either tandem repeats of GGSGG that already present in BKAR (124) or linkers of different sizes (2,8,6,8,10,14 and 20 amino acids) reported by Ibraheem *et al* (107). Rigid linkers utilized are tandem repeats of previously reported EAAAK sequence (132).

It is noteworthy to indicate that 2 of cyan FPs used in this study are new and have not been reported in literature; which are cpTFP193 and cpTFP207. Their spectral properties (credit to Dr. Hiofan Hoi) are summarized in table 2.1

FPs	Wavelength of maximum absorbance	Wavelength of maximum emmision	Extinction coefficient ($mM^{-1}cm^{-1}$)	Φ
cpTFP193	465	491	55	0.59
cpTFP207	465	491	55	0.59

Table 2.1 Spectral properties of cpTFP193 and cpTFP207.

Expression in *E. coli* and image based screening revealed a wide range of biosensor responses. Colonies showing the highest ratio changes (all those with >15% change) were isolated from four different experiments (each experiment had 4 plates), sequenced and the purified proteins of the selected sequences were subjected to our secondary screen. Sequencing of the top variants that were found multiple times revealed that all of them contained the mTFP1-YFP FRET pair, and differed only in the composition of the middle linkers. Although it has been generally accepted that dimerization-prone FPs pairs such as CyPet/YPet and ECFP/YPet generally give superior performance in FRET-based sensors, the mTFP1-YFP FRET pair identified here is not expected to exhibit any tendency for the FPs to dimerize. The clone that showed the highest FRET ratio change (ΔR/R% = 40.9%) carried the '218' internal linker. The other 3 variants were found to carry the $(GGSGG)_2$, $(EAAAK)_3$ and IR middle linkers and exhibited ratio changes of 30.1%, 22.7% and 22.7%, respectively (Figure 2.4).

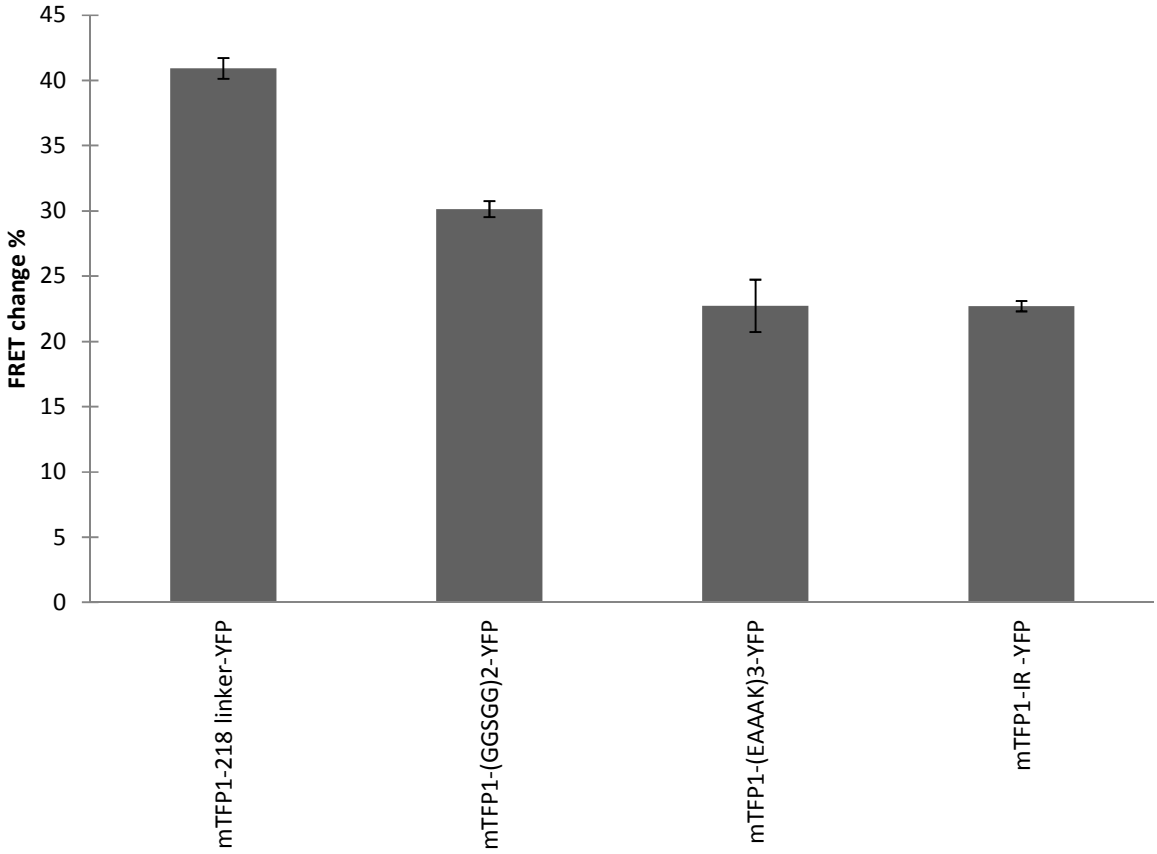

Figure 2.4 Candidates with the highest FRET ratio change of the screened library of PKB biosensors. Each candidate was grown individually under both kinase inducing and repressing conditions, $I_{Acceptor}/I_{Donor}$ were calculated and ΔR/R % were represented with SD (n=4).

The '218' linker is an 18 amino acid linker composed of the sequence (GSTSGSGKPGSGEGSTKG) and was originally designed in such a way to offer both conformational flexibility and resistance to proteolysis by most proteolytic enzymes (133). It is notable that the $(GGSGG)_2$ middle linker clone is very similar to the linker in the original BKAR biosensor. Accordingly, it is not surprising that the $(GGSGG)_2$ variant exhibited a similar emission spectrum and response to that of BKAR. Specifically, the unphosphorylated state is the one that exhibits higher FRET (high acceptor signal) and the phosphorylated state is the one that exhibited lower FRET (low acceptor signal) (Figure 2.5B). Moreover the ratio change of the $(GGSGG)_2$ clone is very similar to that reported with BKAR. In contrast, the variant with the

'218' middle linker clone showed the opposite FRET change profile. That is, the unphosphorylated state was the one with lower FRET efficiency and the FRET efficiency was enhanced significantly upon phosphorylation (Figure 2.5A). This increase in FRET efficiency upon phosphorylation is consistent with the expected mechanism of FRET-based biosensors of this type. That is, the middle domain is expected to become more compact upon modification and this brings the FPs into closer proximity, increasing the FRET efficiency.

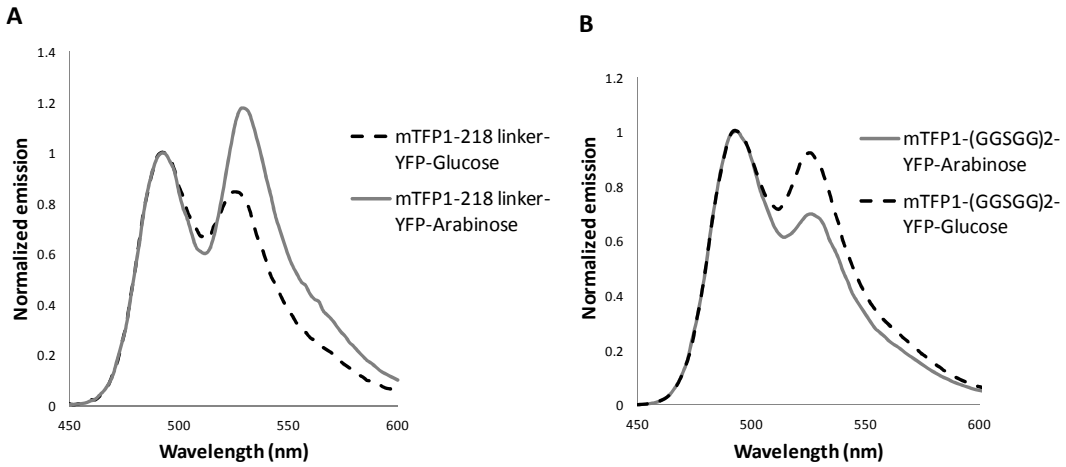

Figure 2.5 Emission spectra of the BKAR variants with the '218' and $(GGSGG)_2$ internal linkers. Emission spectra were measured for proteins expressed under kinase inducing (L-arabinose) and repressing (D-glucose) conditions, All spectra are taken at $\lambda_{excitation}$ of 430 nm and normalized with respect to donor $\lambda_{emission}$. **(A)** An increase in FRET is manifested as an increase in yellow fluorescence signal of '218' linker biosensor upon phosphorylation (presence of L-arabinose). **(B)** A loss of FRET efficiency is manifested as a decrease in yellow fluorescence signal of $(GGSGG)_2$ linker biosensor upon phosphorylation.

To confirm that the change in emission ratio for the '218' variant was due to phosphorylation of the PKB substrate sequence and that constitutively active PKB is indeed expressed and active in the presence of L-arabinose, we performed SDS-PAGE and an anti-phosphothreonine Western blot for the proteins expressed under both repressing (presence of D-glucose) and inducing (presence of L-arabinose) conditions. Coomassie staining of an SDS-PAGE gel showed a band corresponding to the '218' biosensor (expected MW 72 kDa) in both

D-glucose and L-arabinose conditions. In the lane for the protein expressed in the presence of L-arabinsose we observed an extra band for constitutively active PKB enzyme (expected MW 54 kDa). The PKB enzyme contains an N-terminal His_6 tag so co-purifies with the biosensor during Ni-NTA affinity purification. Western blot using an anti-phosphothreonine antibody confirmed the phosphorylation of the biosensor under expression with L-arabinose.

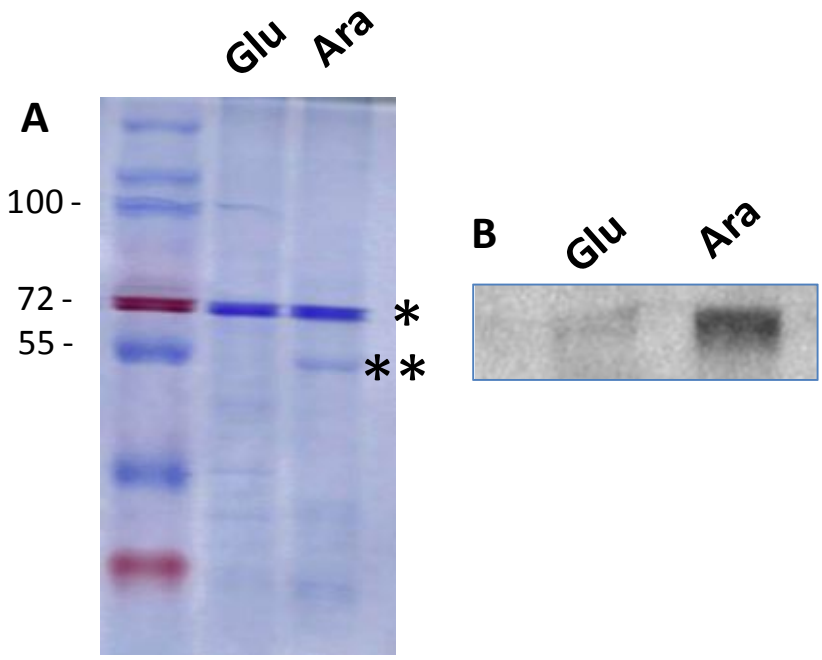

Figure 2.6 Confirmation of enzyme expression and functionality. **(A)** Coomassie blue stained SDS-PAGE of proteins expressed under different induction conditions: enzyme repressing (D-glucose, left lane) and inducing (L-arabinose, right lane); * indicates biosensor and ** indicates enzyme band. **(B)** Western Blot using anti-phosphothreonine antibodies for biosensor expressed under L-arabinose (left lane) and under D-glucose (right lane).

2.3.3 Optimization of a cyclin B1-CDK1 FRET biosensor

The process of mitosis has long been known to be triggered by the activation and nuclear translocation of cyclin B1-associated kinases, the most important of which is cyclin B1-CDK1. Once activated, cyclin B1-CDK1 can phosphorylate a broad spectrum of substrates involved in various steps in mitosis like mitotic spindle generation, chromosome condensation and nuclear envelope breakdown (134-136). Nevertheless, the detailed mechanism of operation and temporal coordination of the various tasks performed by cyclin B1-CDK1 is still unclear. A FRET-based biosensor of CDK1 would greatly facilitate efforts to investigate the spatial and temporal localization of CDK1 activity during mitosis. There is currently only one FP FRET-based biosensor that had been reported for cyclin B1-CDK1 (137, 138). The existing biosensor is composed of an autophosphorylation substrate peptide site from human cyclin B1 (PEPILVDTSSPSPMET) fused to polo-box phosphoamino acid binding domain sandwiched between the mCerulean and YPet FRET pair (137, 138). This biosensor showed a relatively small change in emission ratio of about 10-15% upon cyclin B-CDK1 activation indicated by nuclear envelope breakdown (137, 138). We initially tried to work with the published biosensor design to try and improve its ratio change upon phosphorylation. Nevertheless we were unable to achieve functional expression in *E. coli*. We attribute this failure to the improper folding of the polo-box domain in *E. coli*. Hence we decided to substitute the polo-box domain with the FHA2 domain already used in the earlier section of this chapter and we kept that same substrate (PEPILVDTSSPSPMET) from the earlier cyclin B-CDK1 biosensor in our design.

To apply our colony based screening protocol, we also required a recombinant continuatively active CDK1 that can be expressed, fold well, and function well, in *E. coli*. A literature search led us to Saccharomyces cerevisiae rCdc28–Clb5 (Cyclin B-CDK1 analogue in

S. cerevisiae) from pGEX6P-1/CDC28–CAK1–CKS1–CLB5 plasmid. Expression of active CDK1 requires expression of multiple genes including the Cdc28 kinase itself, its activating Cak1 kinase, the Cks1 subunit, and Clb5 S-phase cyclin in one polycistronic unit that was constructed by Tak *et al*. (139). Consequently, we cloned the complete polycistronic gene downstream of P_{BAD} promoter while we cloned library of different biosensors downstream of the P_{tac} promoter. The biosensor library was similar in design to that discussed in earlier section (as in Figure 1.2).

Application of the colony based screening procedure led to the identification of several variants that showed high emission ratio changes. Each of these variants was isolated individually and propagated under both enzyme inducing and repressing conditions and their percent ratio change determined (Figure 1.7). DNA sequencing of that the biosensor with the highest ratio change (67.0 ± 2.1%) was composed of the mTFP1-YFP FRET pair with $(GGSGG)_2$ as the middle linker between FHA2 and substrate sequence.

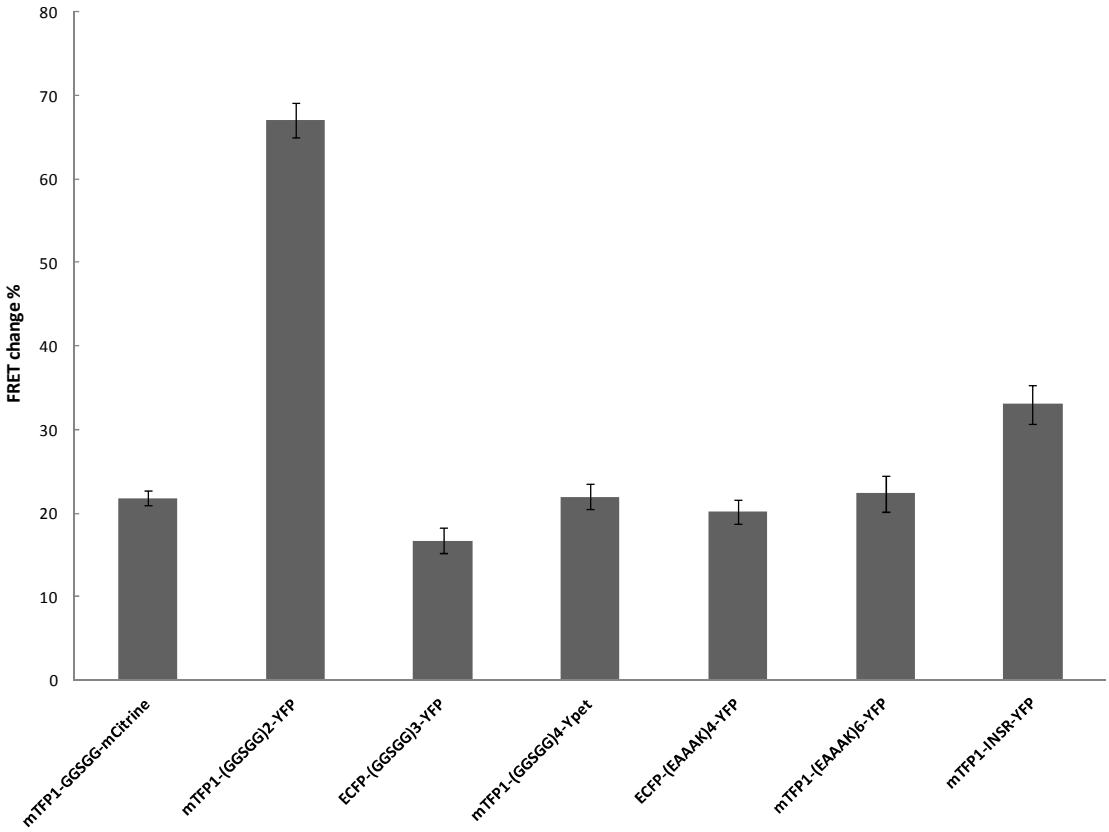

Figure 2.7 Variants with the highest FRET ratio change of the screened library of cyclin B1-CDK1 biosensors. Each candidate was grown individually under both kinase inducing and repressing conditions and ΔR/R% was determined for the purified proteins. Error bars represent standard deviation (n=4).

As with the PKB biosensors, we needed to confirm that the observed high FRET change for the $(GGSGG)_2$ variant was due to phosphorylation post-translational modification. Accordingly, we performed both SDS-PAGE and Western blotting for the $(GGSGG)_2$ proteins expressed in the presence of L-arabinose or D-glucose to either induce or repress kinase expression, respectively.

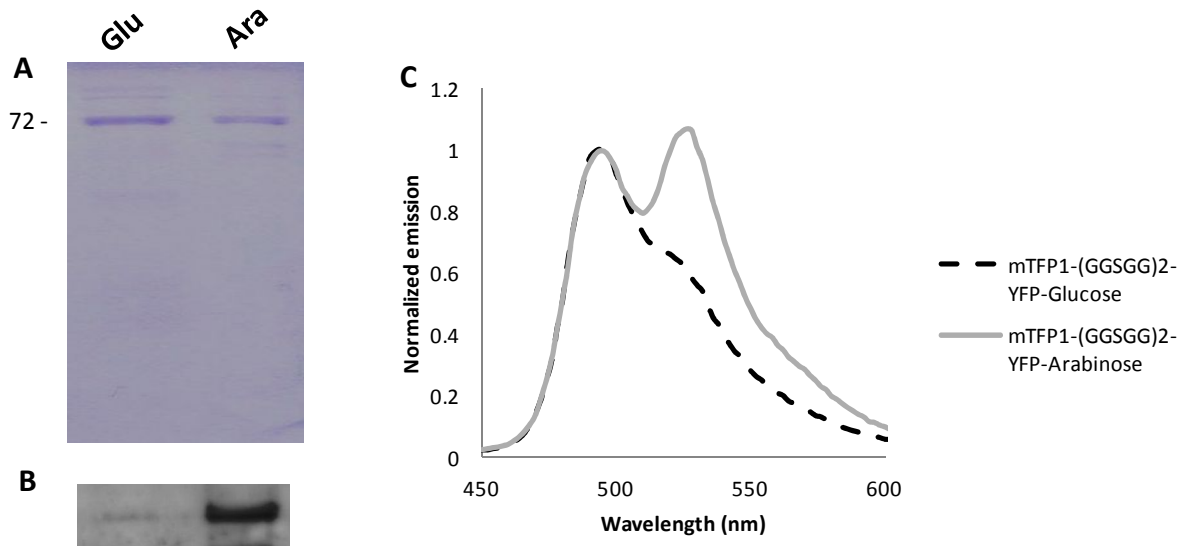

Figure 2.8. Confirmation that the FRET change is a consequence of phosphorylation. (A) Coomassie blue stained SDS-PAGE gel of CDK1 biosensor mTFP1-$(GGSGG)_2$-YFP expressed with D-glucose (enzyme repressive; left panel) or L-arabinose (enzyme inducing; right panel). (B) Western blot of the same biosensor expressed with D-glucose (left panel) or L-arabinose (right panel) using anti-phosphoserine primary antibody. (C) Emission spectra of the same biosensor under kinase inducing (L-arabinose) and repressing (D-glucose) conditions, all spectra are taken at $\lambda_{excitation}$ of 430 nm and normalized with respect to donor $\lambda_{emission}$

Indeed, Coomassie blue staining of one of the replicate gels of the $(GGSGG)_2$ variant (Figure 1.8C) expressed under both kinase repressing and inducing conditions showed a single major band at the expected molecular weight of the biosensor (Figure 1.8A). Moreover, a Western blot of the same protein samples on a replicate gel using anti-phosphoserine primary antibody unequivocally revealed that the FRET change is due to phosphorylation of the biosensor (Figure 1.8C)

2.4 CONCLUSION

Despite the extensive use of FP FRET-based biosensors by many researchers and extensive efforts to optimize such biosensors for high ratio change, the typical strategies employed are extremely labour intensive and almost entirely empirical. Consequently, our lab had been motivated to develop a colony-based screening technique for rapid identification of optimum enzyme biosensors. This strategy relies on a dual expression vector that can express two proteins under two different promoters which enabled us to subject the same colonies to two different scenarios, one with expressing the biosensor alone and one with expressing the active enzyme with the biosensor. By digitally comparing between the images of the same colonies under these two different conditions, we can identify the colony and hence the biosensor with the highest FRET change which will enable us to efficiently screen large libraries of different variants.

In this work we reported a modified version of our previously reported methodology and exploited it for the optimization of kinase activity biosensors. Specifically, we applied the method to optimize biosensors for PKB (Akt) and cyclin B-CDK-1 by screening libraries of different FRET pairs and middle linkers. We successfully improved the previously reported BKAR sensor by improving the ratio change upon phosphorylation from 30% to 40%. In addition we dramatically improved the performance of a cyclin B1-CDK1 biosensor by increasing the ratio change upon phosphorylation from ~10-15% to 67%.

CHAPTER 3

DESIGN AND CONSTRUCTION OF FRET BASED BIOSENSOR FOR MATRIX-METALLOPROTEINASE-2

3.1 INTRODUCTION

Proteases are implicated in almost all biological pathways and networks, and their misregulation is involved in a broad range of diseases, including inflammation, neurodegeneration, cancer, and many cardiovascular disorders (140). They are broadly categorized on the basis of their catalytic mechanisms, and further classified into families based on their tertiary structure and active site residues (141). There are five main classes of proteases: metalloproteinases, serine proteases, cysteine proteases, threonine proteases and aspartic acid proteases (140). Matrix metalloproteinases (MMPs) are a family of zinc-dependent endopeptidases best known for their capacity of proteolyzing extracellular matrix proteins. However, there is mounting evidence that MMPs can also target a growing list of non-extracellular matrix substrates both outside and inside the cell (142). MMP-2 is ubiquitously expressed in cardiomyocytes (heart muscle cells), and is initially synthesized as a 72 kDa zymogen that can be activated by proteolytic removal of the propeptide domain to produce the catalytically active 64 kDa form of MMP-2 (142). However, it can also be activated intracellularly by post-translational modifications including S-glutathiolation and dephosphorylation (142). When activated in cardiomyocytes, MMP-2 specifically proteolyzes certain sarcomeric and cytoskeletal proteins, including troponin I (TnI), myosin light chain-1, α-actinin, and titin, and contributes to acute loss of myocardial contractile function (142).

Fluorescent proteins (FPs) are widely used for investigating intracellular localization and function of proteins. Relative to other types of fluorophores, FPs are particularly well suited for such applications since they are proteins themselves, and as such they can be genetically encoded and transcribed and translated in situ. The utility of the naturally occurring FPs has been dramatically increased by the efforts of protein engineers who have developed FPs with different hues and photophysical properties. Furthermore, FPs can be engineered to be active biosensors

of enzyme activities by taking advantage of the modulation of Förster (also known as fluorescence) resonance energy transfer (FRET) between two FPs with different fluorescence hues (42). This FRET-based biosensing strategy is of particular usefulness when applied to proteolytic enzymes. Proteolytic enzymes were some of the first enzymes to be probed by the earliest examples of FP FRET based biosensors but they continue to be widely used as tool for biological studies and also test new FRET pairs (143, 144). Probing proteolytic enzymes can be carried out by monitoring the protease-dependent loss of FRET between a donor and an acceptor FP (energy donor and acceptor) that are genetically fused to the N- and C-terminal ends of a peptide substrate. Since they are genetically fused together at a distance that is typically similar to or less than the Förster radius, such constructs typically exhibit a high FRET efficiency prior to cleavage. Following cleavage the two fragments are free to dissociate and FRET is completely lost.

In this chapter we demonstrate the design and validation of FRET-based biosensors for the measurement of intracellular MMP-2 activity, based on the use of troponin I as an MMP-2 substrate.

3.2 MATERIALS AND METHODS

3.2.1 General methods and materials

Unless otherwise indicated all chemicals and reagents were purchased from Fisher Scientific (Ottawa, ON, Canada) or Sigma-Aldrich Canada (Oakville, ON, Canada). All primers were purchased from Integrated DNA Technologies (Coralville, IA, USA). Polymerase chain reactions were performed using either Taq DNA polymerase (Invitrogen, Burlington, ON, Canada) or Pfu DNA polymerase (Fermentas, Burlington, ON, Canada) according to the manufacturer's protocols. Fast Digest Endonucleases (Fermentas, Burlington, ON, Canada) were used for restriction digests of all PCR products and plasmids. PCR products and products of restriction digestion were purified by gel electrophoresis and extracted using GeneJet gel extraction kit (Fermentas). DNA ligation was performed using T4 DNA ligase (Invitrogen). *E. coli* ElectroMax DH10B^{TM} (Invitrogen) was used for transformation and subsequent plasmid propagation. Dye terminator cycle sequencing using BigDye (Applied Biosystems, Burlington, ON, Canada) was used to confirm the complete DNA sequencing of all fusion constructs. Sequencing reactions were analyzed at the University of Alberta Molecular Service Unit. Human recombinant active enzymes including: MMP-2 (66 kDa), MMP-3 (22 kDa), MMP-9 (83 kDa), MMP-13 (52 kDa), calpain-1, and caspase-3 were purchased from Calbiochem (Billerica, MA, USA). Recombinant human TnI in 50 mM Tris pH 7.6 containing 0.5 M NaCl, 0.1 mM DTT and 0.1% (w/v) NaN_3, was a gift from Dr. James Potter (Department of Molecular and Cellular Pharmacology, University of Miami, FL, USA). The following were purchased from the sources indicated: trypsin (Worthington, Lakewood, NJ, USA); OmniMMP® fluorogenic peptide substrate (Enzo Life Sciences, Plymouth Meeting, PA, USA); Precision Plus protein dual color molecular weight standard and Coomassie Brilliant Blue R-250 (Bio-Rad, Hercules, CA, USA).

3.2.2 Construction of the FRET-based biosensors

Potential MMP-2 cleavage sites (motifs) were determined according to the conclusions of Turk *et al.* (145) and Chen *et al.* (146). The consensus substrate sequences were aligned with human cardiac troponin I (TnI, Accession P19429), and the result was restricted to the top 15 sites with more than 60% homology using the SIM Alignment tool **(http://web.expasy.org/sim/)** for protein sequence (Figure 3.1). Based on the putative MMP-2 cleavage motifs in the TnI sequence, we constructed 2 FRET-based biosensors, designated as TnI-1 and TnI-2 (Figure 3.2). A 24 amino acid sequence (TnI-1) and a 17 amino acid sequence (TnI-2) derived from human cardiac TnI were inserted between a FP FRET pair (CyPet and YPet, Figure 3.1). A third sensor (Control) contained the sequence GGSGG IPVSLRSG GGSGG, which has been reported to be a selective substrate for MMP-2 (145).

The CyPet donor FP was amplified by PCR from pCyPet-His (Plasmid 14030, Addgene, Cambridge, MA, USA) using a 5' primer containing an *XhoI* restriction site and a 3' primer with a *BglII* restriction site. The PCR product was purified, digested with *XhoI* and *BglII* and ligated into similarly digested pBAD-His B vector. The acceptor FP was amplified via PCR from pYPet-His (Plasmid 14031, Addgene, Cambridge, MA, USA) using specific primers appending 5' *KpnI* and 3' *HindIII* restriction sites. PCR products were purified, digested with appropriate enzymes and ligated into previously ligated pBAD/His B already containing CyPet from the previous step. Genes encoding potential MMP-2 substrates were prepared by overlap PCR with primers appending *BglII* and *KpnI* at 5' and 3' ends respectively. PCR products were purified, digested with appropriate enzymes and ligated into previously ligated pBAD/His B already containing FRET pair from previous steps.

3.2.3 Protein purification

A single colony was used to inoculate 1 L of Lysogeny Broth (LB) medium supplemented with 0.04% ampicillin. Expression of the His_6-tagged protein was induced by L-arabinose (0.2%), and the culture was incubated at 37 °C for 24 hours with shaking at 250 rpm. Cells were harvested by centrifugation at 9800 g and re-suspended in lysis buffer (50 mM sodium phosphate, 300 mM sodium chloride, 10 mM imidazole, pH 7.5). The cells were lysed by cell disruptor (Constant Systems, Daventry, Northants, UK) and debris was separated by centrifugation at 21000 g. Proteins were then purified by Ni-NTA affinity chromatography (Amersham, Buckinghamshire, UK) and dialyzed into the specific buffer of the enzyme to be tested. The buffer for MMP contained 50 mM Tris pH 7.6, 10 mM $CaCl_2$, and 10 μM $ZnSO_4$. The buffer for calpain contained 20 mM Tris-HCl, 25 mM NaCl, 0.15 mM $CaCl_2$, and 10 mM DTT, pH 7.5. The buffer for caspase contained 100 mM HEPES, 2 mM EDTA, 0.1% CHAPS, and 5 mM DTT, pH 7.6. To determine the concentrations of the biosensor proteins, absorbance at 435 nm was recorded on a DU-800 spectrophotometer (Beckman-Coulter, Mississauga, ON, Canada), and concentrations were calculated using Beer-Lambert's law and the previously reported extinction coefficient for CyPet (ε = 35,000 $M^{-1}cm^{-1}$ (144)).

3.2.4 Efficacy of MMP-2 against the FRET-based biosensors

Recombinant human MMP-2 activity was first tested against a known MMP substrate (Omni MMP®), as a positive control for MMP-2 activity. In order to determine if MMP-2 could

catalyze proteolysis of the constructed biosensors, we incubated each biosensor (1 μM) with or without 10 nM MMP-2, and changes in fluorescence were measured for 4 h at 37°C using a Safire2 plate reader (Tecan, Männedorf, Switzerland). Initial assays were made in 120 μl total volume in black polystyrene half-area plates. Full wavelength scans of the biosensor emission spectrum were presented as fluorescence intensity normalized to CyPet.

3.2.5 Calculation of k_{cat}/K_M

Timecourse assays were used to determine the second order rate constant (k_{cat}/K_M) for proteolysis. The two biosensors that were able to cleave MMP-2 (TnI-2 and Control) were used in serial concentrations from 0.25 - 10 μM and were incubated with 10 nM of MMP-2 at 37 °C in a 96-well plate, in order to determine their k_{cat}/K_M. Excitation wavelength was set to 414 nm and fluorescence emission was collected at 475 nm and 527 nm. Measurements were collected every 2 minutes for 16 hours using a Safire2 plate reader (Tecan, Männedorf, Switzerland). The ratio of fluorescence intensity at 475 nm to that at 527 nm was calculated at each time point. Amounts of product were calibrated and determined using the fluorescence ratio from a given biosensor digested to completion with 10 nM trypsin as a 100% product and fluorescence ratio of the intact biosensor in the buffer (without any protease) as 0% product. Appropriate lag time (about 10 minutes) was used to exclude data prior to 37 °C equilibration. Initial rates were determined at various substrate (biosensor) concentrations and data were directly fit with the Michaelis-Menten equation using SOFTmax Pro 4.8 (Molecular Devices, Sunnyvale, CA). For the Control biosensor (for which $K_M >> [S]$), k_{cat}/K_M was calculated by linear regression of initial rates vs. substrate concentrations.

3.2.6 Specificity of biosensors for MMP-2

To examine the specificity of the biosensors toward MMP-2, a variety of recombinant human matrix metalloproteinases (MMP-3, -9, and -13), as well as other recombinant human proteases (calpain-1 and caspase-3) were tested in parallel. All enzymes used were tested against OmniMMP® peptide to check their activity.

To test the ability of these proteases to degrade troponin I, each enzyme (61 nM) was incubated for 120 min at 37 °C with 4.8 mM recombinant human TnI in 50 mM Tris pH 7.6, 10 mM $CaCl_2$, 0.05% Brij detergent, 10 μM $ZnSO_4$. Samples were diluted in reducing Laemmli buffer containing 6% v/v 2-mercaptoethanol (147) and boiled for 3 minutes. Samples were then run on a 10% SDS-PAGE gel which was then stained with Coomassie blue. The reduction in intensity of the full length 25 kDa TnI band and appearance of lower molecular weight fragments below it indicated TnI degradation. As it has been previously reported that caspase-3 is unable to proteolyse TnI *in vitro* (148), this enzyme was not tested in this preliminary experiment.

After checking if the tested proteases were able to degrade TnI *in vitro*, 10 nM of each enzyme were added into individual wells of a 96-well plate, and mixed with 2 μM of each biosensor in a final volume of 120 μL. The excitation wavelength was set to 414 nm and fluorescence emission was collected at 475 nm and 527 nm. Measurements were collected every 2 minutes for 16 h using a Safire2 plate reader (Tecan, Männedorf, Switzerland). The ratio of fluorescence intensity to 475 nm to that at 527 nm was calculated at each time point, and values were plotted against time.

3.2.7 Stability of the TnI-2 and control biosensor in different pH range

To determine the pH dependence of the fluorescence ratio of TnI-2 and Control biosensors, we measured the emission ratio for each biosensor at a range of pH values. Each biosensor (1 μM) was dispensed into wells of a 96-well plate dark-sided with clear bottom plate (Corning, Tewksbury, MA, USA). Each well contained Britton–Robinson buffer (149) adjusted to a specific pH value in the range from 5-10. Measurements were performed in triplicate. The fluorescence emission from 430-650 nm was measured using 414 nm as the excitation wavelength. Ratios of fluorescence intensity at 475 to 527 were calculated at each pH value and ratios were plotted as a function of pH.

3.2.8 Preparation of vector for expression of TnI-2 biosensor in mammalian cells

In order to express TnI-2 biosensor in mammalian cells for the purpose of live cell imaging, the lentiviral LV-GFP vector (Plasmid 25999, Addgene, Cambridge, MA, USA) was modified and subsequently used for gene expression. To simplify gene cloning into this vector, the *HincII* (blunt end producing) restriction site occurring upstream of the open reading frame was mutated to a *SalI* (sticky end producing) restriction site using QuikChange™ site directed mutagenesis kit (Stratagene, La Jolla, CA, USA). The gene encoding CyPet and the TnI-2 substrate was amplified by PCR from the pBAD/His B vector carrying the whole biosensor construct. The PCR primers appended *SalI* and *BamHI* restriction sites at 5' and 3' ends, respectively. The PCR product was purified, double digested and ligated into similarly digested modified LV-GFP. The gene encoding YPet was amplified from pYPet-His appending *BamHI* and *KpnI* restriction sites at 5' and 3' ends, respectively. The PCR product was purified, double

digested and subsequently ligated into the similarly digested modified LV-CyPet-TnI-2 vector. All constructs were confirmed by DNA sequencing.

3.3 RESULTS AND DISCUSSION

The goal of this study was to develop a sensitive, genetically encoded FRET-based MMP-2 biosensor based on the N-terminus sequence of troponin I, a known intracellular MMP-2 substrate. Having such a FRET-based biosensor would allow us to analyze MMP-2 activity and answer some key questions about the conditions under which MMP-2 is activated and the kinetics of the proteolysis.

Our collaborator, Professor Richard Schulz from the Department of Pharmacology, has previously demonstrated that MMP-2 can degrade troponin I (150), among other sarcomeric proteins, during oxidative-stress conditions such as ischemia-reperfusion injury (151, 152). Unpublished data from Professor Richard Schulz's lab has suggested that MMP-2 can cleave TnI between amino acids 17 to 24, which led us to speculate that early degradation events could occur in the N-terminus of the TnI. This inspired us to choose some potential cleavage sites of MMP-2 present in the N-terminus of troponin I, as the basis for constructing a genetically encoded biosensor of MMP-2 activity (see Figure 3.1). Our choice of the potential sequences was further supported by sequence alignment with previously reported MMP-2 consensus substrate motifs (control motifs) (145) located within the troponin I sequence.

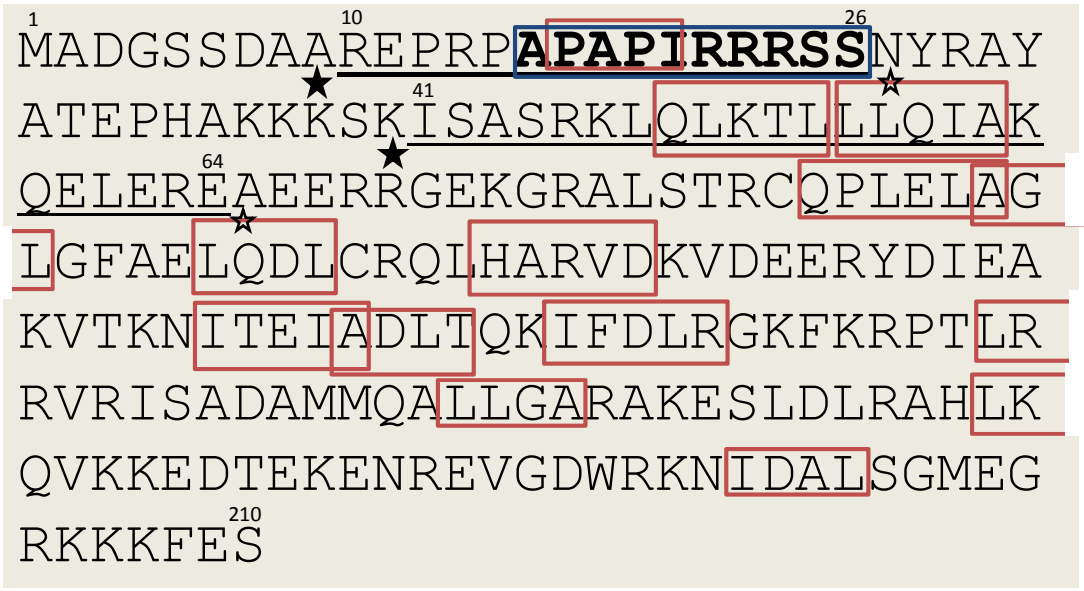

Figure 3.1 TnI sequence showing potential MMP-2 cleavage sites. Indicated on the sequence are putative MMP-2 cleavage motifs in TnI (P19429) (amino acid sequences indicated with red rectangles); a previously confirmed MMP-2 cleavage motif in TnI (indicated with a blue rectangle and bold text); and the localization of the two sequences (underlined) used to prepared potential MMP-2 activity biosensors (black star, fusion point of CyPet; white star, fusion point of YPet).

After these analyses, we came up with two sequences that were promising as MMP-2 substrates. The first sequence extended from residues 41 to 64 (ISASRKLQLKTLLLQIAKQELERE) and was designated TnI-1 (Figure 3.2). The second sequence extended from residues 10 to 26 (REPRPAPAPIRRRSSNY) and was designated TnI-2 (Figure 3.2). It is noteworthy to point out that the former sequence (TnI-1) contains two occurrences (QLKTL and LLQIA) of the consensus motif I/LXXX$_{HY}$ where X$_{HY}$ is a hydrophobic residue. This consensus sequence was argued by Chen *et al.* to be selective for MMP-2 over other MMPs (146). On the other hand the latter sequence (TnI-2) contains the PAPI sequence which corresponds to the consensus motif PXXX$_{HY}$ which been reported to be an optimal substrate for all MMPs (153-155). The TnI-2 sequence also contains the confirmed cleavage site of MMP-2 APIRRRSS (Richard Schulz, unpublished data). We took the sequence

of the previously mentioned control motif (IPVSLRSG) (145) as our positive control (designated Control) for MMP-2 activity (Figure 3.2).

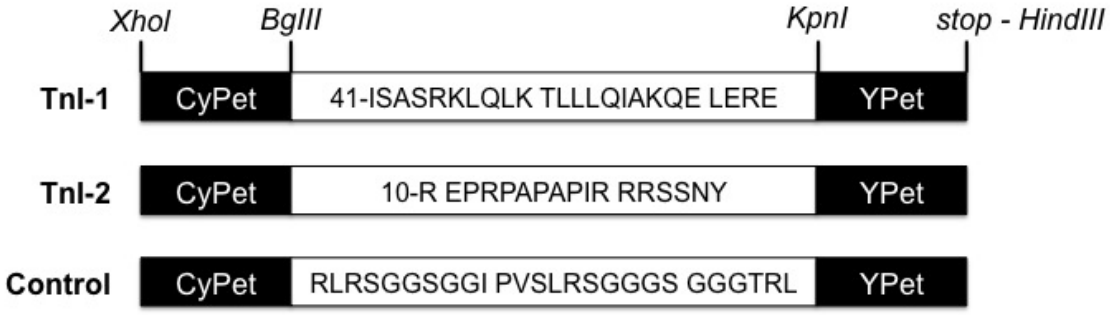

Figure 3.2 An overview of the design of the three different constructs investigated in this study. TnI-1 and TnI-2 contain MMP-2 cleavage sites derived from human cardiac troponin I (TnI), the third construct contained a sequence reported be selective for MMP-2 (*145*).

To construct the FRET biosensor, we chose the CyPet and YPet FRET pair that was engineered through the use of fluorescence activated cell sorting (FACS)-based screening of libraries of CFP and YFP for optimum FRET efficiency. Briefly, a construct containing both CFP and YFP was subjected to multiple evolutionary cycles of random mutagenesis and synthetic DNA shuffling with selection for high FRET efficiency (144). The CyPet and YPet FRET pair typically provides fluorescence ratio changes that are up to six times greater than those provided by CFP and YFP. These large fluorescence changes provide improved contrast and more sensitive detection of proteolytic activity when incorporated into protease biosensors of the type invested in this work (144). In the design used in this work, MMP-2 would cleave the biosensors substrate peptide region, thus separating CyPet and YPet causing a loss of FRET efficiency (Figure 3.3). The FRET change could be monitored by the increase in the emission ratio of CyPet/YPet.

A similar strategy has previously been used to investigate extracellular MMP-2 activity. Yang *et al.* inserted a substrate above mentioned control motif (IPVSLRSG) in a FRET

biosensor based on the CFP and YFP pair (156). In the previous work, the authors did not detect endogenous MMP-2, but rather added high amounts of recombinant MMP-2 to the cell culture medium during live cell imaging. Also, they did not use their biosensor to report on intracellular MMP-2 activity, which is the goal of this study.

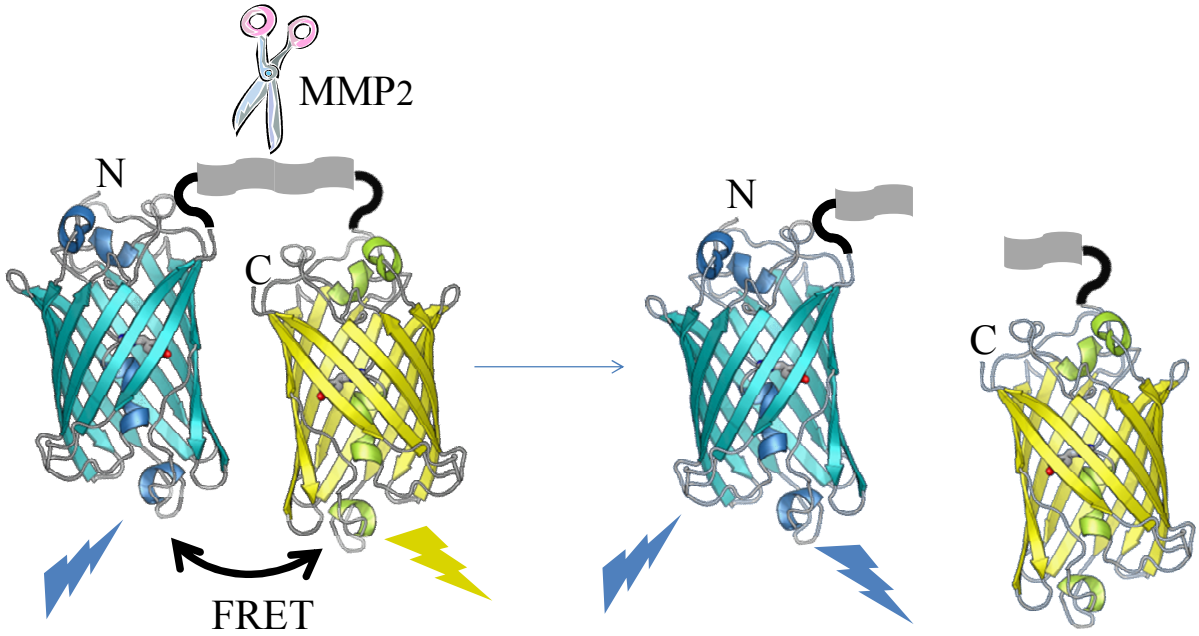

Figure 3.3 Schematic illustration of the MMP-2 biosensor based on FRET from CyPet to YPet.

Following the incubation of the two TnI based biosensors and Control biosensor with 66 kDa MMP-2 a significant increase in CyPet channel (475 nm) with concomitant decrease in YPet channel (527nm) were observed with the TnI-2 based biosensor (Figure 3.4A) and the control biosensor, but not the TnI-1 biosensor. In contrast to the results reported by Chen *et al.* (*146*), the construct that carried the I/LXXX$_{HY}$ consensus motif did not show any significant change in FRET even after treatment with MMP-2 for 16 hours. For this reason, TnI-1 was excluded from further studies. We confirmed the proteolytic cleavage of the TnI-2 biosensor by performing

SDS-PAGE. The biosensor incubated with MMP-2 for 1 hour was cleaved into smaller fragments, but identical samples incubated either without MMP-2 or in the presence of MMP2-inhibitors were not cleaved into smaller fragments (Figure 3.4B).

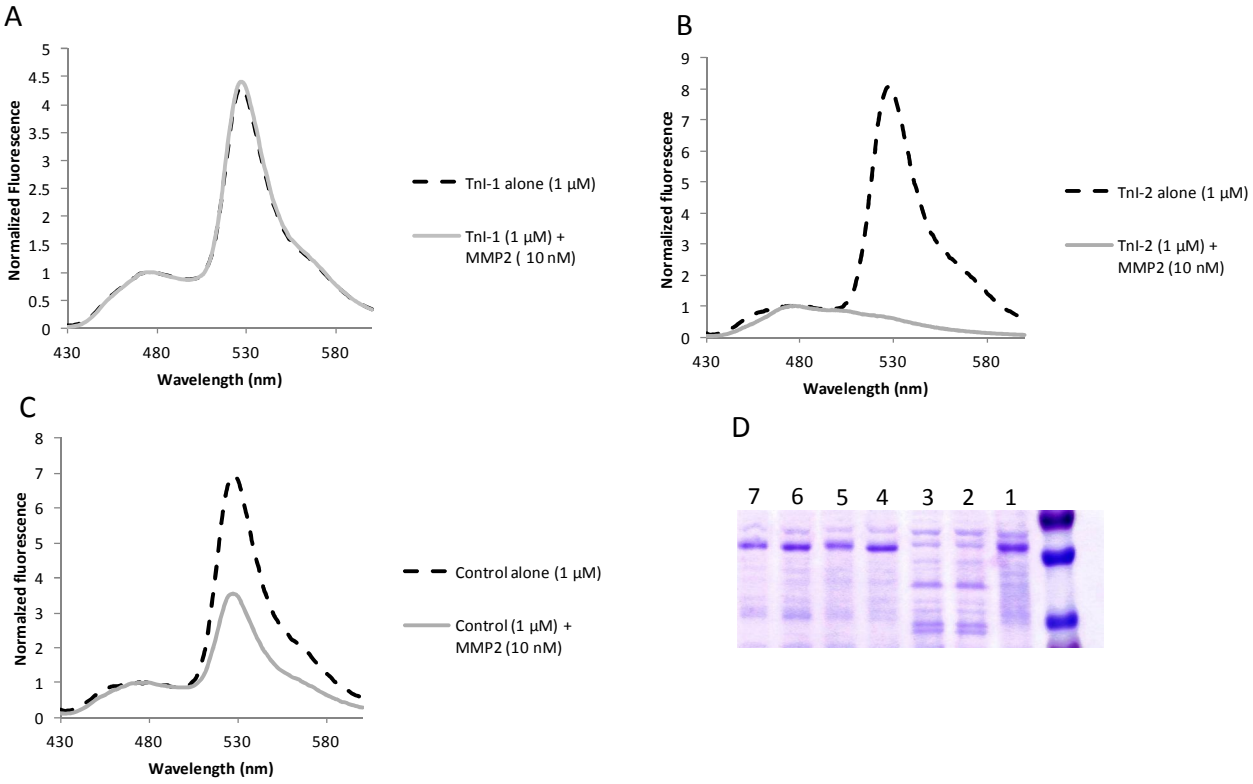

Figure 3.4 Preliminary characterizations of the three designed biosensors. (**A,B,C**) FRET change after incubation of 1 µM of each of TnI-1 (**A**), TnI-2 (**B**) and control (**C**) biosensors with 10 nM MMP-2, for 2 hours. (**D**) Coomassie stained 10% SDS-PAGE of TnI-2 biosensor under different conditions. All lanes contain 1 µM TnI-2. Lane 1 contains TnI-2 alone. Lane 2 and 3 contain TnI-2 plus MMP-2 (10 nM) in 10% methanol and DMSO respectively. Lanes 4-7 contain TnI-2 plus MMP2 plus an MMP inhibitor as follows: lane 4, 1 mM o-phenanthroline (in 10% methanol); lane 5, 10 µM GM 6001 (in 10% DMSO); lane 6, 10 µM ONO-4817 (in 10% DMSO) and; lane 7, 10 µM ARP (in 10% DMSO).

In order to compare the MMP-2 activity against the Control biosensor with the MMP-2 activity against the TnI-2 biosensor, we determined the second order rate constants for proteolysis (k_{cat}/K_M). This parameter allows us to compare the specificity to different substrates of a particular enzyme. Various methods have been previously employed to determine k_{cat}/K_M

including enzyme digestion followed by polyacrylamide gel based Western blot, radioactive labeling, and the use of fluorescently labeled substrates. FRET-based protease assays have been used to study proteases like deubiquitinating enzymes (157) and Sentrin/SUMO-specific proteases (SENPs) (158). In the SENP study, the donor/acceptor emission ratios were used as internally controlled and reliable measurements of the absolute quantities of substrates allowed that "uncleaved" and "100% cleaved" emission ratios were known. In a recent study, the authors suggested that cross-talk between donor and acceptor FPs should be corrected in the calculation of kinetic parameters (159). For our purposes, we reasoned that since we are more interested in comparing two unique substrates in terms of relative rather than absolute kinetic parameters, spectral cross-talk would not significantly affect the comparison. In addition, the high FRET efficiency and relatively high dynamic range provided by the CyPet and YPet FRET pair was expected to minimize the contributions of any errors due to spectral cross-talk.

The kinetic analysis revealed that the TnI-2 biosensor exhibited a k_{cat}/K_M value with MMP-2 that is 4.8 times higher than the Control biosensor. Specifically, k_{cat}/K_M was determined to be 3372 M^{-1} s^{-1} for TnI-2 and 700 M^{-1} s^{-1} for Control as shown in Figure 3.5. This result indicates that the TnI-2 biosensor (containing the TnI-derived substrate peptide) is a better substrate for MMP-2 than the one considered as the positive control. It is noteworthy to mention that the k_{cat}/K_M for the Control biosensor substrate sequence was reported to be two orders of magnitude higher than what we experimentally found (145). The source of this substantial discrepancy in the rate of this substrate turnover remains unclear, but it could potentially be due to batch-to-batch variation in specific activity of commercially available MMP-2. Indeed, we have substantial variation when testing batches from the same supplier and from different suppliers. It is also possible that inclusion of the substrate sequence between two relatively large

FPs might affect the rate significantly by limiting access of the enzyme to the substrate. However, we expect that the relatively long (17 amino acids) substrate sequence should provide sufficient access of the enzyme to its corresponding substrate site.

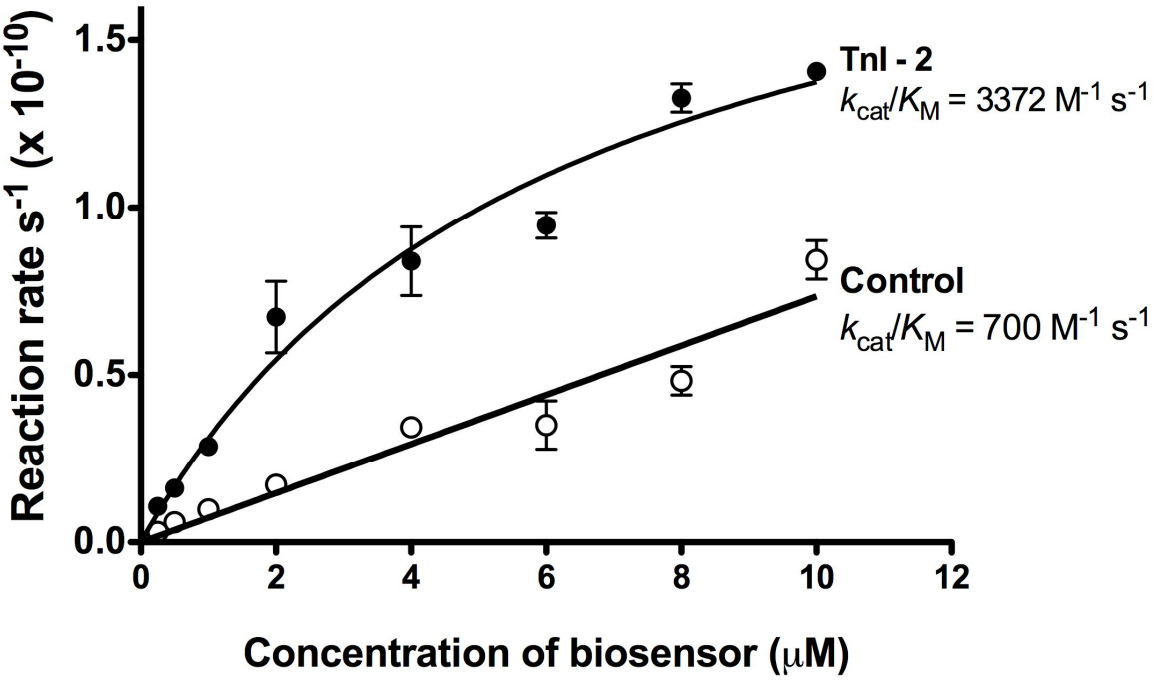

Figure 3.5 Kinetic analysis of TnI-2 and Control biosensors. The k_{cat}/K_M values for TnI-2 and Control biosensors were determined by fitting initial rate data at varying biosensor concentrations to the Michaelis-Menten equation.

To analyze if the constructed biosensors were specific for MMP-2, we wanted to test them against a variety of different MMPs (MMP -3, -9, -13), as well as two other proteases, calpain-1 and caspase-3. Enzyme activities were first tested against a known MMP substrate OmniMMP®, as a positive control for their activity (data not shown). All MMPs were able to proteolyze OmniMMP® whereas calpain-1 and caspase-3 did not.

We then tested the ability of MMPs and calpain-1 to proteolyze human recombinant TnI *in vitro* (Figure 3.6). All tested MMPs, as well as calpain-1, were able to proteolyse TnI. With

the MMPs one sees a degradation band at 23 kDa, while for calpain-1, the TnI hydrolysis band appears at a molecular weight of approximately 17 kDa, which suggests that MMPs and calpain-1 have different cleavage motifs on TnI. Caspase-3 was not tested in this preliminary experiment, as it has previously been shown that caspase-3 is unable to proteolyse TnI *in vitro*(*148*).

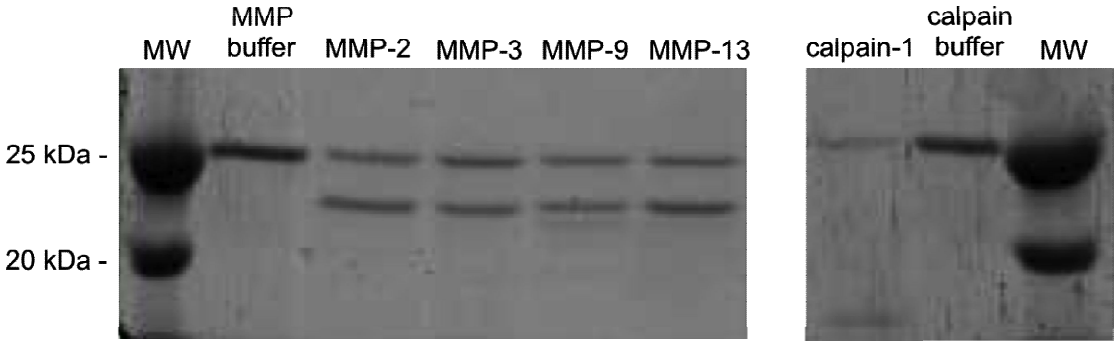

Figure 3.6 TnI degradation by different MMPs and calpain-1. Shown is a 10% SDS-PAGE gel stained with Coomassie blue.

We next compared the rate at which MMPs and other proteases were able to cleave the TnI-2 and Control biosensors. We incubated TnI-2 and Control biosensors with each enzyme (in their respective buffers), and recorded their 475/527 nm fluorescence ratio every 20 minutes for 16 hours (Figure 3.7). We found that both biosensors were specific for MMPs and were not substantially proteolyzed by either calpain-1 or caspase-3. However, the biosensors were not specific for MMP-2 relative to other MMPs. That is, MMPs -3, -9 and -13 all cleaved both the TnI-2 and Control biosensors substantially faster than MMP-2 and gave similar fluorescence ratio vs. time profiles. MMPs -3, -9 and -13 all reached a plateau ratio value of approximately 1.5 within the time frame of the experiment, indicating that complete biosensor cleavage had occured (Figure 3.7). We showed earlier that that calpain-1 proteolyzed TnI at a cleavage site that is distinct from that for MMPs. For this reason it is not surprisingly that calpain-1 was not able to cause changes in FRET for the TnI-2 biosensor.

The biosensors were not specific for MMP-2 relative to other MMPs, which all showed higher activity than MMP-2 towards the TnI-2 and Control biosensors (Figure 3.7). This result could potentially be explained by the other commercial MMP preparations having higher specific activity than the MMP-2 we used in this study. The experiments in this work were done based on the basis of equivalent enzyme and substrate concentration and not normalized by specific activity. Further confounding this issue is the fact that the assays used by the respective providers to measure specific activity were different or each MMP, making it impossible to compare values. One encouraging observation was that our TnI-2 biosensor was degraded by MMP-2 faster than the control biosensor was. That is, the TnI-2 biosensor was proteolzyed at a rate that was faster than the Control biosensor. This result was expected, taking into consideration the higher k_{cat}/K_M value for the TnI-2 biosensor as determined earlier.

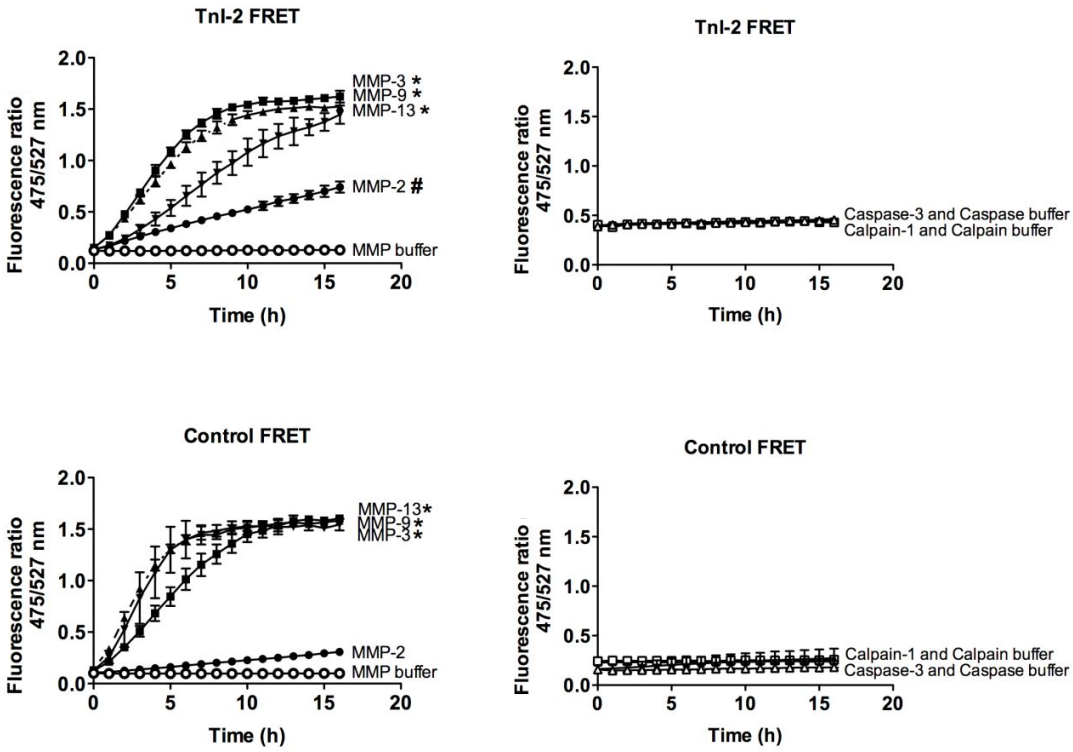

Figure 3.7 Fluorescence ratio (475/527 nm) vs. time observed for different MMPs (left panels), and calpain-1 and caspase-3 (right panels). Upper panels are for the TnI-2 biosensor and lower panels are for the Control biosensor. * denotes significant difference from MMP-2, $p < 0.0001$. # denotes significant difference from negative control, $p < 0.0001$.

The main goal of this study was to design a new tool that would allow us to detect MMP-2 in the intracellular environment. Intracellular MMP-2 activity is expected to increase under conditions of oxidative stress and during ischemia-reperfusion. It has also been reported that intracellular pH (pH_i) drops significantly from around 7.2 to below 6.8 under such conditions (160, 161). Accordingly, we wanted to test how much the biosensors FRET signal might be affected by the expected drop in pH_i. As shown in Figure 3.8, the emission ratio of TnI-2 and Control biosensor is quite stable to small pH_i changes centred around pH 7, and even in a broader pH range from pH 6 to 10 (Figure 3.8).

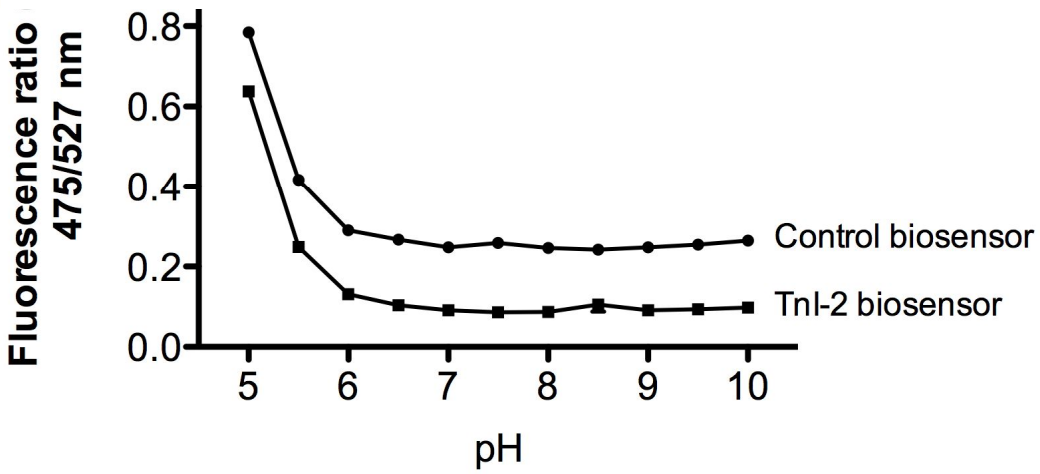

Figure 3.8 Control and TnI-2 biosensors resistance to changes in pH.

3.4 CONCLUSION

Matrix metalloproteinase-2 (MMP-2) is a key protease involved in several oxidative stress related pathologies in the heart and vasculature. Mounting evidence suggests that activated MMP-2 does not only proteolyze extracellular matrix proteins, but also cleaves susceptible intracellular substrates in the heart. One such substrate is the sarcomeric protein troponin I (TnI). FRET-based biosensors have proven very useful in the study of the activity of a variety of proteases. In this work we attempted to apply this technology to determine intracellular MMP-2 activity.

We constructed three potential MMP-2 FRET-based biosensors by inserting amino acid sequences containing putative MMP-2 cleavage sites derived from human cardiac TnI between a donor (CyPet) and an acceptor (YPet) FP. Two of these constructs contained N-terminal TnI amino acid sequences (TnI-1 and TnI-2) based on likely MMP-2 cleavage sites within TnI. The

third sensor (Control) contained the sequence GGSGG IPVSLRSG GGSGG, which has been reported to be selective for MMP-2. Following construction, expression, and purification of the biosensor proteins, we determined their activities by assessing the changes in the CyPet/YPet ratio recorded by digesting the biosensors with human recombinant MMP-2. The k_{cat}/K_M values were determined to be 3372 M^{-1} s^{-1} for TnI-2 and 700 M^{-1} s^{-1} for Control, and TnI-1 was found to not be a substrate for MMP-2. We tested the specificity of these biosensors for MMP-2 relative to a variety of other proteases including MMP-3, -9 and -13, calpain-1, and caspase-3. TnI-2 and Control were selective substrates for all MMPs, but were not highly specific for MMP-2 versus other MMPs. Neither biosensor was cleaved by either calpain-1 or caspase-3. The rates of cleavage observed for MMPs -3, -9 and -13 were very similar for both the TnI-2 and Control biosensors. However, for MMP-2 the TnI-2 biosensor showed a higher rate of proteolysis than the Control biosensor under identical conditions. Overall, these results indicate that identifying specific substrates for an MMP is a challenging process, likely due to the relatively high conservation of the catalytic domain across the multiple MMPs. The biosensors are now being expressed in neonatal cardiomyocytes in order to track intracellular MMP activity following oxidative stress stimuli. While the specificity of the TnI-2 biosensor is not sufficient to provide specific detection of MMP-2 activity, it will be useful as an indicator of general MMP activity in the intracellular milieu.

CHAPTER 4

DESIGN AND DEVELOPMENT OF SINGLE FP BASED BIOSENSORS FOR HYDROGEN PEROXIDE

4.1 INTRODUCTION

For a long period of time, oxidative stress has been primarily concerned with the concept of free radical-induced macromolecular damage (162-164). In other words, many researchers viewed disease related oxidative mechanisms as those that involved molecules or atoms that carry unpaired electrons (i.e., free radicals). Free radicals tend to be highly reactive and are capable of attacking cellular macromolecule such as proteins, nucleic acids, membrane-associated unsaturated fatty acids, and so forth (162-165). This superficial perspective was later refined by the discovery of hydrogen peroxide producing enzymes followed by the elucidation of the role of hydrogen peroxide as a signaling molecule in critical cellular processes such as proliferation, differentiation and apoptosis (163, 164, 166, 167). During the last decade, proteomics and computational approaches lead to the discovery of a plethora of proteins that are selectively regulated by hydrogen peroxide oxidation (163, 164, 166, 168, 169). Obviously, contemporary studies of complex redox processes in biological systems require novel redox-sensitive probes that are capable of providing a fluorescence signal in response to changes in the intracellular redox environment. Genetically encoded FP-based biosensors are a promising technology for such probes. Specifically, FP-based sensors can provide high specificity via biomolecular recognition, high spatio-temporal resolution when used for fluorescence imaging, and yet only minimally perturb the intracellular environment since they are proteins themselves (163, 164, 166, 170).

The FP-based redox probes reported in literature can be classified into four classes. The first class constitutes FPs in which artificial disulfides are introduced into the β-barrel scaffold. Consequently, a change in the redox potential shifts the dithiol-disulfide equilibrium and causes a relatively subtle change in the structure of the FP. This structural change is associated with a

change in the chromophore environment that causes either an intensiometric or ratiomatric signal changes in the FP spectral profile. Specific examples in the first class are redox sensitive yellow fluorescent proteins (rxYFPs) (97, 171) and redox sensitive GFPs (roGFPs) (98, 99, 172-174). The second class are chimeric fusions of redox sensitive FPs (rxYFPs or roGFPs) to redox active enzymes such as glutaredoxin (175, 176) or thioredoxins (170) or peroxidase (177). The rationale for creating a chimera is to increase the specificity and redox sensing efficiency of the redox sensitive FPs. The third class is composed of a redox sensitive linker region sandwiched between a FP FRET pair (178-180). In this case, a change in the FRET efficiency is used as the readout for a redox-dependent change in the linker structure.

The fourth class, which is of particular interest to this study, is represented by the hydrogen peroxide biosensor known as HyPer (181). Hyper is composed of a circularly permuted yellow fluorescent protein (cpYFP) inserted between residues 205 and 206 of the regulatory domain of *Escherichia coli* OxyR protein which is specifically sensitive to H_2O_2 (181). Wild-type OxyR consists of two domains: a DNA binding domain (amino acids 1-79) and a regulatory domain (amino acids 80-310) (182). The oxidized form of OxyR binds specifically to DNA, while the reduced form does not (182). The oxidation involves two key cysteine residues which are C199 and C208 (183). C199 is located in a hydrophobic pocket and hence can't be reached by charged oxidants like superoxide (184). However, H_2O_2 can penetrate into the hydrophobic pocket and oxidize C199 into a charged sulfenic acid that is repelled by its hydrophobic environment (*184*). A dramatic conformational change occurs bringing the sulfenic acid residue in the vicinity of C208 and hence a disulfide bond is formed (184).

HyPer is an excitation ratiometric biosensor with excitation peaks at 420 nm and 500 nm (181). Exposure to H_2O_2 leads to proportional decrease in the 420 nm peak with concomitant

increase in the 500 nm peak (*181*). A later version (HyPer-2) was introduced with a single mutation of A406V (which corresponds to A233V in OxyR) (185). This single mutation caused Hyper-2 to have a dynamic range that was expanded to twice that of Hyper (185). Nonetheless, Hyper-2 forms a strong dimer and shows slow oxidation-reduction kinetics in comparison to Hyper (185). Recently HyPer-3 has been reported, carrying the H34Y mutation which corresponds to H114Y in OxyR, which renders OxyR to be constitutively active (186). Hyper-3 retained the same dynamic range of Hyper-2 but demonstrated faster oxidation-reduction kinetics and lower tendency to undergo dimerization (186).

Our lab has previously developed a palette of single FP genetically encoded Ca^{2+} indicators (GECOs) with a variety of fluorescent hues ranging from blue to red (87). This success inspired us to attempt to similarly expand the palette of genetically encoded Hyper-type H_2O_2 biosensors. The idea in this study was to replace cpYFP by other circular permuted FPs that have previously been optimized in our lab. Out of the several cpFPs that were tried, only the one based on GEM-GECO seems to be particularly promising. Subjecting the latter to cycles of directed evolution along with appropriate screening has lead to the discovery of an intensiometric variant that gives a direct response to H_2O_2 and an intensiometric variant that has an inverse response to H_2O_2.

4.2 MATERIALS AND METHODS

4.2.1 General Materials and Methods

Unless otherwise indicated all chemicals and reagents were purchased from Fisher Scientific (Ottawa, ON, Canada) or Sigma-Aldrich Canada (Oakville, ON, Canada). All primers were purchased from Integrated DNA Technologies (Coralville, IA, USA). Non-mutagenic polymerase chain reactions were performed using Pfu DNA polymerase (Fermentas, Burlington,

ON, Canada) according to the manufacturer's protocol while error-prone PCR amplifications were done using Taq DNA polymerase (Invitrogen, Burlington, ON, Canada) as described in Cirino *et al* (187). Fast Digest Endonucleases (Fermentas, Burlington, ON, Canada) were used for restriction digests of all PCR products and plasmids. PCR products and products of restriction digestion were purified by gel electrophoresis and extracted using GeneJet gel extraction kit (Fermentas). DNA ligation was performed using T4 DNA ligase (Invitrogen). *E. coli* ElectroMax DH10B^{TM} (Invitrogen) was used for transformation and subsequent plasmid propagation. Dye terminator cycle sequencing using BigDye (Applied Biosystems, Burlington, ON, Canada) was used to confirm the complete DNA sequencing of all fusion constructs. Sequencing reactions were analyzed at the University of Alberta Molecular Service Unit.

4.2.2 Construction of chimera of cpFPs and OxyR regulatory domain

The gene fragment encoding the first part of OxyR-regulatory domain (residues 81-205) was PCR amplified from the gene encoding the OxyR2 transcriptional factor. The 5`primer carried an *XhoI* restriction site and the 3`-primer contained either a SAG or PVV linker followed by a region that overlaps with the 5`-primer of the cpFPs. CpFPs were PCR amplified from their genes using 5`-primer carrying either SAG or PVV linker followed by the previously mentioned overlap region and a 3`-primer that carries *KpnI* restriction site. The PCR fragments of OxyR-RD (81-205) and cpFPs are mixed in equimolar amounts and the full length OxyRD(81-205)-SAG or PVV-cpFPs chimeras were assembled by overlap extension PCR using primers *XhoI*-OxyR-(81-205)-FD and cpFP-*KpnI*-BK. The full length product was purified by agarose gel electrophoresis, digested with appropriate enzymes and ligated between the *XhoI* and *KpnI* sites of pBAD/His B (Invitrogen). The gene for the second part of OxyR-regulatory domain (residues

206-305) was also PCR amplified from the gene encoding OxyR2 transcriptional factor. The 5' primer carried a *KpnI* restriction site and the 3' primer carried a *HindIII* site. The PCR product was doubly digested and ligated into previously ligated pBAD/His B already containing OxyRD(81-255)-SAG-cpFPs from the previous step.

4.2.3 Construction and screening of HyPer-cpFPs libraries

Error prone PCR amplifications for construction of libraries of randomly mutated genes were performed using primers *XhoI*-OxyR-(81-205)-FD and cpFP-*KpnI*-BK. The resulting PCR product were digested with *XhoI* and *KpnI* and ligated with similarly digested pBAD/His B already containing OxyR-(205-306) DNA. *E. coli* was transformed with the libraries, and transformants were plated on LB-agar with 0.04% ampicillin and 0.02% L-arabinose in polystyrene Petri dishes and incubated at 37 °C overnight. The imaging system is similar to that discussed in section 2.2.4. For library screening, we picked the top 20 colonies that exhibited the highest intensity change upon spraying with 50 μM H_2O_2 in Tris-HCl (pH 7.4), 150 mM NaCl. Picked colonies were individually cultured in 4 ml LB medium supplemented with 0.02% L-arabinose and 0.04% ampicillin and were shaken (250 rpm) overnight at 37°C. Crude B-PER protein extracts from the picked colonies were subjected to a second stage of screening by comparing emission spectrum of a portion of the crude extract to another portion treated with 250 nM H_2O_2 and variants with the highest change were isolated and sequenced.

4.2.4 Protein purification and characterization

To prepare proteins in sufficient quantity for characterization, a single colony of *E. coli* that had been transformed with pBAD/His B carrying the gene for the variant of interest was used to inoculate 500 ml Lysogeny Broth (LB) medium supplemented with 0.04% ampicillin, 0.2% L-arabinose and 5 mM 2-mercaptoethanol. The culture was allowed to grow overnight

before cells were harvested and lysed by a cell disruptor (Constant Systems, Daventry, Northants, UK). Proteins carrying an N-terminal His_6 tag were then purified by Ni-NTA affinity chromatography (Amersham, Amersham, Buckinghamshire, UK) and exchanged into Tris-HCl (pH 7.4), 150 mM NaCl and 0.5 mM 2-mercaptoethanol. Aliquots of the proteins in the same concentration (approximately 25 nM) were used for H_2O_2 titration. Fluorescence spectra were recorded on a Safire2 plate reader (Tecan, Männedorf, Switzerland). Quantum yields for Hyper-GEM variants were measured using fluorescein in 10 mM NaOH as the reference standard. Emission spectra for quantum yield determination were recorded on QuantaMaster spectrofluorometer (Photon Technology International) and had been corrected for the instrument response.

4.2.5 pH sensitivity determination

The pH dependence of the fluorescence of the selected variants were determined by measuring the emission for each variant at a range of pH values in both reduced and oxidized forms. The oxidized form of the selected variants was obtained by incubating with 500 nM H_2O_2 for half an hour. Each protein (1 μM) was dispensed into wells of a 96-well plate dark-sided with clear bottom plate (Corning, Tewksbury, MA, USA). Each well contained Britton–Robinson buffer adjusted to a specific pH value in the range from 5-10. Measurements were performed in at least four replicates. The pK_a was determined by fitting the experimental data to a four parameter logistic curve using SigmaPlot 12.0 software.

4.3 RESULTS AND DISCUSSION

In an effort to develop a spectral palette of H_2O_2 biosensors with novel spectral properties, I attempted to develop new HyPer analogues based on the incorporation of new circularly permutated FPs that were developed in our lab. The cpFPs variants I used in this study

were either developed separately such as cpmCherry variants 145 and 196 (Dr. Haley J. Carlson, unpublished results) or developed as part of a series of single fluorescent protein based calcium biosensors known as the GECOs (87). Specifically, I used the cpFP domains from GEM-GECO1, G-GECO1.2 and R-GECO1. Each of these cpFPs was sandwiched between split parts of H_2O_2 sensing domain of OxyR2 transcription factor in an analogous way to Hyper. The connection point between the first part of OxyR2 H_2O_2 sensing domain (residues from 81-205) and cpFPs was either SAG as in Hyper or PVV as in R-GECO1. Out of the several candidates prepared and tested only two variants showed a small yet consistent intensiometric response to H_2O_2. These two promising variants were the one that incorporated the cpFP domain from GEM-GECO1 and the one that incorporated the cpmCherry 196 variant (Figure 4.1). Both variants carried the SAG connection linker between OxyR2 (81-205) and the cpFP.

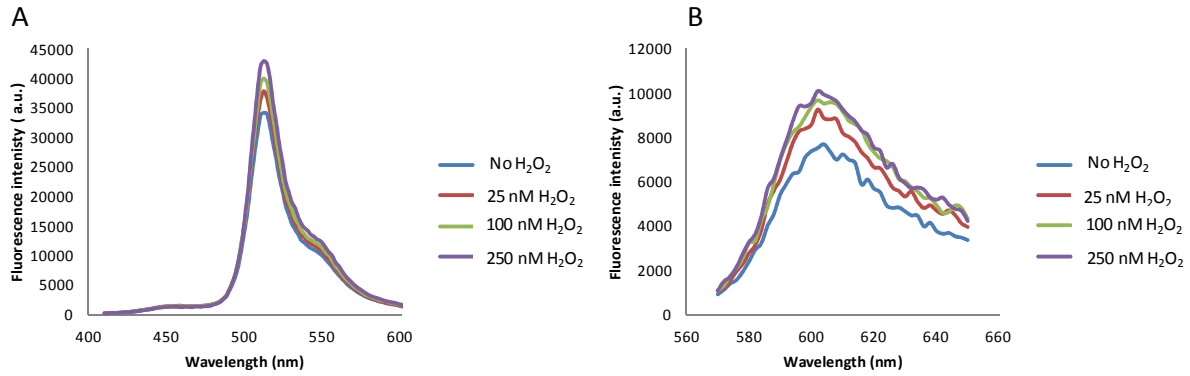

Figure 4.1 Emission spectrum profiles of prototypes biosensors based on a hybrid of HyPer and GEM-GECO1 and cpmCherry196. (A) Titration of prototype of HyPer-GEM with H_2O_2 showing a maximum change of 25.4%; excitation at 390 nm and emission scan from 410-600 nm. (B) Titration of prototype of HyPer-cpmCherry196 with H_2O_2 showing a maximum change of 28.6%; excitation at 550 nm and emission scan from 570-650 nm. Both proteins were prepared at 25 nM in Tris-HCl (pH 7.4), 150 mM NaCl and 0.5 mM 2-mercaptoethanol.

I focused my efforts more on improving these two promising prototypes by directed evolution and screening of large libraries of variants. The method of creating a library for directed evolution was error prone PCR. Unfortunately, after exhaustive screening of numerous

libraries of cpmCherry 196 variants, I did not identify any substantially improved variants. On the other hand, on the first round of evoluting GEM-GECO1 based HyPer analogue an interesting variant named HyPer-GEM1 showing an inverse response upon titration with H_2O_2 (Figure 4.2) and a with 52.4% change in intensity upon full oxidation with H_2O_2.

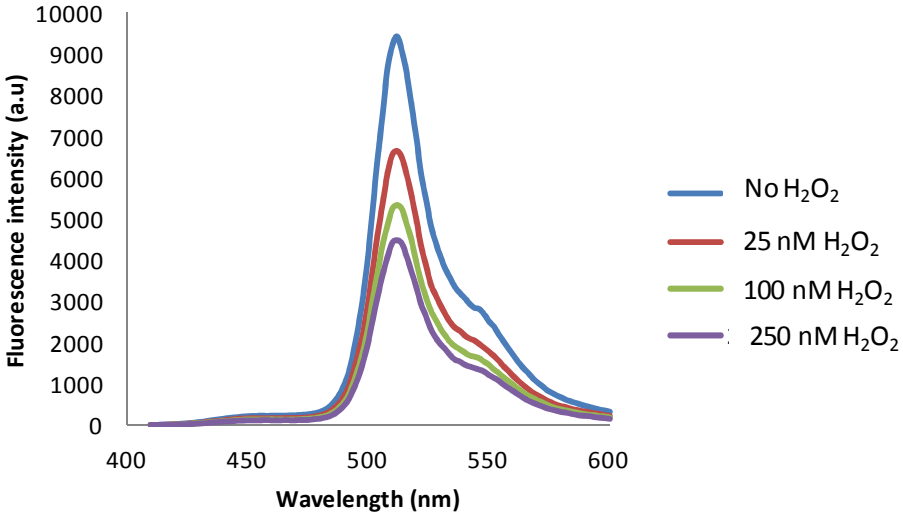

Figure 4.2. Titration of HyPer-GEM1 with H_2O_2 showing an inverse response with a maximum of 52.43%; excitation at 390 nm and emission scan from 410-600 nm. Protein concentration was 25 nM in Tris-HCl (pH 7.4), 150 mM NaCl and 0.5 mM 2-mercaptoethanol.

Exposing Hyper-GEM1 to another round of error-prone PCR followed by screening for highest response change upon H_2O_2 spraying led to the discovery of another interesting variant named Hyper-GEM2. Hyper-GEM2 exhibited a directly proportional intensiometric response upon H_2O_2 titration as demonstrated in Figure 4.3, with a maximum response of 109% change in intensity upon full oxidation with H_2O_2.

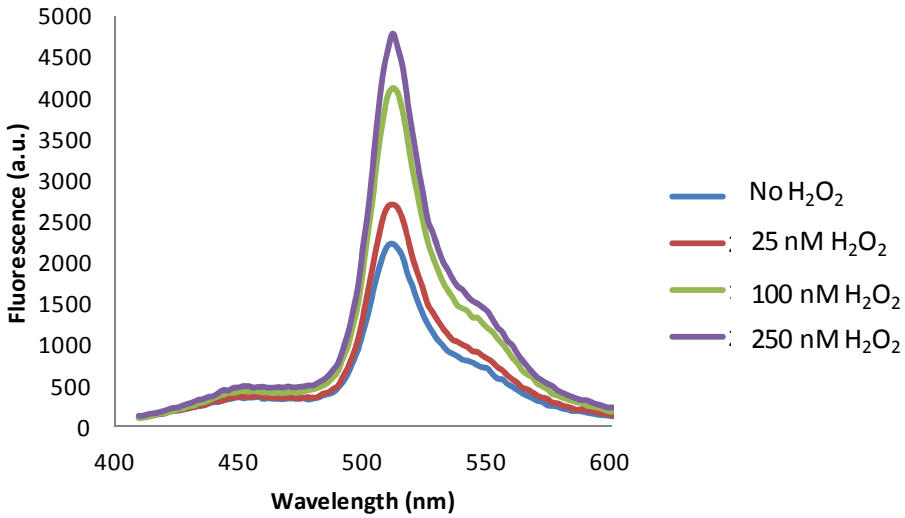

Figure 4.3. Titration of HyPer-GEM2 with H_2O_2 showing a maximum response of 109%; excitation at 390 nm and emission scan from 410-600 nm. Protein concentration was 25 nM in Tris-HCl (pH 7.4), 150 mM NaCl and 0.5 mM 2-mercaptoethanol.

Sequencing of Hyper-GEM1 revealed that it carries two mutations which are N150S and K227R. Both mutations are in the GEM domain and correspond to N83S and K160R in GEM-GECO1. Hyper-GEM2 shares the two mutations of Hyper-GEM1 in addition to three mutations in the N-teminal part of OxyR2 regulatory domain, which are L87Q, M103K and M125I. The latter three mutations correspond to L167Q, M183K and M205I in wild type OxyR2 protein. All sequences are provided in Figure 4.4.

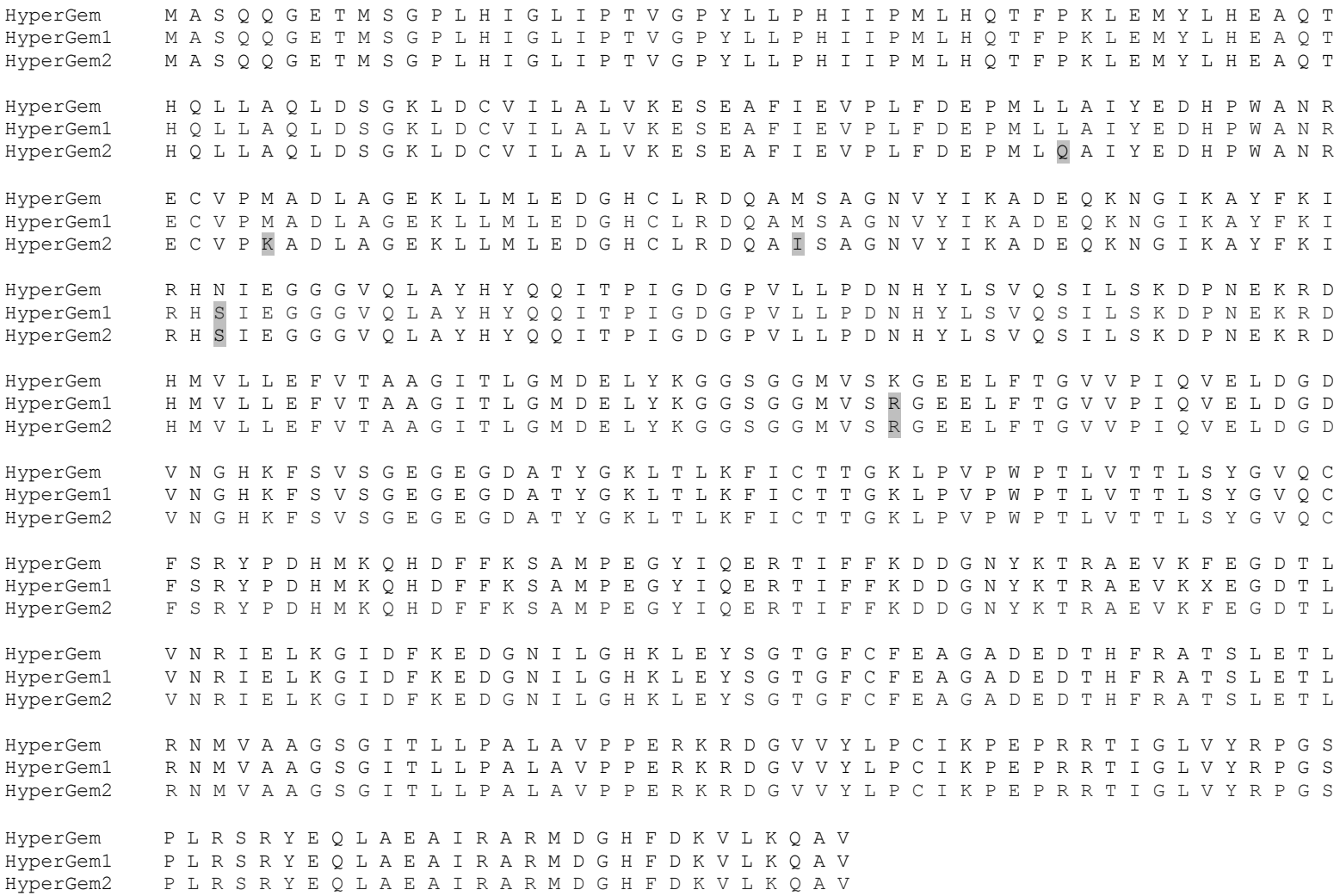

Figure 4.4. Sequence alignment of prototype HyPer-GEM, HyPer-GEM1 and HyPer-GEM2. Mutations found are highlighted in grey shade. Both HyPer-GEM 1 & 2 share two mutations in GEM-domain which are N150S and K227R. HyPer-GEM2 has three additional mutations which are L87Q, M103K and M125I.

By analogy to the GECO series, I expected that the HyPer-GEM variants modulation in fluorescence profile might be attributed to a change in pK_a upon oxidation. On the contrary pH titration of both variants in both oxidized and reduced states didn't show a big change in pK_a comparable to the change in fluorescence (Figure 4.5). HyPer-GEM1 pK_a in the reduced and oxidized states are 6.63 ± 0.17 and 6.73 ± 0.13, respectively. HyPer-GEM2 pK_a in the reduced and oxidized states are 6.74 ± 0.13 and 6.69 ± 0.14.

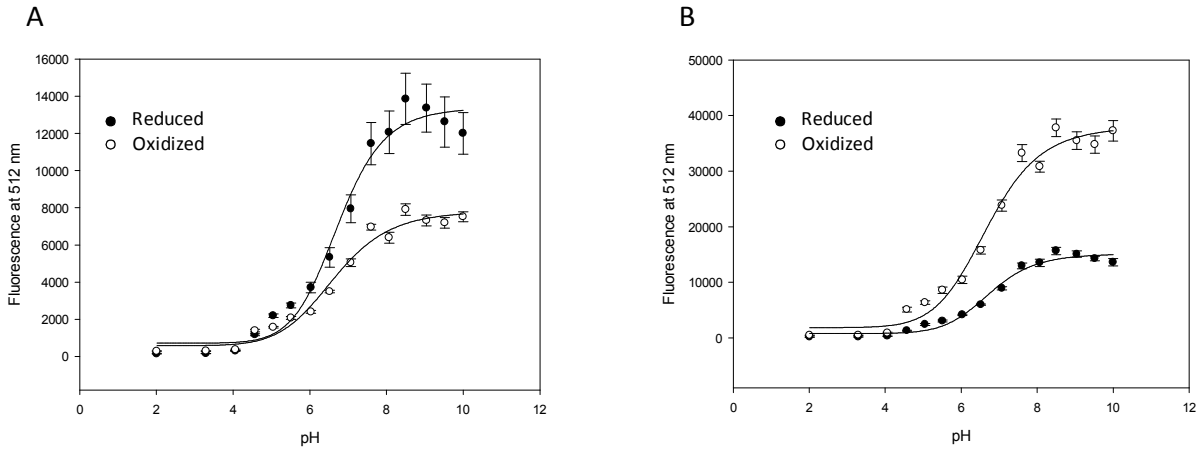

Figure 4.5. pH sensitivity of HyPer-GEM1 and 2. (A) Fluorescence intensity of HyPer-GEM1 as a function of pH in both reduced and oxidized states; the apparent pK_a were 6.63 and 6.73 respectively. (B) Fluorescence intensity of HyPer-GEM2 as a function of pH in both reduced and oxidized states; the apparent pK_a were 6.74 and 6.69. Fluorescence intensity experiments are done in at least triplicates and data ± standard deviation is represented.

Further investigation of the spectral properties of HyPer-GEM 1 and 2 has shown that H_2O_2 response is associated with a change in extinction coefficient and quantum yield as detailed in Table 4.6. HyPer-GEM1 underwent a significant decrease in quantum yield upon oxidation with H_2O_2 with an overall brightness change of about 34%. On the other hand, HyPer-GEM2 underwent a significant increase in both extinction coefficient and quantum yield with an overall brightness change of about 108%.

	Ɛ (mM^{-1} cm^{-1})	Φ	Brightness (mM^{-1} cm^{-1})	pK_a
HyPer-GEM1				
Reduced	34	0.94	24	6.63
Oxidized	33	0.63	16	6.73
HyPer-GEM2				
Reduced	22	0.72	16	6.74
Oxidized	35	0.95	33	6.69

Table 4.1. Spectral properties and pK_a s of HyPer-GEM1 and 2.

4.4 CONCLUSION

The demand for new biosensors for studying the newly discovered biological roles of reactive oxygen species with high spatio-temporal resolution inspired us to try to develop multicolour variants of the previously reported H_2O_2 biosensor HyPer.

Our efforts in trying to develop a red analogue were unfortunately not successful. However we did succeed in developing two long Stoke's shift green HyPer-variants by incorporating the circularly permuted FP present in GEM-GECO into the regulatory domain of OxyR2. Our initial prototype of this sensor was further improved and diversified into two variants with opposing responses to H_2O_2 through the use of molecular evolution. We named these two variants HyPer-GEM1 and HyPer-GEM2. Hyper-GEM1 turned out to be an inverse response H_2O_2 biosensor with an overall change of around 50% upon full oxidation. Hyper-GEM2 is direct response H_2O_2 biosensor with an overall increase of more than 100% upon full oxidation.

Although HyPer-GEM1 and HyPer-GEM2 do not show a comparable signal contrast to one of their parents (i.e., GEM-GECO1 which has a response to calcium ion that is orders of magnitude higher than the variants presented in this chapter), their dynamic range is comparable to that demonstrated by the original HyPer construct (about 120%). In the concluding chapter I will discuss several possible future directions for this project.

CHAPTER 5

CONCLUSIONS AND FUTURE DIRECTIONS

In this thesis, I described the use of fluorescent proteins (FPs) to develop molecular tools that will help other researchers to explore the inner workings of living cells and answer numerous biological questions. One could confidently say that FPs, by the virtue of being proteins and hence genetically encoded, are the best class of fluorophores for converting into biosensors for intracellular applications. For this reason, numerous FP-based biosensors for different application purposes have been engineered and yet there remains much to be done and discovered using these indispensable tools. As I will briefly review in the following sections, our efforts have been focused on developing improved and/or novel biosensors for kinases, matrix metalloproteinase, and hydrogen peroxide.

5.1 FRET-BASED KINASES BIOSENSORS

In Chapter 2 I described the modification of a methodology previously reported by our lab for improving the response of FRET based biosensors for imaging of post-translational modifications (107). The corner stone of the reported methodology is the use of a hybrid expression vector that contains both P_{tac} and P_{BAD} promoters that can operate separately and independently (107). Placing the coding sequence of a constitutive actively enzyme downstream of the tightly controlled P_{BAD} promoter, and the coding sequence of the biosensor downstream of P_{tac}, enables the in-colony screening of biosensor libraries. Specifically, colonies expressing variants of a given FRET based biosensor can be imaged under two conditions. Under one condition (+ arabinose) the constitutively active enzyme is being expressed and the biosensor is primarily in the modified stated. Under the second condition, the constitutively active enzyme is being repressed and the biosensor is primarily in the unmodified state (107). By comparing fluorescence images of Petri dishes containing many hundreds of colonies, those clones that exhibit the largest changes in fluorescence emission between the modified and unmodified states

can be identified. In the original report, it was necessary to randomly pick colonies and then respot them in parallel onto arabinose and glucose containing plates. These two plates are then imaged and the digital images compared to find the most promising clones. This respotting procedure was the limiting step in this procedure and tended to be relatively tedious (107). To increase the throughput of this strategy we avoided respotting by spraying glucose-containing plates with L-arabinose and comparing digital images acquired before and after spraying. We applied our improved procedure to the optimization of a previously reported PKB (Akt) biosensor known as BKAR. In this effort we were successful in increasing the FRET ratio change upon phosphorylation from 30% to 40%. Moreover, we developed a new cyclin B1-CDK1 biosensor with a ratio change upon phosphorylation of 67% which was dramatically improved relative to the ~10-15% change of a previously reported cyclin B1-CDK1 biosensor (137, 138).

Our collaborators, Michael W. Davidson and Brittney R. Sell of the National High Magnetic Field Laboratory, University of Florida, expressed our cyclin B1-CDK1 biosensor in HeLa cells and observed the emission ratio change as cells progressed through mitosis. Indeed, this live cell imaging data was consistent with our *in vitro* data and revealed the expected change in FRET efficiency in response to cyclin B1-CDK1 kinase activity. In one experiment, the emission ratio increased as the cell progressed into prophase reflecting the activation of cyclin B1-CDK1 reaching a maximum plateau as the cell enters to the metaphase as shown in Figure 5.1. The % FRET change observed from the beginning to the end of this experiment is about 60%.

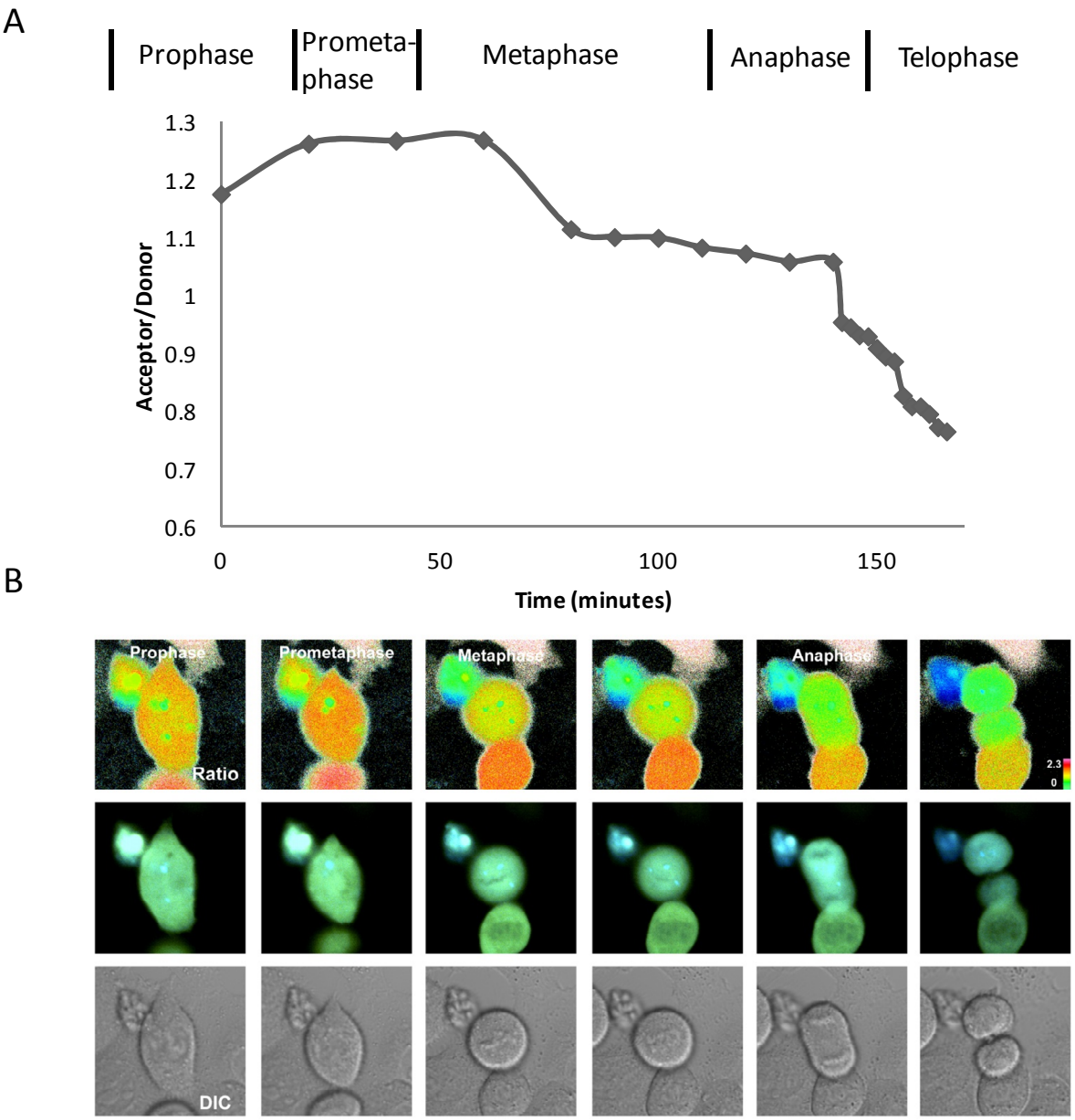

Figure 5.1. Cyclin B1-CDK1 kinase activity during mitotic progression. (A) The FRET signal in the form of emission ratio of Acceptor (YFP) / Donor (TFP) signal over time have been recorded during the mitotic entry in HeLa cells and throughout the whole mitotic process. (B) HeLa S3 cells expressing the cyclin B-Cdk1 activity sensor observed over several hours. Ratiometric (top row), fluorescence merged (middle row), and DIC (bottom row) images of the kinase dynamics during mitotic progression, starting at prophase through cytokinesis. Note that FRET level in prophase is set at ~80% of the dynamic range.

In a second experiment, emission ratio almost remained constant throughout the metaphase before dropping drastically throughout anaphase as shown in Figure 5.2. The % FRET change observed in this run from the beginning till the end is about 70%.

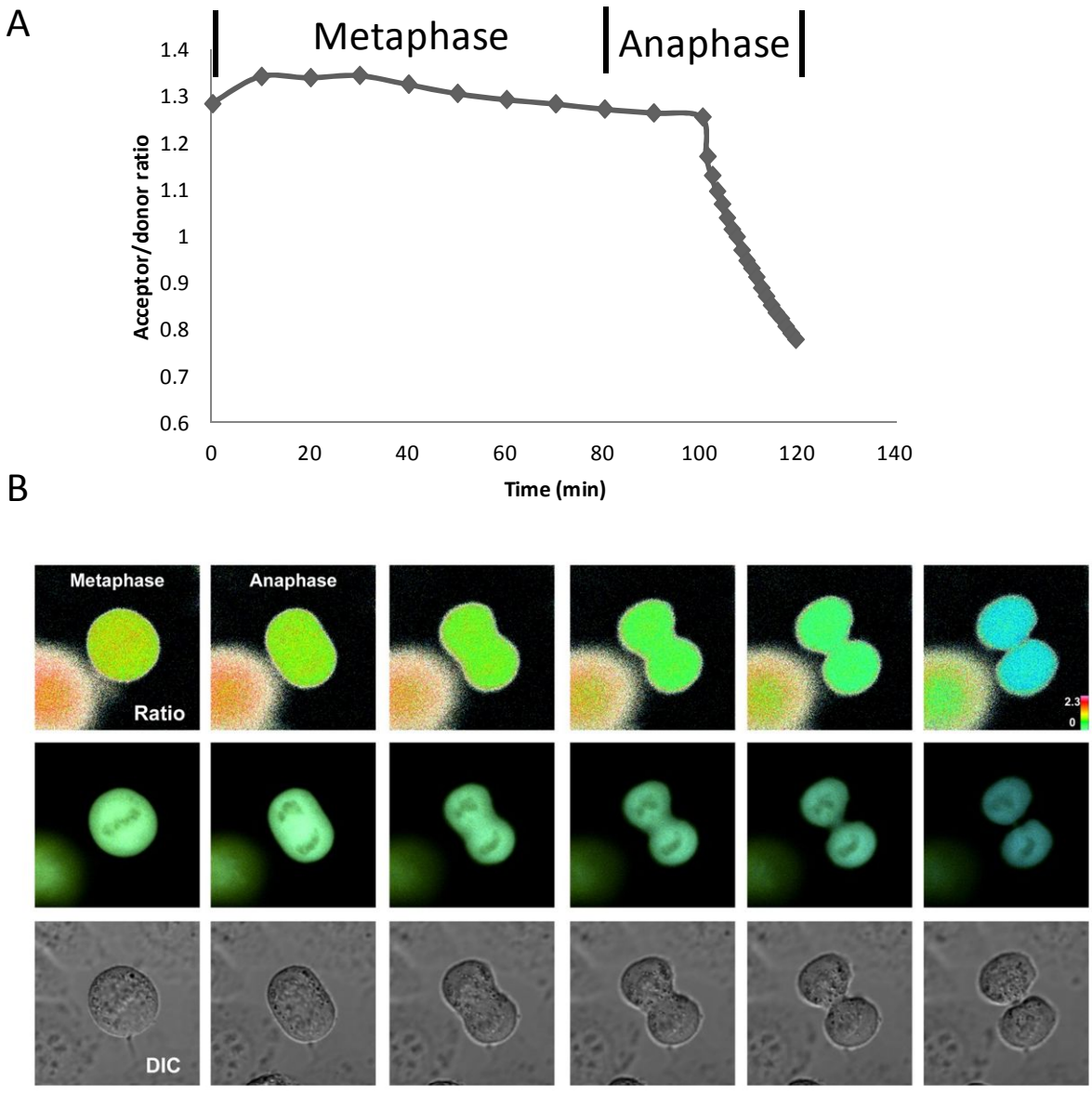

Figure 5.2 Cyclin B1-CDK1 kinase activity during Metaphase and Anaphase. (A) The FRET signal in the form of emission ratio of Acceptor (YFP) / Donor (TFP) signal over time have been recorded during metaphase and anaphase of mitotic cycle. (B) HeLa S3 cells expressing the CyclinB-Cdk1 activity sensor observed over several hours. Ratiometric (top row), fluorescence

merged (middle row), and DIC (bottom row) images of the FRET dynamics during mitotic progression, starting at metaphase through cytokinesis. Note that FRET level in metaphase is set at ~60% of the dynamic range.

It is evident from these imaging results that the emission ratio at the end of the anaphase (and start of G1) is significantly lower than at the start of prophase (and the end of G2). Similar behaviour have been reported with the previously reported biosensor (but of course with lower overall dynamic range) and the authors attributed this to both differential bleaching of the yellow FP versus cyan and cell rounding in HeLa cells (137, 138). Moreover they mentioned that this behaviour was not observed when their biosensor was expressed in RPE cells (137, 138). In contrast to these previous explanations, I would argue that cyclin B1-CDK1 dependant phosphorylation is most likely being reversed during anaphase by the action of a phosphatase and that might be the reason of lower FRET ratio at the end of anaphase compared to start of prophase. This hypothesis will require further investigation and collaboration from research groups with expertise in cell cycle biology. The major challenge that we faced in using this indicator is long term imaging of cells in order to observe a full cell cycle.

The improved dynamic range cyclin B1-CDK1 biosensor we developed will help in better understanding of the kinetics and mechanisms of the roles played by cyclin B1-CDK1 in the cell cycle. I would also suggest that changing the FRET pair with other optimized FRET pairs (for example Clover and mRuby2 (46)) could give a similar if not better response. Switching to alternative color combinations could enable the simultaneous imaging of cyclin B1-CDK1 with spectrally distinct probes for secondary messengers or other post-translational modification known to be involved in the cell cycle process.

5.2 DEVELOPMENT OF TROPONIN-I BASED MMP2 BIOSENSOR

The project described in Chapter 3 was a collaboration with the lab of Professor Richard Schulz in the Department of Pharmacology, University of Alberta. The aim of this work was to provide a genetically encoded probe to investigate the potential intracellular roles of MMP2 during cardiac oxidative-stress conditions such as ischemia-reperfusion injury. This probe took the form of FRET-based substrate for MMP2 consisting of a substrate recognition and cleavage site of the enzyme flanked by a FRET pair of fluorescent proteins. Several substrate sites identified in previous studies (145, 146), and from Professor Richard Schulz's unpublished results, were incorporated into this design and tested *in vitro*. Our kinetic studies of these substrates served to refine previously reported consensus sequences and/or specific MMP2 substrate sequences. While we were not successful in developing a biosensor that is selective for MMP2 over other MMPs, our best biosensor was selective to MMPs in general over other proteases (i.e., calpain) that might be present in cardiomyocytes. As a future direction, our collaborator Professor Richard Schulz will undertake the expression of our biosensor in neonatal cardiomyocytes.

5.3 DEVELOPMENT OF H_2O_2 BIOSENSORS

In Chapter 4 we describe the development of two green fluorescent analogues, designed Hyper-Gem1 and Hyper-Gem2, of the hydrogen peroxide (H_2O_2) biosensor HyPer. The Hyper-Gem1 analogue has an inverse response while the Hyper-Gem2 analogue has a direct response. We propose that future work on this project should involve further investigation and characterization of the two new biosensors. In addition, there is likely addition room for improvement and opportunities for creating new color variants.

We demonstrated that the responses of both Hyper-Gem1 and Hyper-Gem2 to H_2O_2 are not pK_a change dependant. This result stands in contrast to results with the GECO series of Ca^{2+} indicators where the analyte response is primarily attributable to a change in chromophore pK_a (87). Notably, the circular permutated fluorescent protein domain of the Hyper-Gem constructs was derived from the GEM-GECO1 Ca^{2+} indicator. It is therefore somewhat surprising that the response of the Hyper-Gem indicators is primarily based on extinction coefficient and/or quantum yield changes.

One of the most important future directions for this project will be to investigate the mechanism of the Hyper-Gem indicators using mutagenesis studies. It is well established that OxyR2 undergoes dimerization and even higher order oligomerization at high concentrations (188). One interesting questions is whether or not this oligomerization also occurs in the Hyper-Gem indicators and whether this plays a role in the fluorescence response. It might be possible to probe this question by introducing mutations that interfere with oligomerization. Furthermore, there have been a few mutations reported in literature, for either OxyR2 and/or HyPer, that should be introduced into these new indicators. One significant example of such a mutation is A233V in OxyR2 (also present in HyPer-2) that was known to double the dynamic range of HyPer (185). Moreover, the OxyR2 regulatory dimerization interface that constitutes amino acids 226-233 and is also included in HyPer and our new variants might be a fertile soil to improve the dynamic range of HyPer analogues by both site directed and random mutagenesis.

Two specific mutations are known to render OxyR2 to be constitutively active are I110D and H114Y (present in HyPer-3) should also be investigated (186). Another aspect that should be investigated thoroughly is the kinetics of oxidation-reduction of the variants discovered, since faster kinetics are generally more preferred in live cell imaging (186). Finally, further

investigation of the role of the OxyR2 domain change with H_2O_2 in the response of the Gem-Hyper variants can be done by mutating the two critical cysteines C199 and C208 of the OxyR2 portion of the biosensors and determining the effect on the fluorescence response.

In our unsuccessful attempt to develop red variants of HyPer, we made an assumption that the circular permutated red fluorescent protein that had been optimized for Ca^{+2} imaging might be universal and only require slight optimization for biosensing of another analyte of interest. This turned out to be more challenging than expected, so future efforts should probably start from cp-mApple-145 and randomize the linkers connecting different parts of the sensing domain (i.e., OxyR) to the fluorescent protein. We should also try the reported mutations of OxyR regulatory domain that have been mentioned in the above two paragraphs.

Although this project might still be in an early stage of development, we are confident that these tools have lots of potential and will ultimately provide a useful contribution to the scientific community interested in reactive oxygen species.

Overall we tried in this thesis to add to the scientific community of biological interest useful tools that might one day provide answers to critical questions and help in a better understanding of the intracellular workings.

Appendix

Oligonucleotide sequence supplement

OLIGO #	Lay ID	SEQUENCE
2.1	PKB-EcoRI-FD	5'- CGC CTA GAA TTC ATG GAC GAC GTG GCC ATC GT-3'
2.2	PKB-BglII-BK	5'- TAG GCG AGA TCT TCA GGC CGT CGC GCT AG-3'
2.3	YLS-FRET- FD primer	5'- CGC CTA GGT ACC TCC GGA CCT AGG TCC GGA GGG TCG ACA TCC GGA-3'
2.4	YLS-FRET-BK primer	5'- TAG GCG GCC GGC CGT TCC GGA ACC TGC AGG TCC GGA TGT CGA CCC-3'
2.5	TFP-XhoI-FD	5'- CGC CTA CTC GAG CAT GGT GAG CAA GGG CGA GGA-3'
2.6	TFP-AvrII-BK	5'- TAG GCG CCT AGG CTT GTA CAG CTC GTC CAT GCC GTC-3'
2.7	TFP-BglII-BK	5’-TAG GCG AGA TCT CTT GTA CAG CTC GTC CAT GCC GTC GGT-3’
2.8	XbaI-LK-TFP-FD	5’-CGC CTA TCT AGA GGA GGA TCC GGA GGT ATG GTG AGC AAG GGC GAG GAG ACC-3’
2.9	TFP194-FD-XhoI	5’-TAT TCT CGA Ga ATG CTG CCC GAC TAT CAC TTT GTG GAC CAC CG-3’
2.10	TFP193-BK-AvrII	5’-AAT ACC TAG GCT TCA CCG CCT TCT TGG CCC TGT AGA T-3’
2.11	TFP-208-FD-XhoI	5’-TAT TCT CGA Ga AAC CAC GAC AAG GAC TAC AAC AAG GTG-3’
2.12	TFP-207-BK-AvrII	5’-AAT ACC TAG GCA GGA TCT CGA TGC GGT GGT C-3’
2.13	TFP-146-FD-XhoI	5’-TAT TCT CGA Ga ACC GGC TGG GAC GCC TCC-3’
2.14	TFP-145-BK-AvrII	5’-AAT ACC TAG GGG TCT TCT TCT GCA TCA CGG GGC C-3’
2.15	XhoI-CyPet-FD	5’-CGC CTA CTC GAG GAT GTC TAA AGG TGA AGA ATT ATT CGG CGG-3’
2.16	CYpet-AvrII-BK	5’GTT AAC CTA GGT TTG TAC AAT TCA TCC ATA CCA TGG GTA ATA CC-3’3’
2.17	mut-FHA2-sens	5’-GAA GAC AAT AGG TTG TCA CGA GTT CAT TGC TTC-3'
2.18	mut-FHA2-antisens	5’-GAA GCA ATG AAC TCG TGA CAA CCT ATT GTC TTC-3’
2.19	FHA2-AvrII-FD	5'- CGC CTA CCT AGG AAG AAA GTT TGG ACA TTT GGT AGA AAC CC-3'

2.20	FHA2-SalI-BK	5'- TAG GCG GTC GAC TAC ACC AAC GGT TAT TTC ATC ACC TTG -3'
2.21	YFP-SbfI-FD	5’-CGC CTA CCT GCA GGA TGG TGA GCA AGG GCG AGG AG-3’
2.22	YFP-stp-HindIII-BK	5'- TAG GCG AAG CTT TTA CTT GTA CAG CTC GTC CAT GCC GAG -3'
2.23	SbfI-cp-Venus-FD	5’-TAT TCC TGC AGG AAT GGA CGG CGG CGT GCA GC-3’
2.24	Cp-Venus-HindIII-BK	5’-AAT AAA GCT TTT ACT CGA TGT TGT GGC GGA TCT TGA AGT TG-3’
2.25	PKB-SUBS-18link-SalI-FD	5’-CGC CTA GTC GAC GGT TCG ACT AGC GGC AGT GGA AAG CCA GGA TCT GGG GAA GGG TCA ACA AAA GGT AGG AA-3'
2.26	PKB-SUBS-18link-SbfI-BD	5'- TAG GCG CCT GCA GGG ATT CCT AGA GTT CCA AGT CTG TCA CGC TTC CTA CCT TTT GTT GAC CCT TCC CCA GA -3'
2.27	SalI-SGLK1-PKB-Sub-FD	5'- CGC CTA GTC GAC GGC GGC AGC GGC GGC AGG AAG CGT GAC AGA CTT GGA ACT CTA GGA ATC-3’
2.28	SalI-SGLK2-PKB -Sub-FD	5'- CGC CTA GTC GAC GGC GGC AGC GGC GGC GGC GGC AGC GGC GGC AGG AAG CGT GAC AGA CTT GGA ACT CTA GGA ATC-3'
2.29	SalI-SGLK3-PKB -Sub-FD	5'- CGC CTA GTC GAC GGC GGC AGC GGC GGC GGC GGC AGC GGC GGC GGC GGC AGC GGC GGC AGG AAG CGT GAC AGA CTT GGA ACT CTA GGA ATC-3'
2.30	SalI-SGLK4-PKB -Sub-FD	5'- CGC CTA GTC GAC GGC GGC AGC GGC GGC GGC GGC AGC GGC GGC GGC GGC AGC GGC GGC GGC GGC AGC GGC GGC AGG AAG CGT GAC AGA CTT GGA ACT CTA G-3'
2.31	SalI-LK0- PKB -Sub-FD	5'- CGC CTA GTC GAC AGG AAG CGT GAC AGA CTT GGA ACT CTA GGA ATC-3'
2.32	SalI-LK2- PKB -Sub-FD	5'- CGC CTA GTC GAC ATC AGG AGG AAG CGT GAC AGA CTT GGA ACT CTA GGA ATC-3'
2.33	SalI-LK4- PKB -Sub-FD	5'- CGC CTA GTC GAC ATC AAC AGC AGG AGG AAG CGT GAC AGA CTT GGA ACT CTA GGA ATC-3'
2.34	SalI-LK6- PKB -Sub-FD	5'- CGC CTA GTC GAC ATC AAC AGC AGG ATC AGG AGG AAG CGT GAC AGA CTT GGA ACT CTA GGA ATC-3'
2.35	SalI-LK8- PKB -Sub-FD	5'- CGC CTA GTC GAC ATC AAC AGC AGG ATC AGG AAC AGG AGG AAG CGT GAC AGA CTT GGA ACT CTA GGA ATC-3'
2.36	SalI-LK10- PKB -Sub-FD	5'- CGC CTA GTC GAC ATC AAC AGC AGG ATC AGG AAC AGG AGC AGG AGG AAG CGT GAC AGA CTT GGA ACT CTA GGA ATC-3'

2.37	SalI-LK14- PKB -Sub-FD	5'- CGC CTA GTC GAC ATC AAC AGC AGG ATC AGG AAC AGG AGC ATC AGG TAC AGC AGG AGG AAG CGT GAC AGA CTT GGA ACT CTA GGA ATC-3'
2.38	SalI-LK20- PKB -Sub-FD	5'- CGC CTA GTC GAC ATC AAC AGC AGG ATC AGG AAC AGG AGC ATC AGG TAC AGC AGC AGG AAG AGG AAC AGG AGG AGG AAG CGT GAC AGA CTT GGA ACT CTA G-3'
2.39	SalI-YLS-EA1-FD	5’-CGC CTA GTC GAC GAA GCG GCG GCG AAA AGG AAG CGT GAC AGA CTT GGA ACT CTA GGA ATC CCT-3’
2.40	SalI-YLS-EA2-FD	5’-CGC CTA GTC GAC GAA GCG GCG GCG AAA GAA GCG GCG GCG AAA AGG AAG CGT GAC AGA CTT GGA ACT CTA GGA ATC CCT-3’
2.41	SalI-YLS-EA3-FD	5’-CGC CTA GTC GAC GAA GCG GCG GCG AAA GAA GCG GCG GCG AAA GAA GCG GCG GCG AAA AGG AAG CGT GAC AGA CTT GGA ACT CTA GGA ATC CCT-3’
2.42	SalI-YLS-EA4-FD	5’-CGC CTA GTC GAC GAA GCG GCG GCG AAA GAA GCG GCG GCG AAA GAA GCG GCG GCG AAA GAA GCG GCG GCG AAA AGG AAG CGT GAC AGA CTT GGA ACT CTA GGA ATC CCT-3’
2.43	SalI-YLS-EA5-FD	5’-CGC CTA GTC GAC GAA GCG GCG GCG AAA GAA GCG GCG GCG AAA GAA GCG GCG GCG AAA GAA GCG GCG GCG AAA GAA GCG GCG GCG AAA AGG AAG CGT GAC AGA CTT GGA ACT CTA GGA ATC CCT-3’
2.44	SalI-YLS-EA6-FD	5’-CGC CTA GTC GAC GAA GCG GCG GCG AAA GAA GCG GCG GCG AAA GAA GCG GCG GCG AAA GAA GCG GCG GCG AAA GAA GCG GCG GCG AAA GAA GCG GCG GCG AAA AGG AAG CGT GAC AGA CTT GGA ACT CTA GGA ATC CCT-3’
2.45	SalI-YLS-EA7-FD	5’-CGC CTA GTC GAC GAA GCG GCG GCG AAA GAA GCG GCG GCG AAA GAA GCG GCG GCG AAA GAA GCG GCG GCG AAA GAA GCG GCG GCG AAA GAA GCG GCG GCG AAA GAA GCG GCG GCG AAA AGG AAG CGT GAC AGA CTT GGA ACT CTA GGA ATC CCT-3’
2.46	SalI-YLS-EA8-FD	5’-CGC CTA GTC GAC GAA GCG GCG GCG AAA GAA GCG GCG GCG AAA GAA GCG GCG GCG AAA GAA GCG GCG GCG AAA GAA GCG GCG GCG AAA GAA GCG GCG GCG AAA GAA GCG GCG GCG AAA GAA GCG GCG GCG AAA AGG AAG CGT GAC AGA CTT GGA ACT CTA GGA ATC CCT-3’
2.47	SalI-YLS-EA9-FD	5’-CGC CTA GTC GAC GAA GCG GCG GCG AAA GAA GCG GCG GCG AAA GAA GCG GCG GCG AAA GAA GCG GCG GCG AAA GAA GCG GCG GCG AAA GAA GCG GCG GCG AAA GAA GCG GCG GCG AAA GAA GCG GCG GCG AAA GAA GCG GCG GCG AAA AGG AAG CGT GAC AGA CTT GGA ACT CTA GGA ATC CCT-3’
2.48	SalI-YLS-EA10-FD	5’-CGC CTA GTC GAC GAA GCG GCG GCG AAA GAA GCG GCG GCG AAA GAA GCG GCG GCG AAA GAA GCG GCG GCG AAA GAA GCG GCG GCG AAA GAA GCG GCG GCG AAA GAA GCG GCG GCG AAA GAA GCG GCG GCG AAA GAA GCG GCG GCG AAA GAA GCG

		GCG GCG AAA AGG AAG CGT GAC AGA CTT GGA ACT CTA GGA ATC CCT-3’
2.49	EcoRI-XmaI – YPET-FD	5’-CGC CTA GAA TTC CCC GGG ATG TCT AAA GGT GAA GAA TTA TTC ACT GGT GTT GTC CCA ATT TTG-3’
2.50	Ypet-BglII-BK	5’-TAG GCG AGA TCT TTA TTA TTT GTA CAA TTC ATT CAT ACC CTC GGT AAT ACC AGC AGC A-3’
2.51	XmaI-polycis-FD	5’-CGC CTA CCC GGG ATG AGC GGT GAA TTA GCA AAT TAC AAA AGA CTT GAG AAA GTC GGT G-3’
2.52	Polycis-BglII-BK	5’-TAG GCG AGA TCT CTA CTT AAG ATT AAA TAG ATT TTG AAA GTT GCT ATG CAT TTC GGA TGT ACA CCA CTT GAA AG-3’
2.53	SalI-SGLK1-CDK-sub-FD	5'-CGC CTA GTC GAC GGC GGC AGC GGC GGC ACC CCT GAG CCT ATT TTG GTT GAT ACT-3'
2.54	SalI-SGLK2-CDK-sub-FD	5'-CGC CTA GTC GAC GGC GGC AGC GGC GGC GGC GGC AGC GGC GGC ACC CCT GAG CCT ATT TTG GTT GAT ACT-3'
2.55	SalI-SGLK3-CDK-sub-FD	5'-CGC CTA GTC GAC GGC GGC AGC GGC GGC GGC GGC AGC GGC GGC GGC GGC AGC GGC GGC ACC CCT GAG CCT ATT TTG GTT GAT ACT-3'
2.56	SalI-SGLK4-CDK-sub-FD	5'-CGC CTA GTC GAC GGC GGC AGC GGC GGC GGC GGC AGC GGC GGC GGC GGC AGC GGC GGC GGC GGC AGC GGC GGC ACC CCT GAG CCT ATT TTG GTT GAT ACT-3'
2.57	SalI-LK0-CDK-sub-FD	5'-CGC CTA GTC GAC ACC CCT GAG CCT ATT TTG GTT GAT ACT-3'
2.58	SalI-LK2-CDK-sub-FD	5'-CGC CTA GTC GAC ATC AGG ACC CCT GAG CCT ATT TTG GTT GAT ACT-3'
2.59	SalI-LK4-CDK-sub-FD	5'-CGC CTA GTC GAC ATC AAC AGC AGG ACC CCT GAG CCT ATT TTG GTT GAT ACT-3'
2.60	SalI-LK6-CDK-sub-FD	5'-CGC CTA GTC GAC ATC AAC AGC AGG ATC AGG ACC CCT GAG CCT ATT TTG GTT GAT ACT-3'
2.61	SalI-LK8-CDK-sub-FD	5'-CGC CTA GTC GAC ATC AAC AGC AGG ATC AGG AAC AGG ACC CCT GAG CCT ATT TTG GTT GAT ACT-3'
2.62	SalI-LK10-CDK-sub-FD	5'-CGC CTA GTC GAC ATC AAC AGC AGG ATC AGG AAC AGG AGC AGG ACC CCT GAG CCT ATT TTG GTT GAT ACT-3'
2.63	SalI-LK14-CDK-sub-FD	5'-CGC CTA GTC GAC ATC AAC AGC AGG ATC AGG AAC AGG AGC ATC AGG TAC AGC AGG ACC CCT GAG CCT ATT TTG GTT GAT ACT-3'

2.64	SalI-LK20-CDK-sub-FD	5'-CGC CTA GTC GAC ATC AAC AGC AGG ATC AGG AAC AGG AGC ATC AGG TAC AGC AGC AGG AAG AGG AAC AGG AGG ACC CCT GAG CCT ATT TTG GTT GAT ACT-3'
2.65	SalI-EA1-CDK-FD	5'-CGC CTA GTC GAC GAA GCG GCG GCG AAA ACC CCT GAG CCT ATT TTG GTT GAT ACT-3'
2.66	SalI-EA2-CDK-FD	5'-CGC CTA GTC GAC GAA GCG GCG GCG AAA GAA GCG GCG GCG AAA ACC CCT GAG CCT ATT TTG GTT GAT ACT-3'
2.67	SalI-EA3-CDK-FD	5'-CGC CTA GTC GAC GAA GCG GCG GCG AAA GAA GCG GCG GCG AAA GAA GCG GCG GCG AAA ACC CCT GAG CCT ATT TTG GTT GAT ACT-3'
2.68	SalI-EA4-CDK-FD	5'-CGC CTA GTC GAC GAA GCG GCG GCG AAA GAA GCG GCG GCG AAA GAA GCG GCG GCG AAA GAA GCG GCG GCG AAA ACC CCT GAG CCT ATT TTG GTT GAT ACT-3'
2.69	SalI-EA5-CDK-FD	5'-CGC CTA GTC GAC GAA GCG GCG GCG AAA GAA GCG GCG GCG AAA GAA GCG GCG GCG AAA GAA GCG GCG GCG AAA GAA GCG GCG GCG AAA ACC CCT GAG CCT ATT TTG GTT GAT ACT-3'
2.70	SalI-EA6-CDK-FD	5'-CGC CTA GTC GAC GAA GCG GCG GCG AAA GAA GCG GCG GCG AAA GAA GCG GCG GCG AAA GAA GCG GCG GCG AAA GAA GCG GCG GCG AAA GAA GCG GCG GCG AAA ACC CCT GAG CCT ATT TTG GTT GAT ACT-3'
2.71	SalI-EA7-CDK-FD	5'-CGC CTA GTC GAC GAA GCG GCG GCG AAA GAA GCG GCG GCG AAA GAA GCG GCG GCG AAA GAA GCG GCG GCG AAA GAA GCG GCG GCG AAA GAA GCG GCG GCG AAA GAA GCG GCG GCG AAA ACC CCT GAG CCT ATT TTG GTT GAT ACT-3'
2.72	SalI-EA8-CDK-FD	5'-CGC CTA GTC GAC GAA GCG GCG GCG AAA GAA GCG GCG GCG AAA GAA GCG GCG GCG AAA GAA GCG GCG GCG AAA GAA GCG GCG GCG AAA GAA GCG GCG GCG AAA GAA GCG GCG GCG AAA GAA GCG GCG GCG AAA ACC CCT GAG CCT ATT TTG GTT GAT ACT-3'
2.73	SalI-EA8-CDK-FD	5'-CGC CTA GTC GAC GAA GCG GCG GCG AAA GAA GCG GCG GCG AAA GAA GCG GCG GCG AAA GAA GCG GCG GCG AAA GAA GCG GCG GCG AAA GAA GCG GCG GCG AAA GAA GCG GCG GCG AAA GAA GCG GCG GCG AAA ACC CCT GAG CCT ATT TTG GTT GAT ACT-3'
2.74	SALI-EA10-CDK-FD	5'-CGC CTA GTC GAC GAA GCG GCG GCG AAA GAA GCG GCG GCG AAA GAA GCG GCG GCG AAA GAA GCG GCG GCG AAA GAA GCG GCG GCG AAA GAA GCG GCG GCG AAA GAA GCG GCG GCG AAA GAA GCG GCG GCG AAA GAA GCG GCG GCG AAA GAA GCG GCG GCG AAA ACC CCT GAG CCT ATT TTG GTT GAT ACT-3'
2.75	YFP-STp-SbFI-BK	5'-TAG GCG CCT GCA GGT TAC TTG TAC AGC TCG TCC ATG CCG AG-3'

2.76	Ypet-stp-sbfI-BK	5'-TAG GCG CCT GCA GGT TAT TTG TAC AAT TCA TTC ATA CCC TC-3'
3.1	XhoI-CYPET-FR	5'-CGC CTA CTC GAG GAT GTC TAA AGG TGA AGA ATT ATT CGG CGG-3'
3.2	BglII-CYPET-BK	5'-TAG GCG AGA TCT TTT GTA CAA TTC ATC CAT ACC ATG GGT AAT ACC-3'
3.3	KpnI-YPET-FR	5'-CGC CTA GGT ACC ATG TCT AAA GGT GAA GAA TTA TTC ACT GGT GTT-3'
3.4	YPET-STP-HindIII	5'-TAG GCG AAG CTT TTA TTA TTT GTA CAA TTC ATT CAT ACC CTC GGT AAT ACC-3'
3.5	BglII-TnI1-FR	5'-CGC CTA AGA TCT ATT AGC GCG AGC CGC AAA CTG CAG CTG AAA ACC CTG CTG CTG CAG AT-3'
3.6	TnI1-KpnI-BK	5'-TAG GCG GGT ACC TTC GCG TTC CAG TTC CTG TTT CGC AAT CTG CAG CAG CAG GGT TTT C-3'
3.7	BglII-TnI2-FR	5'-CGC CTA AGA TCT CGC GAA CCG CGC CCG GCG CCG GCG CCG ATT CGC C-3'
3.8	TnI2-kpnI-Bk	5'-TAG GCG GGT ACC ATA GTT GCT GCT GCG GCG GCG AAT CGG CGC CGG CG-3'
3.9	BglII-Ctrl-MMP2-Fw	5'-CGC CTA AGA TCT GGC GGC AGC GGC GGC ATT CCG GTG AGC CTG CGC AGC-3'
3.10	Ctrl-MMP2-KpnI-BK	5'-TAG GCG GGT ACC GCC GCC GCT GCC GCC GCC GCT GCG CAG GCT CAC CGG AA-3'
4.1	Oxy-81-XhoI-N-FD	5’-TAT TCT CGA GGG AGA TGG CAA GCC AG-3’
4.2	OxyR-205-PVVSERM-BK	5’-CAT CCG CTC GGA AAC CAC GGG CAT TGC CTG ATC GCG CAA AC-3’
4.3	Oxy-81-206-SAG-RED-BK	5’-CTC GGG GTA CAT CCG CTC GGA GCC CGC GCT CAT TGC CTG ATC GCG CAA ACA GTG ACC A-3’
4.5	SAG-red-GECO-FD	5’- GCA ATG AGC GCG GGC TCC GAG CGG ATG TAC CCC GAG GAC GGC GCC CTG AAG-3’
4.6	Oxy-206-SAG-G-GECO-BK	5’- CTT GTC GGC CTT GAT ATA GAC GTT GCC GGC GGA CAT TGC CTG ATC GCG CA-3’
4.7	SAG-GEM FD	5’-ATG TCC GCC GGC AAC GTG TAT ATA AAG GCC GAC GAG-3’
4.8	SAG-G-GECO-	5- ATG TCC GCC GGC ACG TCT ATA TCA AGG CCG AC-3’

	FD	
4.9	OxyR205-PENV-GEM-BK	5’- GTC GGC CTT TAT ATA CAC GTT CTC TGG TGC CTG ATC GCG CAA AC-3’
4.10	PENV-GEM-FD	5’-CCA GAG AAC GTG TAT ATA AAG GCC GAC G-3’
4.11	GEM-KpnI-BK	5’-TAG GCG GGT ACC GCT GTA CTC CAG CTT GTG CCC-3’
4.12	OxyR205-LENV-G-GECO-BK	5’-GTC GGC CTT GAT ATA GAC GTT CTC GAG TGC CTG ATC GCG CAA AC-3’
4.13	LENV-G-GECO-FD	5’-CTC GAG AAC GTC TAT ATC AAG GCC GAC-3’
4.14	G-GECO-KpnI-BK	5’-TAG GCG GGT ACC CTT GTA GTT GCC GTC GTC CTT-3’
4.15	PVV –RED-cpFP fw	5’-CCC GTG GTT TCC GAG CGG ATG-3’
4.16	RED-cpFP-KpnI-BK	5’-AAT AGG TAC CAG CCT CCC AGC CCA TGG TCT-3’
4.17	OxyR-206-KpnI-FD	5’-GGT ACC GGT TTC TGT TTT GAA GCC GGG G-3’
4.18	OxyR-305-HindIII-BK	5’-AAT AAA GCT TTT AAA CCG CCT GTT TTA AAA CTT T-3’

REFERENCES

1. lakowicz, J. (2006) *Principles of Fluorescence Spectroscopy*, 3rd ed., Springer Science & Business Media, LLC, New York.
2. Coons, A. H., Creech, H. J., Jones, R. N., and Berliner, E. (1942) The Demonstration of Pneumococcal Antigen in Tissues by the Use of Fluorescent Antibody, *Journal of Immunology 45*, 159-170.
3. Bloom, F. E., Wedner, H. J., and Parker, C. W. (1973) Use of Antibodies to Study Cell Structure and Metabolism, *Pharmacological Reviews 25*, 343-358.
4. Ross, A. H., Baltimore, D., and Eisen, H. N. (1981) Phosphotyrosine-Containing Proteins Isolated by Affinity-Chromatography with Antibodies to a Synthetic Hapten, *Nature 294*, 654-656.
5. Heffetz, D., Fridkin, M., and Zick, Y. (1989) Antibodies Directed Against Phosphothreonine Residues as Potent Tools for Studying Protein-Phosphorylation, *European Journal of Biochemistry 182*, 343-348.
6. Kaufmann, H., Bailey, J. E., and Fussenegger, M. (2001) Use of Antibodies for Detection of Phosphorylated Proteins Separated by Two-Dimensional Gel Electrophoresis, *Proteomics 1*, 194-199.
7. Taylor, D. L., and Wang, Y. L. (1978) Molecular Cytochemistry - Incorporation of Fluorescently Labeled Actin into Living Cells, *Proceedings of the National Academy of Sciences. U. S. A. 75*, 857-861.
8. Taylor, D. L., Amato, P. A., Lubyphelps, K., and McNeil, P. (1984) Fluorescent Analog Cyto-Chemistry, *Trends in Biochemical Sciences 9*, 88-91.

9. Tsien, R. Y. (1989) Fluorescent-Probes of Cell Signaling, *The Annual Review of* Neuroscience *12*, 227-253.

10. Shimomura, O., Johnson, F. H., and Saiga, Y. (1962) Extraction, Purification and Properties of Aequorin, a Bioluminescent Protein from *Luminous Hydromedusan*, *Aequorea*, *Journal of Cellular and Comparative Physiology 59*, 223-&.

11. Johnson, F. H., Gershman, L. C., Waters, J. R., Reynolds, G. T., Saiga, Y., and Shimomura, O. (1962) Quantum Efficiency of *Cypridina* Luminescence, with a Note on That of *Aequorea*, *Journal of Cellular and Comparative Physiology 60*, 85-&.

12. Shimomura, O. (1979) Structure of the Chromophore of *Aequorea* Green Fluorescent Protein, *FEBS Letters 104*, 220-222.

13. Cody, C. W., Prasher, D. C., Westler, W. M., Prendergast, F. G., and Ward, W. W. (1993) Chemical-Structure of the Hexapeptide Chromophore of the *Aequorea* Green-Fluorescent Protein, *Biochemistry 32*, 1212-1218.

14. Prasher, D. C., Eckenrode, V. K., Ward, W. W., Prendergast, F. G., and Cormier, M. J. (1992) Primary Structure of the *Aequorea Victoria* Green-Fluorescent Protein, *Gene 111*, 229-233.

15. Chalfie, M., Tu, Y., Euskirchen, G., Ward, W. W., and Prasher, D. C. (1994) Green Fluorescent Protein as a Marker for Gene-Expression, *Science 263*, 802-805.

16. Inouye, S., and Tsuji, F. I. (1994) *Aequorea* Green Fluorescent Protein - Expression of the Gene and Fluorescence Characteristics of the Recombinant Protein, *FEBS Letters 341*, 277-280.

17. Heim, R., Prasher, D. C., and Tsien, R. Y. (1994) Wavelength Mutations and Posttranslational Autoxidation of Green Fluorescent Protein, *Proceedings of the National Academy of Sciences. U. S. A. 91*, 12501-12504.

18. Cubitt, A. B., Heim, R., Adams, S. R., Boyd, A. E., Gross, L. A., and Tsien, R. Y. (1995) Understanding, Improving and Using Green Fluorescent Proteins, *Trends in Biochemical Sciences 20*, 448-455.

19. Rosenow, M. A., Huffman, H. A., Phail, M. E., and Wachter, R. M. (2004) The Crystal Structure of the Y66L Variant of Green Fluorescent Protein Supports a Cyclization-Oxidation-Dehydration Mechanism for Chromophore Maturation, *Biochemistry 43*, 4464-4472.

20. Zhang, L. P., Patel, H. N., Lappe, J. W., and Wachter, R. M. (2006) Reaction Progress of Chromophore Biogenesis in Green Fluorescent Protein, *Journal of the American Chemical Society 128*, 4766-4772.

21. Pouwels, L. J., Zhang, L., Chan, N. H., Dorrestein, P. C., and Wachter, R. M. (2008) Kinetic Isotope Effect Studies on the De novo Rate of Chromophore Formation in Fast- and Slow-Maturing GFP Variants, *Biochemistry 47*, 10111-10122.

22. Matz, M. V., Fradkov, A. F., Labas, Y. A., Savitsky, A. P., Zaraisky, A. G., Markelov, M. L., and Lukyanov, S. A. (1999) Fluorescent Proteins from Nonbioluminescent *Anthozoa* Species, *Nature Biotechnology 17*, 969-973.

23. Baird, G. S., Zacharias, D. A., and Tsien, R. Y. (2000) Biochemistry, Mutagenesis, and Oligomerization of DsRed, a Red Fluorescent Protein from Coral, *Proceedings of the National Academy of Sciences. U. S. A. 97*, 11984-11989.

24. Gross, L. A., Baird, G. S., Hoffman, R. C., Baldridge, K. K., and Tsien, R. Y. (2000) The Structure of the Chromophore within DsRed, a Red Fluorescent Protein from Coral, *Proceedings of the National Academy of Sciences. U. S. A. 97*, 11990-11995.

25. Strack, R. L., Strongin, D. E., Mets, L., Glick, B. S., and Keenan, R. J. (2010) Chromophore Formation in DsRed Occurs by a Branched Pathway, *Journal of the American Chemical Society 132*, 8496-8505.

26. Bravaya, K. B., Subach, O. M., Korovina, N., Verkhusha, V. V., and Krylov, A. I. (2012) Insight into the Common Mechanism of the Chromophore Formation in the Red Fluorescent Proteins: The Elusive Blue Intermediate Revealed, *Journal of the American Chemical Society 134*, 2807-2814.

27. Ormo, M., Cubitt, A. B., Kallio, K., Gross, L. A., Tsien, R. Y., and Remington, S. J. (1996) Crystal structure of the *Aequorea Victoria* green fluorescent protein, *Science 273*, 1392-1395.

28. Yang, F., Moss, L. G., and Phillips, G. N. (1996) The Molecular Structure of Green Fluorescent Protein, *Nature Biotechnology 14*, 1246-1251.

29. Cubitt, A. B., Woollenweber, L. A., and Heim, R. (1999) Understanding Structure-Function Relationships in the *Aequorea Victoria* Green Fluorescent Protein, *Methods in Cell Biology, Vol 58 58*, 19-+.

30. Shaner, N. C., Campbell, R. E., Steinbach, P. A., Giepmans, B. N. G., Palmer, A. E., and Tsien, R. Y. (2004) Improved Monomeric Red, Orange and Yellow Fluorescent Proteins Derived from *Discosoma* Sp Red Fluorescent Protein, *Nature Biotechnology 22*, 1567-1572.

31. Hein, R., and Tsien, R. Y. (1996) Engineering Green Fluorescent Protein for Improved Brightness, Longer Wavelengths and Fluorescence Resonance Energy Transfer, *Current Biology 6*, 178-182.

32. Wachter, R. M., Elsliger, M. A., Kallio, K., Hanson, G. T., and Remington, S. J. (1998) Structural Basis of Spectral Shifts in the Yellow-Emission Variants of Green Fluorescent Protein, *Structure with Folding & Design 6*, 1267-1277.

33. Wall, M. A., Socolich, M., and Ranganathan, R. (2000) The Structural Basis for Red Fluorescence in the Tetrameric GFP Homolog DsRed, *Nature Structural Biology 7*, 1133-1138.

34. Yarbrough, D., Wachter, R. M., Kallio, K., Matz, M. V., and Remington, S. J. (2001) Refined Crystal Structure of DsRed, a Red Fluorescent Protein from Coral, at 2.0-Angstrom Resolution, *Proceedings of the National Academy of Sciences. U. S. A. 98*, 462-467.

35. Campbell, R. E., Tour, O., Palmer, A. E., Steinbach, P. A., Baird, G. S., Zacharias, D. A., and Tsien, R. Y. (2002) A Monomeric Red Fluorescent Protein, *Proceedings of the National Academy of Sciences. U. S. A. 99*, 7877-7882.

36. Shaner, N. C., Lin, M. Z., McKeown, M. R., Steinbach, P. A., Hazelwood, K. L., Davidson, M. W., and Tsien, R. Y. (2008) Improving the Photostability of Bright Monomeric Orange and Red Fluorescent Proteins, *Nature Methods 5*, 545-551.

37. Davidson, M. W., and Campbell, R. E. (2009) Engineered Fluorescent Proteins: Innovations and Applications, *Nature Methods 6*, 713-717.

38. Kogure, T., Karasawa, S., Araki, T., Saito, K., Kinjo, M., and Miyawaki, A. (2006) A Fluorescent Variant of a Protein from the Stony Coral *Montipora* Facilitates Dual-Color

Single-Laser Fluorescence Cross-Correlation Spectroscopy, *Nature Biotechnology 24*, 577-581.

39. Lim, D. V., Simpson, J. M., Kearns, E. A., and Kramer, M. F. (2005) Current and Developing Technologies for Monitoring Agents of Bioterrorism and Biowarfare, *Clinical Microbiology Reviews 18*, 583-607.

40. Forster, T. (1959) 10th Spiers Memorial Lecture - Transfer Mechanisms of Electronic Excitation, *Discussions of the Faraday Society*, 7-17.

41. Forster, T. (1946) Energiewanderung Und Fluoreszenz, *Naturwissenschaften 33*, 166-175.

42. Campbell, R. E. (2009) Fluorescent-Protein-Based Biosensors: Modulation of Energy Transfer as a Design Principle, *Analytical Chemistry 81*, 5972-5979.

43. Ibraheem, A., and Campbell, R. E. (2010) Designs and Applications of Fluorescent Protein-Based Biosensors, *Current Opinion in Chemical Biology 14*, 30-36.

44. Ai, H.-w., Hazelwood, K. L., Davidson, M. W., and Campbell, R. E. (2008) Fluorescent Protein FRET Pairs for Ratiometric Imaging of Dual Biosensors, *Nature Methods 5*, 401-403.

45. Ouyang, M., Huang, H., Shaner, N. C., Remacle, A. G., Shiryaev, S. A., Strongin, A. Y., Tsien, R. Y., and Wang, Y. (2010) Simultaneous Visualization of Protumorigenic Src and MT1-MMP Activities with Fluorescence Resonance Energy Transfer, *Cancer Research 70*, 2204-2212.

46. Lam, A. J., St-Pierre, F., Gong, Y., Marshall, J. D., Cranfill, P. J., Baird, M. A., McKeown, M. R., Wiedenmann, J., Davidson, M. W., Schnitzer, M. J., Tsien, R. Y., and

Lin, M. Z. (2012) Improving FRET Dynamic Range with Bright Green and Red fluorescent proteins, *Nature Methods 9*, 1005-1012.

47. Miyawaki, A., Llopis, J., Heim, R., McCaffery, J. M., Adams, J. A., Ikura, M., and Tsien, R. Y. (1997) Fluorescent Indicators for Ca2+ Based on Green Fluorescent Proteins and Calmodulin, *Nature 388*, 882-887.

48. Miyawaki, A., Griesbeck, O., Heim, R., and Tsien, R. Y. (1999) Dynamic and Quantitative Ca2+ Measurements Using Improved Cameleons, *Proceedings of the National Academy of Sciences. U. S. A. 96*, 2135-2140.

49. Palmer, A. E., Giacomello, M., Kortemme, T., Hires, S. A., Lev-Ram, V., Baker, D., and Tsien, R. Y. (2006) Ca2+ Indicators Based on Computationally Redesigned Calmodulin-Peptide Pairs, *Chemistry & Biology 13*, 521-530.

50. Quiocho, F. A., and Ledvina, P. S. (1996) Atomic Structure and Specificity of Bacterial Periplasmic Receptors for Active Transport and Chemotaxis: Variation of Common Themes, *Molecular Microbiology 20*, 17-25.

51. Dwyer, M. A., and Hellinga, H. W. (2004) Periplasmic Binding Proteins: a Versatile Superfamily for Protein Engineering, *Current Opinion in Structural Biology 14*, 495-504.

52. Lager, I., Fehr, M., Frommer, W. B., and Lalonde, S. W. (2003) Development of a Fluorescent Nanosensor for Ribose, *FEBS Lett. 553*, 85-89.

53. Deuschle, K., Chaudhuri, B., Okumoto, S., Lager, I., Lalonde, S., and Frommer, W. B. (2006) Rapid Metabolism of Glucose Detected with FRET Glucose Nanosensors in Epidermal Cells and Intact Roots of Arabidopsis RNA-Silencing Mutants, *Plant Cell 18*, 2314-2325.

54. Lager, I., Looger, L. L., Hilpert, M., Lalonde, S., and Frommer, W. B. (2006) Conversion of a Putative Agrobacterium Sugar-Binding Protein into a FRET Sensor with High Selectivity for Sucrose, *Journal of Biological Chemistry 281*, 30875-30883.

55. Hires, S. A., Zhu, Y., and Tsien, R. Y. (2008) Optical Measurement of Synaptic Glutamate Spillover and Reuptake by Linker Optimized Glutamate-Sensitive Fluorescent Reporters, *Proceedings of the National Academy of Sciences. U. S. A. 105*, 4411-4416.

56. Kaper, T., Looger, L. L., Takanaga, H., Platten, M., Steinman, L., and Frommer, W. B. (2007) Nanosensor Detection of an Immunoregulatory Tryptophan Influx/Kynurenine Efflux Cycle, *Plos Biology 5*, 2201-2210.

57. Gu, H., Lalonde, S., Okumoto, S., Looger, L. L., Scharff-Poulsen, A. M., Grossman, A. R., Kossmann, J., Jakobsen, I., and Frommer, W. B. (2006) A Novel Analytical Method for *in Vivo* Phosphate Tracking, *FEBS Letters 580*, 5885-5893.

58. Zhang, J., and Allen, M. D. (2007) FRET-based Biosensors for Protein Kinases: Illuminating the Kinome, *Molecular Biosystems 3*, 759-765.

59. Lin, C. W., Jao, C. Y., and Ting, A. Y. (2004) Genetically Encoded Fluorescent Reporters of Histone Methylation in Living Cells, *Journal of the American Chemical Society 126*, 5982-5983.

60. Carrillo, L. D., Krishnamoorthy, L., and Mahal, L. K. (2006) A cellular FRET-Based Sensor for Beta-O-GlcNAc, a Dynamic Carbohydrate Modification Involved in Signaling, *Journal of the American Chemical Society 128*, 14768-14769.

61. Ai, H.-w., Henderson, J. N., Remington, S. J., and Campbell, R. E. (2006) Directed Evolution of a Monomeric, Bright and Photostable Version of *Clavularia* Cyan

Fluorescent Protein: Structural Characterization and Applications in Fluorescence Imaging, *Biochemical Journal 400*, 531-540.

62. Tsai, M.-T., Cheng, Y.-H., Liu, Y.-N., Liao, N.-C., Lu, W.-W., and Kung, S.-H. (2009) Real-Time Monitoring of Human Enterovirus (HEV)-Infected Cells and Anti-HEV 3C Protease Potency by Fluorescence Resonance Energy Transfer, *Antimicrobial Agents and Chemotherapy 53*, 748-755.

63. Sabariegos, R., Picazo, F., Domingo, B., Franco, S., Martinez, M.-A., and Llopis, J. (2009) Fluorescence Resonance Energy Transfer-Based Assay for Characterization of Hepatitis C Virus NS3-4A Protease Activity in Live Cells, *Antimicrobial Agents and Chemotherapy 53*, 728-734.

64. Hwang, Y.-C., Chu, J. J.-H., Yang, P. L., Chen, W., and Yates, M. V. (2008) Rapid Identification of Inhibitors that Interfere with Poliovirus Replication Using a Cell-Based Assay, *Antiviral Research 77*, 232-236.

65. Chumakov, S. P., Kravchenko, Y. E., and Chumakov, P. M. (2012) Protein Complementation as Tool for Studying Protein-Protein Interactions in Living Cells, *The Journal of Molecular Biology 46*, 627-638.

66. Johnsson, N., and Varshavsky, A. (1994) Split Ubiquitin as a Sensor of Protein Interactions in-Vivo, *Proceedings of the National Academy of Sciences. U. S. A. 91*, 10340-10344.

67. Hu, C. D., Chinenov, Y., and Kerppola, T. K. (2002) Visualization of Interactions among BZip and Rel Family Proteins in Living Cells Using Bimolecular Fluorescence Complementation, *Molecular Cell 9*, 789-798.

68. Jach, G., Pesch, M., Richter, K., Frings, S., and Uhrig, J. F. (2006) An Improved mRFP1 Adds Red to Bimolecular Fluorescence Complementation, *Nature Methods 3*, 597-600.

69. Kodama, Y., and Hu, C.-D. (2010) An Improved Bimolecular Fluorescence Complementation Assay with a High Signal-to-Noise Ratio, *Biotechniques 49*, 793-805.

70. Pelletier, J. N., Campbell-Valois, F. X., and Michnick, S. W. (1998) Oligomerization Domain-Directed Reassembly of Active Dihydrofolate Reductase From Rationally Designed Fragments, *Proceedings of the National Academy of Sciences. U. S. A. 95*, 12141-12146.

71. Chumakov, S. P., Ilyinskaya, G. V., Kravchenko, J. E., Frolova, E. I., Prasolov, V. S., and Chumakov, P. M. (2008) Lentiviral Vector-Based Aassay System for Quantitative Detection of Intracellular Ttranslocations of Recombinant Proteins, *The Journal of Molecular Biology 42*, 894-900.

72. Moosmann, P., and Rusconi, S. (1996) Alpha Complementation of LacZ in Mammalian Cells, *Nucleic Acids Research 24*, 1171-1172.

73. Wehr, M. C., Laage, R., Bolz, U., Fischer, T. M., Gruenewald, S., Scheek, S., Bach, A., Nave, K.-A., and Rossner, M. J. (2006) Monitoring Regulated Protein-Protein Interactions Using Split TEV, *Nature Methods 3*, 985-993.

74. Paulmurugan, R., and Gambhir, S. S. (2003) Monitoring Protein-Protein Interactions Using Split Synthetic Renilla Luciferase Protein-Fragment-Assisted Complementation, *Analytical Chemistry 75*, 1584-1589.

75. Ghosh, I., Hamilton, A. D., and Regan, L. (2000) Antiparallel Leucine Zipper-Directed Protein Reassembly: Application to the Green Fluorescent Protein, *Journal of the American Chemical Society 122*, 5658-5659.

76. Kerppola, T. K. (2008) Biomolecular Fluorescence Complementation (BiFC) Analysis as a Probe of Protein Interactions in Living Cells, in *Annual Review of Biophysics*, pp 465-487.

77. Kerppola, T. K. (2008) Bimolecular fluorescence complementation: Visualization of Molecular Interactions in Living Cells, *Methods in Cell Biology 85,* 431-470.

78. Ding, Z., Liang, J., Lu, Y., Yu, Q., Zhou, S., Lin, S.-Y., and Mills, G. B. (2006) A Retrovirus-Based Protein Complementation Assay Screen Reveals Functional AKT1-Binding Partners, *Proceedings of the National Academy of Sciences. U. S. A. 103*, 15014-15019.

79. Kojima, T., Karasawa, S., Miyawaki, A., Tsumuraya, T., and Fujii, I. (2011) Novel Screening System for Protein-Protein Interactions by Bimolecular Fluorescence Complementation in *Saccharomyces Cerevisiae*, *Journal of Bioscience and Bioengineering 111*, 397-401.

80. Shyu, Y. J., Liu, H., Deng, X. H., and Hu, C. D. (2006) Identification of New Fluorescent Protein Fragments for Bimolecular Fluorescence Complementation Analysis under Physiological Conditions, *Biotechniques 40*, 61-66.

81. Ohashi, K., Kiuchi, T., Shoji, K., Sampei, K., and Mizuno, K. (2012) Visualization of Cofilin-actin and Ras-Raf Interactions by Bimolecular Fluorescence Complementation Assays Using a New Pair of Split Venus Fragments, *Biotechniques 52*, 45-50.

82. Fan, J.-Y., Cui, Z.-Q., Wei, H.-P., Zhang, Z.-P., Zhou, Y.-F., Wang, Y.-P., and Zhang, X.-E. (2008) Split MCherry as a New Red Bimolecular Fluorescence Complementation System for Visualizing Protein-Protein Interactions in Living Cells, *Biochemical and Biophysical Research Communications 367*, 47-53.

83. Chu, J., Zhang, Z., Zheng, Y., Yang, J., Qin, L., Lu, J., Huang, Z.-L., Zeng, S., and Luo, Q. (2009) A Novel Far-red Bimolecular Fluorescence Complementation System that Allows for Efficient Visualization of Protein Interactions under Physiological Conditions, *Biosensors & Bioelectronics 25*, 234-239.

84. Hu, C. D., and Kerppola, T. K. (2003) Simultaneous Visualization of Multiple Protein Interactions in Living Cells Using Multicolor Fluorescence Complementation Analysis, *Nature Biotechnology 21*, 539-545.

85. Grinberg, A. V., Hu, C. D., and Kerppola, T. K. (2004) Visualization of Myc/Max/Mad Family Dimers and the Competition for Dimerization in Living Cells, *Molecular and Cellular Biology 24*, 4294-4308.

86. Frommer, W. B., Davidson, M. W., and Campbell, R. E. (2009) Genetically Encoded Biosensors Based on Engineered Fluorescent Proteins, *Chemical Society Reviews 38*, 2833-2841.

87. Zhao, Y., Araki, S., Jiahui, W., Teramoto, T., Chang, Y.-F., Nakano, M., Abdelfattah, A. S., Fujiwara, M., Ishihara, T., Nagai, T., and Campbell, R. E. (2011) An Expanded Palette of Genetically Encoded Ca2+ Indicators, *Science 333*, 1888-1891.

88. Patterson, G. H., Knobel, S. M., Sharif, W. D., Kain, S. R., and Piston, D. W. (1997) Use of the Green Fluorescent Protein and its Mutants in Quantitative Fluorescence Microscopy, *Biophysical Journal 73*, 2782-2790.

89. Llopis, J., McCaffery, J. M., Miyawaki, A., Farquhar, M. G., and Tsien, R. Y. (1998) Measurement of Cytosolic, Mitochondrial, and Golgi pH in Single Living Cells with Green Fluorescent Proteins, *Proceedings of the National Academy of Sciences. U. S. A. 95*, 6803-6808.

90. Miesenbock, G., De Angelis, D. A., and Rothman, J. E. (1998) Visualizing Secretion and Synaptic Transmission with pH-Sensitive Green Fluorescent Proteins, *Nature 394*, 192-195.

91. Nakabayashi, T., Wang, H.-P., Kinjo, M., and Ohta, N. (2008) Application of Fluorescence Lifetime Imaging of Enhanced Green Fluorescent Protein to Intracellular pH Measurements, *Photochemical & Photobiological Sciences 7*, 668-670.

92. Bizzarri, R., Serresi, M., Luin, S., and Beltram, F. (2009) Green fluorescent protein Based pH Indicators for *In Vivo* Use: a Review, *Analytical and Bioanalytical Chemistry 393*, 1107-1122.

93. Johnson, D. E., Ai, H.-w., Wong, P., Young, J. D., Campbell, R. E., and Casey, J. R. (2009) Red Fluorescent Protein pH Biosensor to Detect Concentrative Nucleoside Transport, *Journal of Biological Chemistry 284*, 20499-20511.

94. Serresi, M., Bizzarri, R., Cardarelli, F., and Beltram, F. (2009) Real-time Measurement of Endosomal Acidification by a Novel Genetically Encoded Biosensor, *Analytical and Bioanalytical Chemistry 393*, 1123-1133.

95. Jayaraman, S., Haggie, P., Wachter, R. M., Remington, S. J., and Verkman, A. S. (2000) Mechanism and Cellular Applications of a Green Fluorescent Protein-Based Halide Sensor, *Journal of Biological Chemistry 275*, 6047-6050.

96. Wachter, R. M., Yarbrough, D., Kallio, K., and Remington, S. J. (2000) Crystallographic and Energetic Analysis of Binding of Selected Anions to the Yellow Variants of Green Fluorescent Protein, *Journal of Molecular Biology 301*, 157-171.

97. Ostergaard, H., Henriksen, A., Hansen, F. G., and Winther, J. R. (2001) Shedding Light on Disulfide Bond Formation: Engineering a Redox Switch in Green Fluorescent Protein, *Embo Journal 20*, 5853-5862.

98. Dooley, C. T., Dore, T. M., Hanson, G. T., Jackson, W. C., Remington, S. J., and Tsien, R. Y. (2004) Imaging Dynamic Redox Changes in Mammalian Cells with Green Fuorescent Protein Indicators, *Journal of Biological Chemistry 279*, 22284-22293.

99. Hanson, G. T., Aggeler, R., Oglesbee, D., Cannon, M., Capaldi, R. A., Tsien, R. Y., and Remington, S. J. (2004) Investigating Mitochondrial Redox Potential with Redox-Sensitive Green Fluorescent Protein Indicators, *Journal of Biological Chemistry 279*, 13044-13053.

100. Baird, G. S., Zacharias, D. A., and Tsien, R. Y. (1999) Circular Permutation and Receptor Insertion within Green Fluorescent Proteins, *Proceedings of the National Academy of Sciences. U. S. A. 96*, 11241-11246.

101. Nagai, T., Sawano, A., Park, E. S., and Miyawaki, A. (2001) Circularly Permuted Green Fluorescent Proteins Engineered to Sense Ca2+, *Proceedings of the National Academy of Sciences. U. S. A. 98*, 3197-3202.

102. Akerboom, J., Rivera, J. D. V., Guilbe, M. M. R., Malave, E. C. A., Hernandez, H. H., Tian, L., Hires, S. A., Marvin, J. S., Looger, L. L., and Schreiter, E. R. (2009) Crystal Structures of the GCaMP Calcium Sensor Reveal the Mechanism of Fluorescence Signal Change and Aid Rational Design, *Journal of Biological Chemistry 284*, 6455-6464.

103. Souslova, E. A., Belousov, V. V., Lock, J. G., Stromblad, S., Kasparov, S., Bolshakov, A. P., Pinelis, V. G., Labas, Y. A., Lukyanov, S., Mayr, L. M., and Chudakov, D. M. (2007)

Single Fluorescent Protein-Based Ca2+ Sensors with Increased Dynamic Range, *BMC Biotechnology 7*.

104. Mizuno, T., Murao, K., Tanabe, Y., Oda, M., and Tanaka, T. (2007) Metal-Ion-Dependent GFP Emission *In Vivo* by Combining a Circularly Permutated Green Fluorescent Protein with an Engineered Metal-ion-Binding Coiled-Coil, *Journal of the American Chemical Society 129*, 11378-11383.

105. Nausch, L. W. M., Lecloux, J., Bonev, A. D., Nelson, M. T., and Dostmann, W. R. (2008) Differential Patterning of cGMP in Vascular Smooth Muscle Cells Revealed by Single GFP-Linked Biosensors, *Proceedings of the National Academy of Sciences. U. S. A. 105*, 365-370.

106. Berg, J., Hung, Y. P., and Yellen, G. (2009) A Genetically Encoded Fluorescent Reporter of ATP:ADP Ratio, *Nature Methods 6*, 161-166.

107. Ibraheem, A., Yap, H., Ding, Y. D., and Campbell, R. E. (2011) A Bacteria Colony-Based Screen for Optimal Linker Combinations in Genetically Encoded Biosensors, *BMC Biotechnology 11*, 105.

108. Förster, T. (1948) Zwischenmolekulare Energiewanderung und Fluoreszenz, *Annalen der Physik 437*, 55-75.

109. Jares-Erijman, E. A., and Jovin, T. M. (2003) FRET Imaging, *Nature Biotechnology 21*, 1387-1395.

110. Aoki, K., Komatsu, N., Hirata, E., Kamioka, Y., and Matsuda, M. (2012) Stable Expression of FRET Biosensors: A New Light in Cancer Research, *Cancer Science 103*, 614-619.

111. Piljic, A., de Diego, I., Wilmanns, M., and Schultz, C. (2011) Rapid Development of Genetically Encoded FRET Reporters, *ACS Chemical Biology 6*, 685-691.

112. Schifferer, M., and Griesbeck, O. A Dynamic FRET Reporter of Gene Expression Improved by Functional Screening, *Journal of the American Chemical Society 134*, 15185-15188.

113. Cheng, Z., and Campbell, R. E. (2006) Assessing the Structural Stability of Designed Beta-Hairpin Peptides in the Cytoplasm of Live Cells, *Chembiochem 7*, 1147-1150.

114. Schagger, H., and Vonjagow, G. (1987) Tricine Sodium Dodecyl-Sulfate Polyacrylamide-Gel Electrophoresis for the Separation of Proteins in the Range from 1-Kda to 100-Kda, *Analytical Biochemistry 166*, 368-379.

115. Franke, T. F. (2008) PI3K/Akt: Getting It Right Matters, *Oncogene 27*, 6473-6488.

116. Bellacosa, A., Franke, T. F., Gonzalezportal, M. E., Datta, K., Taguchi, T., Gardner, J., Cheng, J. Q., Testa, J. R., and Tsichlis, P. N. (1993) Structure, Expression and Chromosomal Mapping of C-Akt - Relationship to V-Akt and Its Implications, *Oncogene 8*, 745-754.

117. Bellacosa, A., Testa, Staal, S. P., and Tsichlis, P. N. (1991) A Retroviral Oncogene, akt, Encoding a Serine-Threonine Kinase Containing an SH2-like Region, *Science 254*, 274-277.

118. Wong, K. K., Engelman, J. A., and Cantley, L. C. (2010) Targeting the PI3K Signaling Pathway in Cancer, *Current Opinion in Genetics and Development. 20*, 87-90.

119. Farese, R. V., Sajan, M. P., and Standaert, M. L. (2005) Insulin-Sensitive Protein Kinases (Atypical Protein Kinase C and Protein Kinase B/Akt): Actions and Defects in Obesity and Type II Diabetes, *Experimental Biology and Medicine 230*, 593-605.

120. Brazil, D. P., and Hemmings, B. A. (2001) Ten Years of Protein Kinase B Signalling: a Hard Akt to Follow, *Trends in Biochemical Sciences 26*, 657-664.

121. Andjelkovic, M., Alessi, D. R., Meier, R., Fernandez, A., Lamb, N. J. C., Frech, M., Cron, P., Cohen, P., Lucocq, J. M., and Hemmings, B. A. (1997) Role of Translocation in the Activation and Function of Protein Kinase B, *Journal of Biological Chemistry 272*, 31515-31524.

122. Franke, T. F., Kaplan, D. R., Cantley, L. C., and Toker, A. (1997) Direct Regulation of the Akt Proto-Oncogene Product by Phosphatidylinositol-3,4-bisphosphate, *Science 275*, 665-668.

123. James, S. R., Downes, C. P., Gigg, R., Grove, S. J. A., Holmes, A. B., and Alessi, D. R. (1996) Specific Binding of the Akt-1 Protein Kinase to Phosphatidylinositol 3,4,5-trisphosphate without Subsequent Activation, *Biochemical Journal 315*, 709-713.

124. Kunkel, M. T., Ni, Q., Tsien, R. Y., Zhang, J., and Newton, A. C. (2005) Spatio-temporal Dynamics of Protein Kinase B/Akt Signaling Revealed by a Genetically Encoded Fluorescent Reporter, *Journal of Biological Chemistry 280*, 5581-5587.

125. Gao, X., and Zhang, J. (2008) Spatiotemporal Analysis of Differential Akt Regulation in Plasma Membrane Microdomains, *Molecular Biology of the Cell 19*, 4366-4373.

126. Alessi, D. R., James, S. R., Downes, C. P., Holmes, A. B., Gaffney, P. R. J., Reese, C. B., and Cohen, P. (1997) Characterization of a 3-Phosphoinositide-Dependent Protein Kinase which Phosphorylates and Activates Protein Kinase B Alpha, *Current Biology 7*, 261-269.

127. Stephens, L., Anderson, K., Stokoe, D., Erdjument-Bromage, H., Painter, G. F., Holmes, A. B., Gaffney, P. R. J., Reese, C. B., McCormick, F., Tempst, P., Coadwell, J., and

Hawkins, P. T. (1998) Protein Kinase B Kinases that Mediate Phosphatidylinositol 3,4,5-Trisphosphate-Dependent Activation of Protein Kinase B, *Science 279*, 710-714.

128. Stokoe, D., Stephens, L. R., Copeland, T., Gaffney, P. R. J., Reese, C. B., Painter, G. F., Holmes, A. B., McCormick, F., and Hawkins, P. T. (1997) Dual Role of Phosphatidylinositol-3,4,5-Trisphosphate in the Activation of Protein Kinase B, *Science 277*, 567-570.

129. Toker, A., and Newton, A. C. (2000) Akt/protein Kinase B is Regulated by Autophosphorylation at the Hypothetical PDK-2 Site, *Journal of Biological Chemistry 275*, 8271-8274.

130. Alessi, D. R., Andjelkovic, M., Caudwell, B., Cron, P., Morrice, N., Cohen, P., and Hemmings, B. A. (1996) Mechanism of Activation of Protein Kinase B by Insulin and IGF-1, *EMBO Journal 15*, 6541-6551.

131. Scheid, M. P., Marignani, P. A., and Woodgett, J. R. (2002) Multiple Phosphoinositide 3-Kinase-Dependent Steps in Activation of Protein Kinase B, *Molecular and Cellular Biology 22*, 6247-6260.

132. Adams, S. R., Campbell, R. E., Gross, L. A., Martin, B. R., Walkup, G. K., Yao, Y., Llopis, J., and Tsien, R. Y. (2002) New Biarsenical Ligands and Tetracysteine Motifs for Protein Labeling in Vitro and in Vivo: Synthesis and Biological Applications, *Journal of the American Chemical Society 124*, 6063-6076.

133. Whitlow, M., Bell, B. A., Feng, S. L., Filpula, D., Hardman, K. D., Hubert, S. L., Rollence, M. L., Wood, J. F., Schott, M. E., Milenic, D. E., Yokota, T., and Schlom, J. (1993) An Improved Linker for Single-Chain Fv with Reduced Aggregation and Enhanced Proteolytic Stability, *Protein Engineering 6*, 989-995.

134. Egloff, A. M., Vella, L. A., and Finn, O. J. (2006) Cyclin B1 and Other Cyclins as Tumor Antigens in Immunosurveillance and Immunotherapy of Cancer, *Cancer Research 66*, 6-9.

135. Gallegos, L. L., Kunkel, M. T., and Newton, A. C. (2006) Targeting Protein Kinase C Activity Reporter to Discrete Intracellular Regions Reveals Spatiotemporal Differences in Agonist-Dependent Signaling, *Journal of Biological Chemistry 281*, 30947-30956.

136. Wang, Q., Su, L., Liu, N., Zhang, L., Xu, W., and Fang, H. (2011) Cyclin Dependent Kinase 1 Inhibitors: A Review of Recent Progress, *Current Medicinal Chemistry 18*, 2025-2043.

137. Gavet, O., and Pines, J. (2010) Progressive Activation of CyclinB1-Cdk1 Coordinates Entry to Mitosis, *Developmental Cell 18*, 533-543.

138. Gavet, O., and Pines, J. (2010) Activation of Cyclin B1-Cdk1 Synchronizes Events in the Nucleus and the Cytoplasm at Mitosis, *Journal of Cell Biology 189*, 247-259.

139. Tak, Y.-S., Tanaka, Y., Endo, S., Kamimura, Y., and Araki, H. (2006) A CDK-Catalysed Regulatory Phosphorylation for Formation of the DNA Replication Complex Sld2-Dpb11, *EMBO Journal 25*, 1987-1996.

140. Drag, M., and Salvesen, G. S. (2010) Emerging Principles in Protease-Based Drug Discovery, *Nature Reviews Drug Discovery 9*, 690-701.

141. Oliveira, L. C. G., Silva, V. O., Okamoto, D. N., Kondo, M. Y., Santos, S. M. B., Hirata, I. Y., Vallim, M. A., Pascon, R. C., Gouvea, I. E., Juliano, M. A., and Juliano, L. (2012) Internally Quenched Fluorescent Peptide Libraries with Randomized Sequences Designed to Detect Endopeptidases, *Analytical Biochemistry 421*, 299-307.

142. Ali, M. A. M., Fan, X., and Schulz, R. (2011) Cardiac Sarcomeric Proteins: Novel Intracellular Targets of Matrix Metalloproteinase-2 in Heart Disease, *Trends in Cardiovascular Medicine 21*, 112-118.

143. Ai, H. W., Olenych, S. G., Wong, P., Davidson, M. W., and Campbell, R. E. (2008) Hue-shifted Monomeric Variants of *Clavularia* Cyan Fluorescent Protein: Identification of the Molecular Determinants of Color and Applications in Fluorescence Imaging, *BMC Biology 6*.

144. Nguyen, A. W., and Daugherty, P. S. (2005) Evolutionary Optimization of Fluorescent Proteins for Intracellular FRET, *Nature Biotechnology 23*, 355-360.

145. Turk, B. E., Huang, L. L., Piro, E. T., and Cantley, L. C. (2001) Determination of Protease Cleavage Site Motifs Using Mixture-Based Oriented Peptide Libraries, *Nature Biotechnology 19*, 661-667.

146. Chen, E. I., Kridel, S. J., Howard, E. W., Li, W. Z., Godzik, A., and Smith, J. W. (2002) A Unique Substrate Recognition Profile for Matrix Metalloproteinase-2, *Journal of Biological Chemistry 277*, 4485-4491.

147. Laemmli, U. K. (1970) Cleavage of Structural Proteins During Assembly of Head of Bacteriophage-T4, *Nature 227*, 680-&.

148. Communal, C., Sumandea, M., de Tombe, P., Narula, J., Solaro, R. J., and Hajjar, R. J. (2002) Functional Consequences of Caspase Activation in Cardiac Myocytes, *Proceedings of the National Academy of Sciences. U. S. A. 99*, 6252-6256.

149. Britton, H. T. S., and Robinson, R. A. (1931) CXCVIII.-Universal Buffer Solutions and the Dissociation Constant of Veronal, *Journal of the Chemical Society (Resumed) 0*, 1456-1462.

150. Wang, W. J., Schulze, C. J., Suarez-Pinzon, W. L., Dyck, J. R. B., Sawicki, G., and Schulz, R. (2002) Intracellular Action of Matrix Metalloproteinase-2 Accounts for Acute Myocardial Ischemia and Reperfusion Injury, *Circulation 106*, 1543-1549.

151. Kandasamy, A. D., Chow, A. K., Ali, M. A. M., and Schulz, R. (2010) Matrix Metalloproteinase-2 and Myocardial Oxidative Stress Injury: Beyond the Matrix, *Cardiovascular Research 85*, 413-423.

152. Schulz, R. (2007) Intracellular Targets of Matrix Metalloproteinase-2 in Cardiac Disease: Rationale and Therapeutic Approaches, *Annual Review of Pharmacology and Toxicology*, pp 211-242.

153. Knauper, V., Cowell, S., Smith, B., LopezOtin, C., Oshea, M., Morris, H., Zardi, L., and Murphy, G. (1997) The Role of the C-terminal Domain of Human Collagenase-3 (MMP-13) in the Activation of Procollagenase-3, Substrate Specificity, and Tissue Inhibitor of Metalloproteinase Interaction, *Journal of Biological Chemistry 272*, 7608-7616.

154. Kridel, S. J., Chen, E., Kotra, L. P., Howard, E. W., Mobashery, S., and Smith, J. M. (2001) Substrate Hydrolysis by Matrix Metalloproteinase-9, *Journal of Biological Chemistry 276*, 20572-20578.

155. Landry, F., Lombardo, C. R., and Smith, J. W. (2000) A Method for Application of Samples to Matrix-Assisted Laser Desorption Ionization Time-of-Flight Targets that Enhances Peptide Detection, *Analytical Biochemistry 279*, 1-8.

156. Yang, J., Zhang, Z., Lin, J., Lu, J., Liu, B.-f., Zeng, S., and Luo, Q. (2007) Detection of MMP Activity in Living Cells by a Genetically Encoded Surface-Displayed FRET Sensor, *Biochimica et Biophysica Acta (BBA) - Molecular Cell Research 1773*, 400-407.

157. Horton, R. A., Strachan, E. A., Vogel, K. W., and Riddle, S. M. (2007) A Substrate for Deubiquitinating Enzymes Based on Time-Resolved Fluorescence Resonance Energy Transfer Between Terbium and Yellow Fluorescent Protein, *Analytical Biochemistry 360*, 138-143.

158. Martin, S. F., Hattersley, N., Samuel, I. D. W., Hay, R. T., and Tatham, M. H. (2007) A Fluorescence-Resonance-Energy-Transfer-Based Protease Activity Assay and its Use to Monitor Paralog-Specific Small Ubiquitin-Like Modifier Processing, *Analytical Biochemistry 363*, 83-90.

159. Liu, Y., Song, Y., Madahar, V., and Liao, J. (2012) Quantitative Forster Resonance Energy Transfer Analysis for Kinetic Determinations of SUMO-Specific Protease, *Analytical Biochemistry 422*, 14-21.

160. Kawasaki, H., Otani, H., Mishima, K., Imamura, H., and Inagaki, C. (2001) Involvement of Anion Exchange in the Hypoxia/Reoxygenation-Induced Changes in pH(i) and [Ca2+](i) in Cardiac Myocyte, *European. Journal of Pharmacology. 411*, 35-43.

161. Sipos, I., Torocsik, B., Tretter, L., and Adam-Vizi, V. (2005) Impaired Regulation of pH Homeostasis by Oxidative Stress in Rat Brain Capillary Endothelial Cells, *Cellular and Molecular Neurobiology 25*, 141-151.

162. Hansen, J. M., Go, Y. M., and Jones, D. P. (2006) Nuclear and Mitochondrial Compartmentation of Oxidative Stress and Redox Signaling, in *Annual Review of Pharmacology and Toxicology*, pp 215-234.

163. Bindoli, A., and Rigobello, M. P. (2013) Principles in Redox Signaling: From Chemistry to Functional Significance, *Antioxidants & Redox Signaling 18*, 1557-1593.

164. Bachi, A., Dalle-Donne, I., and Scaloni, A. (2013) Redox Proteomics: Chemical Principles, Methodological Approaches and Biological/Biomedical Promises, *Chemical Reviews 113*, 596-698.

165. Aslund, F., Zheng, M., Beckwith, J., and Storz, G. (1999) Regulation of the OxyR Transcription Factor by Hydrogen Peroxide and the Cellular Thiol - Disulfide Status, *Proceedings of the National Academy of Sciences. U. S. A. 96*, 6161-6165.

166. Jones, D. P. (2006) Redefining Oxidative Stress, *Antioxidants & Redox Signaling 8*, 1865-1879.

167. Droge, W. (2002) Free Radicals in the Physiological Control of Cell Function, *Physiological Reviews 82*, 47-95.

168. Fomenko, D. E., Xing, W., Adair, B. M., Thomas, D. J., and Gladyshev, V. N. (2007) High-throughput Identification of Catalytic Redox-active Cysteine Residues, *Science 315*, 387-389.

169. Weerapana, E., Wang, C., Simon, G. M., Richter, F., Khare, S., Dillon, M. B. D., Bachovchin, D. A., Mowen, K., Baker, D., and Cravatt, B. F. (2010) Quantitative Reactivity Profiling Predicts Functional Cysteines in Proteomes, *Nature 468*, 790-U779.

170. Meyer, A. J., and Dick, T. P. (2010) Fluorescent Protein-Based Redox Probes, *Antioxidants & Redox Signaling 13*, 621-650.

171. Hansen, R. E., Ostergaard, H., and Winther, J. R. (2005) Increasing the Reactivity of an Artificial Dithiol-disulfide Pair Through Modification of the Electrostatic Milieu, *Biochemistry 44*, 5899-5906.

172. Cannon, M. B., and Remington, S. J. (2006) Re-engineering Redox-Sensitive Green Fluorescent Protein for Improved Response Rate, *Protein Science 15*, 45-57.

173. Meyer, A. J., Brach, T., Marty, L., Kreye, S., Rouhier, N., Jacquot, J.-P., and Hell, R. (2007) Redox-sensitive GFP in *Arabidopsis Thaliana* is a Quantitative Biosensor for the Redox Potential of the Cellular Glutathione Redox Buffer, *Plant Journal 52*, 973-986.

174. Lohman, J. R., and Remington, S. J. (2008) Development of a Family of Redox-sensitive Green Fluorescent Protein Indicators for Use in Relatively Oxidizing Subcellular Environments, *Biochemistry 47*, 8678-8688.

175. Bjornberg, O., Ostergaard, H., and Winther, J. R. (2006) Mechanistic Insight Provided by Glutaredoxin within a Fusion to Redox-sensitive Yellow Fluorescent Protein, *Biochemistry 45*, 2362-2371.

176. Gutscher, M., Pauleau, A.-L., Marty, L., Brach, T., Wabnitz, G. H., Samstag, Y., Meyer, A. J., and Dick, T. P. (2008) Real-time Imaging of the Intracellular Glutathione Redox Potential, *Nature Methods 5*, 553-559.

177. Gutsche, M., Sobotta, M. C., Wabnitz, G. H., Ballikaya, S., Meyer, A. J., Samstag, Y., and Dick, T. P. (2009) Proximity-based Protein Thiol Oxidation by H_2O_2-scavenging Peroxidases, *Journal of Biological Chemistry 284*, 31532-31540.

178. Kolossov, V. L., Spring, B. Q., Clegg, R. M., Henry, J. J., Sokolowski, A., Kenis, P. J. A., and Gaskins, H. R. (2011) Development of a High-Dynamic Range, GFP-based FRET Probe Sensitive to Oxidative Microenvironments, *Experimental Biology and Medicine 236*, 681-691.

179. Kolossov, V. L., Spring, B. Q., Sokolowski, A., Conour, J. E., Clegg, R. M., Kenis, P. J. A., and Gaskins, H. R. (2008) Engineering Redox-Sensitive Linkers for Genetically Encoded FRET-based Biosensors, *Experimental Biology and Medicine 233*, 238-248.

180. Yano, T., Oku, M., Akeyama, N., Itoyama, A., Yurimoto, H., Kuge, S., Fujiki, Y., and Sakai, Y. (2010) A Novel Fluorescent Sensor Protein for Visualization of Redox States in the Cytoplasm and in Peroxisomes, *Molecular and Cellular Biology 30*, 3758-3766.

181. Belousov, V. V., Fradkov, A. F., Lukyanov, K. A., Staroverov, D. B., Shakhbazov, K. S., Terskikh, A. V., and Lukyanov, S. (2006) Genetically Encoded Fluorescent Indicator for Intracellular Hydrogen Peroxide, *Nature Methods 3*, 281-286.

182. Kim, S. O., Merchant, K., Nudelman, R., Beyer, W. F., Keng, T., DeAngelo, J., Hausladen, A., and Stamler, J. S. (2002) OxyR: A Molecular Code for Redox-Related Signaling, *Cell 109*, 383-396.

183. Zheng, M., Aslund, F., and Storz, G. (1998) Activation of the OxyR Transcription Factor by Reversible Disulfide Bond Formation, *Science 279*, 1718-1721.

184. Choi, H. J., Kim, S. J., Mukhopadhyay, P., Cho, S., Woo, J. R., Storz, G., and Ryu, S. E. (2001) Structural Basis of the Redox Switch in the OxyR Transcription Factor, *Cell 105*, 103-113.

185. Markvicheva, K. N., Bilan, D. S., Mishina, N. M., Gorokhovatsky, A. Y., Vinokurov, L. M., Lukyanov, S., and Belousov, V. V. (2011) A Genetically Encoded Sensor for H_2O_2 with Expanded Dynamic Range, *Bioorganic & Medicinal Chemistry 19*, 1079-1084.

186. Bilan, D. S., Pase, L., Joosen, L., Gorokhovatsky, A. Y., Ermakova, Y. G., Gadella, T. W. J., Grabher, C., Schultz, C., Lukyanov, S., and Belousov, V. V. (2013) HyPer-3: A Genetically Encoded H_2O_2 Probe with Improved Performance for Ratiometric and Fluorescence Lifetime Imaging, *ACS Chemical Biology 8*, 535-542.

187. Cirino, P. C., Mayer, K. M., and Umeno, D. (2003) Generating Mutant Libraries Using Error-prone PCR, *Methods in molecular biology*, 3-9.

188. Kullik, I., Stevens, J., Toledano, M. B., and Storz, G. (1995) Mutational Analysis of the Redox-Sensitive Transcriptional Regulator Oxyr - Regions Important for DNA-Binding and Multimerization, *Journal of Bacteriology 177*, 1285-1291.